JRC TECHNICAL REPORTS

Theoretical framework for In-Car Navigation based on Integrated GPS/IMU Technologies

Giorgio M. Vitetta,
Gianmarco Baldini

2015

Report EUR 27042 EN

Joint
Research
Centre

European Commission
Joint Research Centre
Institute for the Protection and Security of the citizen

Contact information
Gianmarco Baldini Surname
Address: Joint Research Centre, via Enrico Fermi 2749, TP 360, 21027 Ispra, Italy
E-mail: gianmarco.baldini@jrc.ec.europa.eu
Tel.: +39 0332 78 6618

JRC Science Hub
https://ec.europa.eu/jrc

JRC93775

EUR 27042 EN

ISBN 978-92-79-44729-7

ISSN 1831-9424

doi:10.2788/509569

Luxembourg: Publications Office of the European Union, 2015

Abstract

In this report the problem of vehicular navigation based on the integration of the global positioning system and an inertial navigation system is tackled. After analysing some fundamental technical issues about reference systems, vehicle modelling and sensors, a novel solution, combining extended Kalman Filtering with particle Fitering, is developed. This solution allows to embed highly nonlinear constraints originating from digital maps in the position estimation process and is expected to be implementable on commercial hardware platforms equipped with low cost inertial sensors.

Theoretical framework for In-Car Navigation based on Integrated GPS/IMU Technologies

Giorgio M. Vitetta,*

Gianmarco Baldini

18th December 2014

1 Proof of Concept - Integration of positioning technologies for improved accuracy

This report has been created in the context of the Proof of Concept "'Integration of positioning technologies for improved accuracy"', funded by JRC.DDG.03 Intellectual Property and Technology Transfer.

Research in positioning technologies has a long history because of the unquestionable benefits in various domains, but its application in the everyday life has increased enormously in recent years with the use of Global Navigation Satellite Systems (GNSS) for road transportation, Location Based Services (LBS) and so on. Even if the GNSS is the predominant positioning technology, it has limitations, which makes its use in many applications not viable: the accuracy of GNSS is limited to 10 meters or more, GNSS signal may not be available in underground areas or urban areas (e.g., due to urban canyons) and it may be subject to attacks like jamming or spoofing. GNSS is not the only available positioning technology. Wireless Communication technologies based on ranging can also provide accurate position depending on the environment and the features of the wireless communication technology (e.g., bandwidth, power). A third class of positioning systems is based on Inertial Measurements Unit (IMU), based on the use of orientation, and gravitational forces through a combination of accelerometers and gyroscopes. Other techniques uses different parts of the RF spectrum (e.g., infrared) or sound based. Each of this technology has its own advantage and disadvantages. A recent overview of the limitation and trade-offs of positioning technologies for the specific application of firefighting in indoor environments is presented in http://spectrum.ieee.org/static/how-new-indoor-navigation-systems-will-protect-emergency-responders). In addition, some of these technologies can be rather expensive and they cannot be applicable to

*Giorgio M. Vitetta is with the CNIT Research Unit of the University of Modena and Reggio Emilia (Address: Department of Engineering "Enzo Ferrari", Via Vignolese, 905/B, 41125 Modena, Italy; Phone: +390592056157; e-mail: giorgio.vitetta@unimore.it

many applications due to cost reasons. In the third quarter of 2013, JRC.G.06 submitted a proposal for a Proof of Concept (PoC) on positioning technologies to JRC.DDG.03, which was funded from February 2014.
The objective of this PoC is to design a low cost positioning solution, which is able to overcome the disadvantage of the single technology and enhance the accuracy by fusion of the data and by the design and implementation of sophisticated algorithms, which can be tested in specific use cases like Intelligent Transport Systems. The approach of the proposal is on the definition of sophisticated algorithms, which can mitigate the deficiencies of low-cost and not high performing components and devices (e.g., IMU units, radio frequency front end). The rationale of this approach is that the processing power needed for the execution of sophisticated algorithms is available by increasing powerful electronic circuits while low cost devices for various positioning technologies (e.g., IMU, sensors, GNSS receivers) are becoming mass market produced.

The PoC was structured in the following work packages:

- WP1) Requirements and system architecture. This work-package has the objective to define the main uses cases, the operational requirements and the high level system architecture.
- WP2) Theoretical framework. This work-package has the objective to identify and described the main elements of the theoretical framework in the different areas of the proposal: data fusion, evaluation of the accuracy, robustness and other requirements.
- WP3) Design and Implementation. This work-package has the objective to describe the low level architecture, the main design solutions and the implementation of the prototype.
- WP4) Evaluation and testing. This work package has the objective to describe the evaluation and testing activity of the framework and the prototype against the requirements and use cases defined in WP1.

This specific report has the objective to describe the theoretical framework for Work Package 2.

The design of the theoretical framework has been assigned to CNIT Research Unit of the University of Modena and Reggio Emilia. The research work has been coordinated by Prof. Giorgio M. Vitetta.

The theoretical framework has been completely defined by Prof. Giorgio M. Vitetta and his group. Gianmarco Baldini has provided the input requirements, definition of the scenarios and description of the overall context of the project.

2 Introduction to the Theoretical Framework

It is well known that in-car positioning systems based on *Global Positioning System* (GPS) technology only suffer from *vulnerability* [9]. A substantial improvement in positioning accuracy, integrity, availability, and continuity of service can be achieved by combining (i.e., by fusing) GPS measurements with additional information coming from various vehicle sensors and, in particular, from an *inertial measurement unit* (IMU). Unluckily, solving the data fusion problem may entail a formidable complexity mainly due to a) the intrisic nonlinearity of the involved measurement and state models, and b) the large dimensionality of the system state. The data fusion problem becomes even more complicated if map information has to be combined with sensor measurements. For this reason, map information is commonly exploited in the last phase of the positioning procedure, where a digital map is employed to put constraints on the solution generated by in-car navigation systems (this process is known as *map matching*).

In recent years different architectures have been proposed for integrating an IMU with GPS data. The proposed solutions are usually based on: a) reformulating the whole data fusion problem as a set of subproblems, which can be tackled more easily; b) solving each subproblem separately; c) combining all these partial solutions in a solution to the whole problem. The substantial differences between distinct architectures can be related to the level of integration (i.e., *coupling*) to be achieved between the GPS receiver and the IMU (and, eventually, other sensors) and to the use of specific signal processing algorithms, often characterized by substantially different levels of complexity. Examples of integration of GPS and inertial sensors can be found in [6], [7], [55] and [59], where, however, map matching is not taken into consideration; on the contrary, map matching in GPS/IMU based navigation systems has been investigated in [32], [33], [34], [35], [36], [38], [47] and [48]. Various details on the possible architectural options available for these systems can be found in [29], [30] and [31].

In this manuscript the problem of navigation based on the integration of an IMU (and, in particular, of an *inertial navigation system*, INS) and GPS is analysed from a theoretical viewpoint; then it is shown how filtering methods for mixed linear/nonlinear systems, like *particle filtering* (PF) and *extended Kalman filtering* (EKF), can be exploited to solve this problem at an acceptable complexity. The problem of embedding map information in the filtering process is also analysed. The main goal of this manuscript is to show how the above mentioned advanced signal processing techniques can be employed to develop a novel navigation technique fusing GPS data, INS data and map information. Such a technique is required to have an acceptable complexity (i.e., to be implementable on commercial hardware platforms) and to outperform other technical solutions already available in the technical literature in terms of one or more of the following parameters: a) *accuracy* (intended as the degree of conformity of the estimated position, velocity, etc., to their actual values); b) *integrity* (trustfulness that can be put in the information provided by the navigation system);

3) *availability* (intended as a measure of the percentage of the intended coverage area in which the navigation system works); 4) *continuity of service* (expressing the system probability of continuously providing information without nonscheduled interruptions during a given working period).

This manuscripts aims also at providing a framework for a) the analysis of integrated GPS/INS navigation in the presence of map information and b) the development of data fusion algorithms. For this reason, an analysis of two state-space models for four wheel vehicles and of the measurement models for standard sensors employed in vehicular navigation is provided.

The remaining part of this report is organized as follows. In Section 3 a description of the employed coordinate systems and that of well known state models for a four wheel vehicle are provided. In Section 4 the measurement models of various sensors for navigation systems are briefly described. Different architectures for the integration of INS and GPS are illustrated in Section 5. The problem of integrating map knowledge in a navigation system is tackled in Section 6. A new technique for integrated INS/GPS navigation is illustrated in Section 7, whereas some conclusions are provided in Section 8. Finally, an introduction to quaternion algebra is given in the Appendix.

3 System Description

In this Section the following two technical issues are analysed: a) the use of coordinate systems in navigation systems; b) state-space models for a four-wheel vehicle.

3.1 Coordinate Systems

Because of the 3-D nature of the quantities sensed byan IMU and by other sensors installed on a vehicle, the coordinate spaces and the adopted notation need to be clearly defined. In the following two different coordinate systems (also called *frames*) are taken into consideration: the *body* (or *vehicle*) *frame*, rigidly attached to the IMU sensor (and, consequently, to the considered vehicle) and the *navigation frame*, rigidly attached to some fixed point of the environment where navigation takes place and with its z axis pointing away from Earth. The vehicle coordinate system usually has its origin at the center of gravity of the vehicle, and the coordinate axes are aligned with the forward, sideway (to the right), and down directions associated with the vehicle. The information provided by vehicle-mounted sensors, and the motion and dynamic constraints imposed by the vehicle model are generally expressed with reference to this coordinate system.

In this document, when *Euler angles* are employed, the angle sequence $(1, 2, 3)$ is always used and the rotation angles (ϕ, θ, ψ) are called *roll*, *pitch* and *yaw*, respectively [8, Sec. 5.6], so that the roll angle refers to the rotation around the x axis, the pitch around the y axis and the yaw around the z axis. Note that the notation (ϕ, θ, ψ) entails that rotations occur in reverse order:

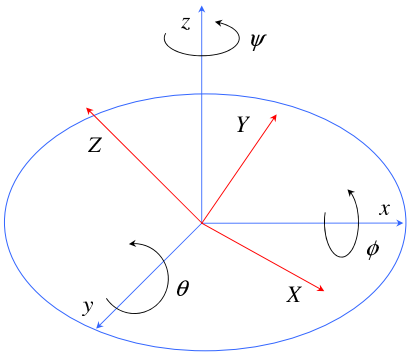

Figure 1: Conventions adopted for the IMU coordinate frame. The navigation frame is shown in blue, the vehicle (or body) frame is shown in red. The Euler angle sequence $(1, 2, 3)$ for a navigation to body (vehicle) transformation, corresponds to the figure angles (ϕ, θ, ψ), *roll*, *pitch* and *yaw*, where all the angles are positive.

first a rotation by ψ degrees around the z axis, then a rotation by θ around the y axis and, finally, by ϕ around the x axis (see Fig. 1, which summarizes such conventions). Positive angles denote counter-clockwise rotations when the observer is looking at a given rotation axis so that it points toward him; moreover, a positive angular velocity $\omega = \alpha/T$ represents a counterclockwise rotation by positive angle α occurring in T s.

A vector expressed in some coordinate frame can be transformed in a vector lying in a different coordinate frame by employing different transformations. For tracking applications, representations avoiding singularities (arising from the so-called *gimbal lock*[1]) are particularly well-suited; a representation with thes properties is provided by the adoption of unit *quaternions* for vehicle to navigation transformations (and viceversa). In practice a *navigation to vehicle*

[1] A gimbal lock is the loss of one degree of freedom in a three-dimensional, three-gimbal mechanism that occurs when the axes of two of the three gimbals are driven into a parallel configuration, so "locking" the system into rotation in a degenerate two-dimensional space.

transformation can be represented a unit quaternion $q^{n\triangleright b} \triangleq \left(q_0^{n\triangleright b}, \mathbf{q}^{n\triangleright b}\right) = (q_0, q_1, q_2, q_3)$ belonging to the so called $\mathbb{H}_1$ space; then, the trasformation of a vector $\mathbf{x}^n \in \mathbb{R}^3$ in the *navigation* frame into its representation $\mathbf{x}^b$ expressed in the *body* (*vehicle*) frame can be expressed as (e.g., see [10, Sec. B] and [61, Eq. (5.11)])

$$\mathbf{x}^b = q^{n\triangleright b} \odot \mathbf{x}^n \odot \left(q^{n\triangleright b}\right)^* = \mathbf{R}\left(q^{n\triangleright b}\right)\mathbf{x}^n, \tag{1}$$

where $\odot$ denotes the *multiplication operator* defined in the quaternion algebra (see the Appendix for further details about this algebra and the operations defined over it). This transformation can be also represented a

$$\mathbf{x}^b = \mathbf{R}\left(q^{n\triangleright b}\right)\mathbf{x}^n, \tag{2}$$

where $\mathbf{R}\left(q^{n\triangleright b}\right) \in \mathbb{R}^{3\times 3}$ is the *rotation matrix* associated with the quaternion $q^{n\triangleright b}$ and is defined as (e.g., see [74, Eq. (B.1)] and [61, Eq. (5.11)]):

$$\mathbf{R}(q) \triangleq \begin{bmatrix} 2q_0^2 + 2q_1^2 - 1 & 2q_1q_2 - 2q_0q_3 & 2q_1q_3 + 2q_0q_2 \\ 2q_1q_2 + 2q_0q_3 & 2q_0^2 + 2q_2^2 - 1 & 2q_2q_3 - 2q_0q_1 \\ 2q_1q_3 - 2q_0q_2 & 2q_2q_3 + 2q_0q_1 & 2q_0^2 + 2q_3^2 - 1 \end{bmatrix}. \tag{3}$$

Note that this matrix coincides with the transpose of the matrix (e.g., see [8, eq. (125)])

$$\mathbf{C}_b^n \triangleq \begin{bmatrix} \cos\theta\cos\psi & \sin\phi\sin\theta\cos\psi - \cos\phi\sin\psi & \cos\phi\sin\theta\cos\psi + \sin\phi\sin\psi \\ \cos\theta\sin\psi & \sin\phi\sin\theta\sin\psi + \cos\phi\cos\psi & \cos\phi\sin\theta\sin\psi - \sin\phi\cos\psi \\ -\sin\theta & \sin\phi\cos\theta & \cos\phi\cos\theta \end{bmatrix} \tag{4}$$

expressing the *body* (*vehicle*) *to navigation* transformation. It is worth noting that:

- The product in (1) formally involves a mapping of $\mathbf{x}^n$ into the space $\mathbb{H}_0$ of pure quaternions (i.e., two quaternion multiplications in the space $\mathbb{H}$ that produce a new quaternion in $\mathbb{H}_0$), which can then be easily mapped back to $\mathbb{R}^3$; these conceptual operations can be represented graphically, as shown in Fig. 2 (see also [61, Sec. 5]).
- Quaternions can be related to Euler angles. If the angle sequence $(1, 2, 3)$ is considered, then the angles $(\phi, \theta\psi)$ can be obtained from the $q^{n\triangleright b}$ quaternion, representing the *navigation to vehicle* transformation, as $\phi = \phi(q^{n\triangleright b})$, $\theta = \theta(q^{n\triangleright b})$ and $\psi = \psi(q^{n\triangleright b})$, where (e.g., see [10, Eq. (B.2)]):

$$\phi(q) \triangleq \arctan\frac{2(q_2q_3 - q_0q_1)}{2q_0^2 + 2q_3^2 - 1}, \tag{5}$$

$$\theta(q) \triangleq -\arcsin 2(q_1q_3 + q_0q_2) \tag{6}$$

and

$$\psi(q) \triangleq \arctan\frac{2(q_1q_2 - q_0q_3)}{2q_0^2 + 2q_1^2 - 1}. \tag{7}$$

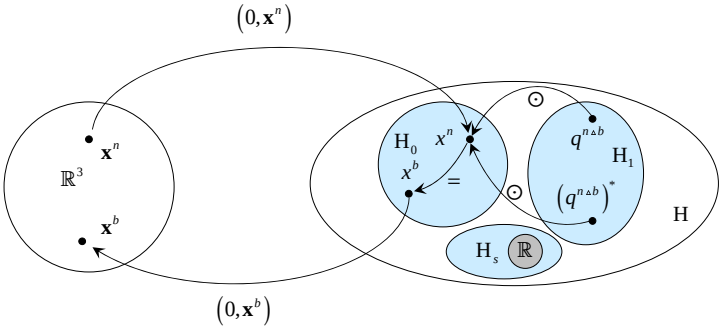

Figure 2: Graphical representation of (1) stressing the relations between vectors in $\mathbb{R}^3$ and quaternions in $\mathbb{H}_0$ and $\mathbb{H}_1$. The relations among $\mathbb{H}$, $\mathbb{H}_s$ (the space of scalar quaternions) and $\mathbb{R}$ are also shown.

> Note that these equations coincide with those provided by [8, Eq. (290)] if the conjugate quaternion is considered (in other words, [8] gives similar equations referring, however, to the opposite transformation); further details about these transformations can be found in [8], [10], [61] and [74].

3.2 Vehicle Modelling

3.2.1 Introduction

Ideally, a vehicle moving on a planar path experiences no wheel slip and no motion in the direction perpendicular to the path itself. Consequently, in a real world scenario the downward and sideway components of vehicle velocity are constrained to be close to zero. It is well known that these results can be interpreted as *nonholonomic constraints*[2], which can be profitably exploited in

[2]Generally speaking, a *nonholonomic system* is a system whose state depends on the path taken to reach it. Such a system is described by a set of parameters subject to differential constraints (known as *noholonomic constraints*), such that when the system evolves along a path in its parameter space and finally returns to the original set of values at the start of the

the development of in-car navigation techniques for GNSS-aided INSs (see [6], [7] and [14]). In fact, its has been shown that the position error growth during GNSS outages can be substantially mitigated and the attitude accuracy can be improved if nonholonomic constraints are exploited in the navigation system; further improvements can be obtained by complementing INS with velocity measurements (provided by velocity encoders). However, it is important to point out that, *from the viewpoint of estimation theory*, sensor and vehicle model information play an equivalent role in the estimation of the vehicle state [12]. This means that, if there were a perfect vehicle model such that the vehicle state could be perfectly predicted from control inputs, sensor information would be superfluous. On the contrary, if perfect sensors were available, the vehicle model would provide no additional information; unluckily, since this does not occur, vehicle modelling can improve navigation system performance or, for a given performance, may allow the use of less-costly sensors. Numerous vehicle models and motion constraints are available in the technical literature, ranging from the aforementioned nonholonomic constraints to more advanced models incorporating wheel slip, tire stiffness, etc. (e.g., see [2], [7], [12], [13], [14], [15] and [16]). In particular, in [12], a theoretical framework for analyzing the impact of various vehicle models is developed and it is shown that, if more refined vehicle models are employed, significant gains can be obtained, particularly in the accuracy of the orientation estimate. However, it is difficult to find good vehicle models independent of the driving situation [2]. More advanced models require knowledge about several parameters such as vehicle type, tires, and environmental specifics [7]. To adapt the model to different driving conditions, these parameters must be estimated in real time. Alternatively, the driving conditions must be detected and used to switch between different vehicle models. An example of this approach can be found in [2], where a technical solution based on an interactive multimodel *extended Kalman filter* (EKF) is employed.

In the following we first focus on the vehicle model proposed in [7], which explicitly exploits the nonholonomic constraints mentioned above; then we take into consideration the multimodel approach proposed in [1] and [2], which implicitly incorporates such constraints.

3.2.2 Vehicle model proposed by Dissanayake et al.

In [7] a wheeled vehicle moving on the earth surface is considered. As explained in the previous Section, the *navigation frame* is the coordinate frame with respect to which the location of the vehicle needs to be estimated, whereas the *body frame* is attached to the vehicle and is aligned with the axes of the IMU. Without any loss of generality, it is assumed that:

1. The IMU is placed at the center of the rear axle of the vehicle such that the y axis is in the direction of the rear axle and the x axis is in the direction of the forward motion of the vehicle.

path, the system itself may not have returned to its original state. In robotics a system is non-holonomic if the controllable degrees of freedom are less than the total degrees of freedom.

2. The vehicle is steered using its front wheels.

3. The position of the vehicle $\mathbf{p}_n \triangleq [p_{nx}, p_{ny}, p_{nz}]^T$ is the position vector of the origin of the body frame in the navigation frame and the velocity of the vehicle $\mathbf{v}_n \triangleq [v_{nx}, v_{ny}, v_{nz}]^T$ is the rate of change of $\mathbf{p}_n$ (the time variable is omitted for simplicity).

4. The orientation of the vehicle is represented by the three Euler angles (ϕ, θ, ψ) (see the previous Paragraph) and the orientation of body frame with respect to the navigation frame is described by the rotation matrix (see (4))

$$\mathbf{C}_b^n \triangleq \begin{bmatrix} \cos\theta\cos\psi & \sin\phi\sin\theta\cos\psi - \cos\phi\sin\psi & \cos\phi\sin\theta\cos\psi + \sin\phi\sin\psi \\ \cos\theta\sin\psi & \sin\phi\sin\theta\sin\psi + \cos\phi\cos\psi & \cos\phi\sin\theta\sin\psi - \sin\phi\cos\psi \\ -\sin\theta & \sin\phi\cos\theta & \cos\phi\cos\theta \end{bmatrix}. \tag{8}$$

5. The acceleration and angular velocity in the body frame are denoted $\mathbf{a}_b \triangleq [a_{bx}, a_{by}, a_{bz}]^T$ and $\omega_b \triangleq [\omega_{bx}, \omega_{by}, \omega_{bz}]^T$, respectively; these quantities can be measured by a means of a 3D accelerometer and a 3D gyroscope, respectively (i.e., by an IMU).

6. The vehicle state is defined by the vector $\mathbf{x} \triangleq [\mathbf{p}_n^T, \mathbf{v}_n^T, \phi, \theta, \psi]^T$ (9-dimensional vector).

7. The rate of rotation of the earth is negligible.

8. The gravity vector $\mathbf{g}$ is constant and parallel to the z axis of the navigation frame, so that acceleration measured in the body frame $\mathbf{a}_b$ is related to the acceleration $\mathbf{a}_n$ in the navigation frame by

$$\mathbf{a}_b = (\mathbf{C}_b^n)^T [\mathbf{a}_n + \mathbf{g}]. \tag{9}$$

Then, using the kinematic relationship between ω_b and the rates of changes of the Euler angles, the state equations for vehicle motion can be written as

$$\dot{\mathbf{p}}_n = \mathbf{v}_n \tag{10}$$

$$\dot{\mathbf{v}}_n = \mathbf{C}_b^n \mathbf{a}_b - \mathbf{g} \tag{11}$$

$$\dot{\phi} = \omega_{bx} + (\omega_{by}\sin\phi + \omega_{bz}\cos\phi)\tan\theta \tag{12}$$

$$\dot{\theta} = \omega_{by}\cos\phi - \omega_{bz}\sin\phi \tag{13}$$

$$\dot{\psi} = \frac{\omega_{by}\sin\phi + \omega_{bz}\cos\phi}{\cos\theta} \tag{14}$$

Equations (10)–(14) enable the computation of the state of the vehicle from an initial state and a series of measurements on $\mathbf{a}_b$ and ω_b generated by an IMU. Their use deserves the following comments:

- These equations hold for the motion of any rigid body in a three-dimensional space. In some inertial applications, various effects, such as the Schuler frequency, Earth rotation, and the fact that gravity is not necessarily constant as a vehicle travels over large distances, should be kept into account in the the equations shown above. However, for low cost IMU's which cannot measure such effects, or changes in these effects, these terms are not included. This choice is motivated by the fact that in many land, civilian applications, like the one considered in this report, the error drift in the INS solutions is relevant enough to require constant aiding by GPS.

- Equations (11)–(14) represent a set of nonlinear differential equations that can be solved using a variety of different techniques. If the sampling time is sufficiently small, as usually is the case in many practical applications, a simple Euler's method is adequate.

- These equations, for sufficiently small sampling intervals, can be linearized by incorporating all the elements of the direction cosine matrix $\mathbf{C}_b^n$ into the state equations themselves. Alternative schemes for representing orientation of a body can also be used (e.g., quaternions) in the formulation of state equations.

- When $\theta = \pm\pi/2$, the set of equations presented above is singular; this condition is equivalent to driving up or down a 90 degree slope and does not occur in the case of land vehicles.

Some nonholonomic constraints can be added to the equations (10)–(14) in order to limit the rate of growth of the position errors due to incorrect estimates of $\mathbf{a}_b$ and ω_b. In fact, when a vehicle does not jump off the ground and does not slide on the ground, its velocity in the plane perpendicular to the forward direction is zero. In addition, under ideal conditions, there is no side slip along the direction of the rear axle and no motion normal to the road surface, so that

$$v_{bz} = 0 \tag{15}$$

and

$$v_{by} = 0, \tag{16}$$

if $\mathbf{v}_b \triangleq [v_{bx}, v_{by}, v_{bz}]^T$ denotes the velocity in the body frame. In practice, these constraints are somewhat violated due to the presence of a) side slips during cornering and b) vibrations caused by the engine and suspension system; note also that side slips are influenced by the vehicle state as well as by the interaction between the vehicle tyres and the terrain. A number of models are available for determining side slips, but such models require various information (e.g., the knowledge of the vehicle, tyre and ground characteristics) that are not usually available. Alternatively, information from external sensors can be used to accomplish on-line estimation of side slip. However, as a first approximation, constraint violations can be modelled by replacing (15) and (16) with

$$v_{by} = n_y \tag{17}$$

and

$$v_{bz} = n_z, \tag{18}$$

respectively, where n_z and n_y are Gaussian noise processes with zero mean and variances σ_z^2 and σ_y^2 , respectively (note that noise strength should be adapted in a way to account for the extent of the expected constraint violations). Since

$$\mathbf{v}_b = \left(\mathbf{C}_b^n\right)^T \mathbf{v}_n, \tag{19}$$

the constraints (17) and (18) can be reformulated as

$$v_{by} = v_{nx}\cos\theta\cos\psi + v_{ny}\cos\theta\sin\psi - v_{nz}\sin\theta = n_y \tag{20}$$

and

$$\begin{aligned} v_{bz} = v_{nx}\left(\sin\phi\sin\theta\cos\psi - \cos\phi\sin\psi\right) + v_{ny}\left(\sin\phi\sin\theta\sin\psi + \cos\phi\cos\psi\right) \\ + v_{nz}\sin\phi\cos\theta = n_z, \end{aligned} \tag{21}$$

respectively; these equations relate both constraints to the vehicle state. In an IMU-based navigation system it is required to obtain the best estimate for the state vector modeled by the state equations (11)–(14) from a series of measurements about $\mathbf{a}_b$ and ω_b under the constraints (20)-(21). In principle, state estimation can be accomplished as follows. Discrete-time state equations can be easily derived by discretising (11)–(14) and can be put in the form (a sampling period equal to T s is implictly assumed in the derivation of the following equations)

$$\mathbf{x}\left[k\right] = f\left(\mathbf{x}\left[k-1\right], \mathbf{u}\left[k-1\right]\right), \tag{22}$$

where $\mathbf{x}\left[k\right] \triangleq \left[\mathbf{p}_n^T\left[k\right], \mathbf{v}_n^T\left[k\right], \phi\left[k\right], \theta\left[k\right], \psi\left[k\right]\right]^T$ is the state vector and $\mathbf{u}\left[k\right] \triangleq \left[\mathbf{a}_b^T\left[k\right], \omega_b^T\left[k\right]\right]^T$ denotes the input vector. A discrete time version of the constraint equations (20)-(21) can be also derived and can be put in the form

$$\mathbf{z}\left[k\right] = h\left(\mathbf{x}\left[k\right], \mathbf{n}\left[k\right]\right), \tag{23}$$

where $\mathbf{n}\left[k\right] \triangleq \left[n_y\left[k\right], n_z\left[k\right]\right]^T$ and $\mathbf{z}\left[k\right] \triangleq \left[v_{by}\left[k\right], v_{bz}\left[k\right]\right]^T$. Note that $\mathbf{z}\left[k\right]$ is expected to be zero and that (23) can be treated as an observation equation where the "virtual observation" (pseudo measurement) at each time instant is identical to zero. An extended Kalman filter can be adopted to recursively compute state estimates on the basis of the process model (22) and of the observation model (23). Further details can be found in [7, Par. II-C].

3.2.3 Vehicle Model Proposed by Toledo-Moreo et al.

In [1] and [2] an *interactive multimodel* (IMM)-based method is developed for fusing inertial, odometry and satellite data. In the proposed approach, the use of an IMM method allows to exploit the benefits of high dynamic models in the problem of road vehicle positioning while avoiding their relevant disadvantages (namely, large computational load and unrealistic assumptions about noise models). In practice, two *planar* models of a vehicle are proposed to reproduce

its movements along roads. The *straight* (or *nonmaneuvering*) model (model #1, briefly) reproduces properly straight and mild trajectories of the vehicle, whereas the *curved* (or *maneuvering*) model (model #2, briefly) describes sharp turns and brusque accelerations in the vehicle state at the expense of higher noise considerations. An IMM-EKF filter allows to evaluate the probability of success of each model at every filter execution scan, supplying a realistic combined solution for vehicle behavior; these probabilities are calculated according to a Markov model for the transition between the two maneuver states.

In the derivation of model #1 the considered vehicle is assumed to undergo piecewise constant linear and angular accelerations with a nearly constant velocity direction in a straight motion. The model is based on the rigid solid definition of a four-wheel vehicle; its back wheels can rotate only around the transversal axis of the vehicle, whereas the turn of its forward wheels follows curves centered around an instant rotation center, as shown in Fig. 3 (the notation defined in [1] and [2] is adopted in the following). In the proposed model the following variables are defined for the k-th observation instant (a sampling period equal to T s is assumed):

- $(x_c(k), y_c(k))$ denote the position (coordinates) of the *geometrical center* (g.c.) of the vehicle with respect to the navigation frame;
- the variable $v_c(k)$ represents the speed of the vehicle measured in its g.c. (and expressed in m/s);
- the variables $\theta(k)$ and $\dot{\theta}(k)$ denote the orientation of the vehicle with respect to the navigation frame and its angular velocity, respectively;
- the variable $\phi_c(k)$ denotes the nominal angle of the velocity (projected steering angle to the g.c. of the vehicle in the absence of slips);
- the variable $s_c(k)$ represents the *slide correction angle*, i.e. the slip bias angular component in g.c. (generally speaking, it is due to unbalanced weight distribution and/or inaccurate wheel alignment).
- the variables v_{fl}, v_{fr}, v_{rl} and v_{rr} represent the velocities of the forward left, forward right, rear left and rear right wheels, respectively;
- the variables $\delta_{fl}, \delta_{fr}, \delta_{rl}$ and δ_{rr} represent the steering angles of the forward left, forward right, rear left and rear right wheels, respectively;
- the parameters l and b are the wheel tread and the wheel base, respectively;
- the parameter Δ is the angle between the longitudinal axis of the vehicle and the line connecting the center of a wheel with the g.c. (see Fig. 3; this angle is expressed by $\tan^{-1}(b/l)$);
- the point I represents the instant center of rotation.

Given the quantities defined above, in model #1 the *vehicle state* at the k-th observation instant can be defined as the 7-dimensional vector

$$\mathbf{x}(k) \triangleq \left[x_c(k),\, y_c(k),\, \theta(k),\, \dot{\theta}(k),\, v_c(k),\, \phi_c(k),\, s_c(k)\right]^T. \tag{24}$$

The state update equations are

$$\begin{aligned} x_c(k+1) = x_c(k) + Tv_c(k)\cos(\theta(k) + \phi_c(k) + s_c(k)) \\ +0.5T^2\dot{v_c}(k)\cos(\theta(k) + \phi_c(k) + s_c(k)) \\ -0.5T^2 v_c(k)\dot{\theta}(k)\sin(\theta(k) + \phi_c(k) + s_c(k)), \end{aligned} \tag{25}$$

$$\begin{aligned} y_c(k+1) = y_c(k) + Tv_c(k)\sin(\theta(k) + \phi_c(k) + s_c(k)) \\ +0.5T^2\dot{v_c}(k)\sin(\theta(k) + \phi_c(k) + s_c(k)) \\ -0.5T^2 v_c(k)\dot{\theta}(k)\cos(\theta(k) + \phi_c(k) + s_c(k)), \end{aligned} \tag{26}$$

$$\theta(k+1) = \theta(k) + T\dot{\theta}(k) + 0.5T^2\ddot{\theta}(k), \tag{27}$$

$$\dot{\theta}(k+1) = \dot{\theta}(k) + T\ddot{\theta}(k), \tag{28}$$

$$v_c(k+1) = v_c(k) + T\dot{v_c}(k), \tag{29}$$

$$\phi_c(k+1) = \phi_c(k) + T\dot{\phi_c}(k) \tag{30}$$

and

$$s_c(k+1) = s_c(k) + T\dot{s_c}(k). \tag{31}$$

Then, if the 4-dimensional vector

$$\mathbf{v}(k) \triangleq \left[\ddot{\theta}(k),\, \dot{v_c}(k),\, \dot{\phi_c}(k),\, \dot{s_c}(k)\right]^T \tag{32}$$

is defined, the state transition equations (25)-(31) can be put in the form

$$\mathbf{x}(k+1) = \mathbf{f}(\mathbf{x}(k)) + \mathbf{G}(\mathbf{x}(k))\mathbf{v}(k), \tag{33}$$

where

$$\begin{aligned} \mathbf{f}(\mathbf{x}(k)) \triangleq [x_c(k) + Tv_c(k)\cos(\theta(k) + \phi_c(k) + s_c(k)) \\ -0.5T^2 v_c(k)\dot{\theta}(k)\sin(\theta(k) + \phi_c(k) + s_c(k)), \\ y_c(k) + Tv_c(k)\sin(\theta(k) + \phi_c(k) + s_c(k)) \\ -0.5T^2 v_c(k)\dot{\theta}(k)\cos(\theta(k) + \phi_c(k) + s_c(k)), \\ \theta(k) + T\dot{\theta}(k), \dot{\theta}(k), v_c(k), \phi_c(k), s_c(k)\Big]^T \end{aligned} \tag{34}$$

and

$$\mathbf{G}(\mathbf{x}(k)) \triangleq \begin{bmatrix} 0 & 0.5T^2\cos(\theta(k) + \phi_c(k) + s_c(k)) & 0 & 0 \\ 0 & 0.5T^2\sin(\theta(k) + \phi_c(k) + s_c(k)) & 0 & 0 \\ 0.5T^2 & 0 & 0 & 0 \\ T & 0 & 0 & 0 \\ 0 & T & 0 & 0 \\ 0 & 0 & T & 0 \\ 0 & 0 & 0 & T \end{bmatrix}. \tag{35}$$

Note that in model #1 the changes in the steering angle $\phi_c(k)$ are described by a first-order equation (see (30)).

Both parallel-change lane and turn motions can be described by slightly modifying the structure of model #1: this leads to model #2. Like in the derivation of model #1, the vehicle is assumed to undergo piecewise constant linear and angular accelerations; however, a nearly constant change in velocity direction is assumed now. In the description of model #2 the notation is the same as that adopted above, but the variations in the steering projected angle are described by a second-order equation in order to account for sharp curves. Then, the state update equations are given by (25),-(29), (31),

$$\phi_c\left(k+1\right) = \phi_c\left(k\right) + T\dot{\phi}_c\left(k\right) + 0.5T^2\ddot{\phi}_c\left(k\right) \tag{36}$$

and

$$\dot{\phi}_c\left(k+1\right) = \dot{\phi}_c\left(k\right) + T\ddot{\phi}_c\left(k\right). \tag{37}$$

In model #2 the proposed *state vector* is 8-dimensional, since its is obtained by including the new variable $\dot{\phi}_c\left(k\right)$ in the state vector $\mathbf{x}\left(k\right)$ (24); for this reason, the new state vector is

$$\mathbf{x}\left(k\right) = \left[x_c\left(k\right), y_c\left(k\right), \theta\left(k\right), \dot{\theta}\left(k\right), v_c\left(k\right), \phi_c\left(k\right), \dot{\phi}_c\left(k\right), s_c\left(k\right)\right]^T. \tag{38}$$

Then, if the 4-dimensional vector

$$\mathbf{v}\left(k\right) = \left[\ddot{\theta}\left(k\right), \dot{v_c}\left(k\right), \ddot{\phi}_c\left(k\right), \dot{s_c}\left(k\right)\right]^T \tag{39}$$

is defined, the new state transition equations (25)-(29), (31), (36) and (37) can be still put in the form (33), where, however,

$$\begin{aligned}\mathbf{f}(\mathbf{x}\left(k\right)) \triangleq [&x_c\left(k\right) + Tv_c\left(k\right)\cos\left(\theta(k) + \phi_c\left(k\right) + s_c\left(k\right)\right)\\ &-0.5T^2v_c\left(k\right)\dot{\theta}(k)\sin\left(\theta\left(k\right) + \phi_c\left(k\right) + s_c\left(k\right)\right),\\ &y_c\left(k\right) + Tv_c\left(k\right)\sin\left(\theta\left(k\right) + \phi_c\left(k\right) + s_c\left(k\right)\right)\\ &-0.5T^2v_c\left(k\right)\dot{\theta}\left(k\right)\cos\left(\theta\left(k\right) + \phi_c\left(k\right) + s_c\left(k\right)\right),\\ &\theta\left(k\right) + T\dot{\theta}\left(k\right), \dot{\theta}\left(k\right), v_c\left(k\right), \phi_c\left(k\right) + T\dot{\phi}_c\left(k\right), \dot{\phi}_c\left(k\right), s_c\left(k\right)\Big]^T\end{aligned} \tag{40}$$

and

$$\mathbf{G}(\mathbf{x}\left(k\right)) \triangleq \begin{bmatrix} 0 & 0.5T^2\cos\left(\theta\left(k\right) + \phi_c\left(k\right) + s_c\left(k\right)\right) & 0 & 0\\ 0 & 0.5T^2\sin\left(\theta\left(k\right) + \phi_c\left(k\right) + s_c\left(k\right)\right) & 0 & 0\\ 0.5T^2 & 0 & 0 & 0\\ T & 0 & 0 & 0\\ 0 & T & 0 & 0\\ 0 & 0 & 0.5T^2 & 0\\ 0 & 0 & T & 0\\ 0 & 0 & 0 & T \end{bmatrix}. \tag{41}$$

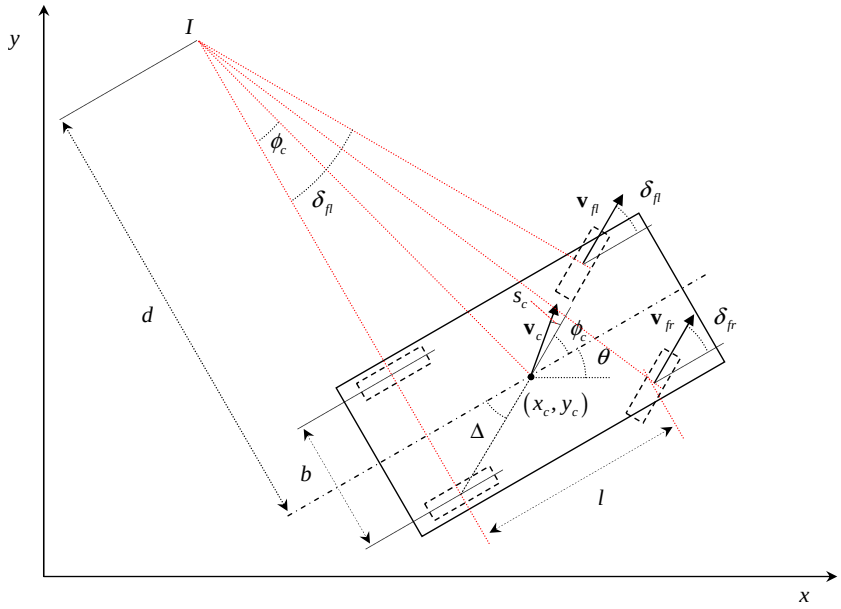

Figure 3: Representation of a four-wheel vehicle accomplishing an instantaneous rotation around the point I.

Finally, it is worth stressing that the underlying vehicle representation for both models is the same; such models, however, are characterized by different noise contributions.

4 Sensor Description and Models

In this Section a short description is provided for each of the following sensors: a) an IMU; b) an odometer; c) a GPS receiver.

4.1 IMU

In this report the following assumptions are made about the considered IMU:

1. This device consists of three accelerometers and three gyroscopes, where the sensitivity axes of the accelerometers are mounted to be orthogonal and span a 3-D space, and the gyroscopes measure the rotations around these axes.

2. IMU-sensed quantities are expressed with respect to the vehicle frame (see Paragraph 3.1).

3. IMU data are available in "raw mode", i.e., the raw sensor outputs can be acquired as integer numbers and then scaled.

4. Calibration procedures on the sensors can be performed.

The most common signal model for a 3-D accelerometer is (assuming the sensor to be still) [21], [22]

$$\mathbf{a}_{bm} = \mathbf{G}_a \mathbf{a}_b + \hat{\mathbf{b}}_a + \mathbf{n}_a, \tag{42}$$

where $\mathbf{a}_{bm} \in \mathbb{Z}^3$ is the vector of measured accelerations (in body frame); $\mathbf{a} \in \mathbb{R}^3$ is the vector of true accelerations (in body frame); $\mathbf{G}_a \in \mathbb{R}^{3\times 3}$ is the gain matrix (diagonal if only scale factors are accounted for, or a generic invertible matrix if cross-couplings are also accounted for); $\hat{\mathbf{b}}_a \in \mathbb{R}^3$ is a deterministic bias vector (in vehicle frame) and $\mathbf{n}_a \in \mathbb{R}^3$ is the noise vector (in vehicle frame); noise is assumed to be zero-mean Gaussian with covariance matrix $\mathbf{\Sigma}_a = \sigma_a^2 \mathbf{I}_3$. It is important to mention that

1. Any accelerometer requires *calibration*; this task consists in estimating the matrix $\mathbf{G}_a$ and the vector $\mathbf{b}_a$ by observing $\mathbf{a}_{bm}$ and can be accomplished as follows. If the IMU sensor is still and the orientation of the sensor with respect to the navigation frame is known in the form of the rotation matrix $\mathbf{C}_b^n$, then $\mathbf{a}_{bm}$ must satisfy the constraint $\mathbf{C}_b^n \mathbf{a}_{bm} = [0, 0, g]^T$, where g is the gravitational acceleration (assumed known); in principle this form of a priori knowledge makes the accelerometer calibration possible, as shown in [21], [22]. A simple calibration procedure can be found in [43]. This procedure is similar to that described in [21], [22], but does not require any additional hardware (besides the IMU itself), such as expensive motion

rate tables; moreover, it can be accomplished only once. Note that the resulting bias estimate $\hat{\mathbf{b}}_a$ has to be considered as an estimate of the *deterministic* (systematic) errors affecting the accelerometer sensor.

2. The stochastic noise affecting is usually a combination of at least three different stochastic processes: *acceleration random walk* (ARW), *bias instability* (BI), *rate random walk* (RRW) (see [51, 52] for further details). Such contributions can be investigated analysing long sequences of sensor outputs acquired while the sensor is still (the Allan variance method is employed).

The most common signal model for a 3-D gyroscope is

$$\boldsymbol{\omega}_{bm} = \mathbf{G}_\omega \boldsymbol{\omega}_b + \hat{\mathbf{b}}_\omega + \mathbf{n}_\omega, \tag{43}$$

where $\boldsymbol{\omega}_{bm} \in \mathbb{Z}^3$ is the vector of measured angular velocities (in body frame); $\boldsymbol{\omega}_b \in \mathbb{R}^3$ is the vector of true angular velocities (in body frame); $\mathbf{G}_\omega \in \mathbb{R}^{3\times 3}$ is the gain matrix (diagonal if only scale factors are accounted for, or a generic invertible matrix if cross-couplings are also accounted for); $\mathbf{b}_\omega \in \mathbb{R}^3$ is the bias vector, in body frame and $\mathbf{n}_\omega \in \mathbb{R}^3$ is the noise vector (in body frame) and is assumed to be zero-mean Gaussian noise with covariance matrix $\boldsymbol{\Sigma}_\omega = \sigma_\omega^2 \mathbf{I}_3$. The sensor calibration task consists in estimating $\mathbf{G}_\omega$ and $\hat{\mathbf{b}}_\omega$, by observing $\boldsymbol{\omega}^m$; similarly as the accelerometer, the resulting bias estimate $\hat{\mathbf{b}}_\omega$ has to be considered as an estimate of the *deterministic* errors affecting the gyroscope output. Unluckily, gyroscope calibration is a difficult task since it requires expensive dedicated hardware platforms, capable of producing precisely known values of angular velocity.

4.2 Odometer

An odometer provides information on the traveled curvilinear distance of a vehicle by measuring the number of full and fractional rotations of vehicle wheels [20]; this result is achieved by means of an encoder generating an integer number of pulses for each revolution of the wheel. The number of pulses during a time slot is then mapped to an estimate of the traveled distance during the slot itself by multiplying such a number by a scale factor, depending on the wheel radius. It can be shown that, if the vehicle model illustrated in Paragraph 3.2.3 is adopted, an estimate of the velocity $v_c(k)$ in the g.c. of the vehicle itself can be evaluated as [2]

$$v_c^o(k) = v_{fl}(k) \frac{\cos\left(\Delta - \delta_{fl}(k)\right)}{\cos\left(\Delta - \phi_c(k) - s_c(k)\right)} \tag{44}$$

in the k-th observation interval, where $\delta_{fl}(k)$ and $v_{fl}(k)$ are the angle and the velocity of the left wheel, respectively. A more refined estimation method is proposed in [1], wher the speeds

$$v_1^o(k) = v_{fl}(k) \frac{\cos\left(\Delta - \delta_{fl}(k)\right)}{\cos\left(\Delta - \phi_c(k) - s_c(k)\right)} \tag{45}$$

of the front-left wheel and the speed

$$v_2^o(k) = v_{rr}(k)\frac{\cos\left(\Delta - \delta_{rr}(k)\right)}{\cos\left(\Delta - \phi_c(k) - s_c(k)\right)} \tag{46}$$

and of the rear right wheel are computed first; then, an estimate $v_c^o(k)$ of $v_c(k)$ is evaluated as the mean of $v_1^o(k)$ and $v_2^o(k)$. Finally, it is worth mentioning that:

- If the data coming from the front wheels are compared with those of the rear wheels, an estimate of the angular velocity of the vehicle can be computed; further details about this issue can be found in [1] and [2].
- The availability of odometers substantially simplifies the development of in-car navigation systems. In fact, when these sensors are available, the use of accelerometers is no more required and the estimation of a single Euler angle (namely, the yaw) is really needed to generate an estimate of the car trajectory [47].

4.3 GPS

In the GPS navigation system navigation messages are broadcasted by multiple satellites synchronized with the same reference time. Messages arrive at a specific GPS user at different times, due to the different receiver/satellite distances; however, even if the transmission epoch of a specific navigation messages and position of the satellite radiating it are known to the user's receiver, the receiver itself is unable to compute its distance from the satellite since its local reference time is different from the satellite one (i.e., from the GPS reference time). On the basis of the reception epochs on the user time scale and of the relative delays between navigation message originating from distinct satellites, the so called *pseudoranges* can be estimated. Let us assume that the considered GPS user receives the navigation messages from N distinct satellites. The pseudorange evaluated on the basis of the message coming from the i-th satellite can be expressed as [60]

$$\varrho_i = d_i + c\, b_u + \epsilon_{\rho_i} \tag{47}$$

with $i = 0, 1, ..., N-1$, where d_i

$$d_i = \sqrt{(x_u - x_i)^2 + (y_u - y_i)^2 + (z_u - z_i)^2} \tag{48}$$

denotes the geometric range between the GPS receiver (having coordinates (x_u, y_u, z_u)) and the satellite (having coordinates (x_i, y_i, z_i)), c is the speed of light, b_u denotes the so called *clock bias*[3] between the receiver and satellite and ϵ_{ρ_i} is the composite error. This error can be expressed as

$$\epsilon_{\rho_i} = \epsilon_{orb,i} + \epsilon_{trop,i} + \epsilon_{ion,i} + \epsilon_{mup,i} + \epsilon_{\rho,i} \tag{49}$$

[3]Note that this quantity is unknown and consequenty needs to be estimated jointly with the user position.

where $\epsilon_{orb,i}$, $\epsilon_{trop,i}$ and $\epsilon_{ion,i}$ are the orbital error, the error due to the troposphere delay and the error due to ionosphere delay, respectively, $\epsilon_{mup,i}$ is the pseudorange multipath effect and $\epsilon_{\rho,i}$ is the measurement noise in the pseudorange. If $N \geq 4$ the N pseudoranges $\{\varrho_i; i = 0, 1, ..., N-1\}$ can be processed to estimate (x_u, y_u, z_u) by means of a least square method (if a single-point solution is needed) or Kalman filter (to include known user dynamics and reducing the dependence of the solution accuracy on the instantaneous satellite geometry), which output the position $\hat{\mathbf{p}}_n$ and velocity $\hat{\mathbf{v}}_n$ estimates with respect to the navigation frame in the n-th observation interval. In a loosely coupled scheme (see Paragraph 5.1) the measurement equations

$$\hat{\mathbf{p}}_n = \mathbf{p}_n + \mathbf{n}_{p,n} \tag{50}$$

and

$$\hat{\mathbf{v}}_n = \mathbf{v}_n + \mathbf{n}_{v,n} \tag{51}$$

can be adopted [59], where the position error $\mathbf{n}_{p,n}$ and velocity error $\mathbf{n}_{v,n}$ can be assumed to be zero mean white Gaussian processes with covariance matrices $\mathbf{Q}_p$ and $\mathbf{Q}_v$, respectively.

5 Integration Architectures for INS/GPS

An INS can be integrated with GPS so that the short term stability of INS and the long term one of GPS can be exploited in a synergistic fashion. In doing so, distinct types of integration architectures (providing different levels of system integrity) can be considered. In the following *loosely coupled*, *tightly coupled* and *ultra-tightly/deeply coupled* architectures are briefly described and the advantages/disadvantages they offer are illustrated. A comparative analysis of a) the integrity provided by different architectures and b) the techniques for integrity monitoring can be found in [29], [30] and [31].

5.1 Loosely coupled systems

Loosely coupled systems are based on *position domain coupling*. In fact, they combine the *position* (P), *velocity* (V) and *time* (T) generated by a GPS receiver with the position, velocity and *attitude* (A) provided by a INS by means of a navigation processor (typically a Kalman filter) which generates a navigation solution; such a solution allows to improve the accuracy of the sensors and their calibration (see Fig. 4), since some feedback about gyro/accelometer bias and scale factor errors can be provided to the INS.

Disadvantages - The Kalman filter of a a loosely coupled system heavily depends upon the GPS solution. In fact, when the GPS solution is unavailable (e.g., when less than four satellites are available) generating an integrated solution is no longer possible. In such a case the performance of the integrated system is limited to its *coasting capability*, which depends primarily on the quality of the employed inertial sensors.

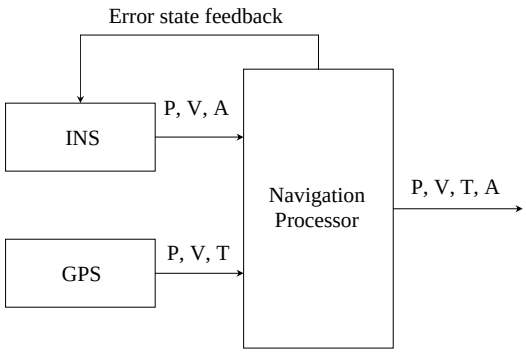

Figure 4: Loosely coupled architecture.

Advantages - A loosely coupled system provides benefits over individual systems in terms of navigation performance (namely, accuracy, integrity, continuity and availability). In fact, an integrated system is more accurate, achieves a high integrity provided by an additional navigation system, is capable of a higher rate than GPS because of the higher data rate of INS, makes the navigation service available even during GPS outage for a period limited by the quality of the INS.

However, to achieve real benefits in integrity monitoring, *measurement domain coupling* methods are needed.

5.2 Tightly coupled systems

In a tightly coupled system (e.g., see [63], [62] and [64]) position, *velocity* and *attitude variations* (denoted ΔV and ΔA, respectively) originating from the INS are combined with *raw* GPS measurements (more precisely, *pseudoranges*, PR, and *differential pseudoranges*, DPR) by means of a navigation filter (see Fig. 5); moreover, the GPS receiver clock drift and bias are included in the system state. The navigation filter processes GPS raw measurements and their corresponding values predicted on the basis of INS measurements.

Disadvantages - A tightly coupled system responds more slowly to INS errors than a loosely coupled system [23].

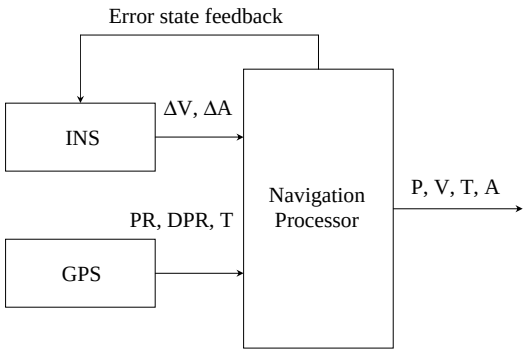

Figure 5: Tightly coupled architecture.

Advantages - A tightly coupled system outperforms a loosely coupled system in terms of integrity monitoring, because individual pseudoranges can be accessed. Even with fewer than four available satellites, a navigation solution can be still evaluated.

5.3 Ultra-tight coupling

In ultra-tight coupling (see Fig. 6), the measurements originating from the GPS receiver are the in-phase and quadrature-phase signals produced by the receiver itself and the tracking loop of the GPS receiver is aided by external information (for this reason this approach is also referred to as *deep* or *ultra-tight integration*). Different variants of ultra-tight coupling are available in the technical literature. The main difference between these couplings is represented by the the method employed for combining INS and GPS observables; for instance, the use of a minimum variance non-linear filter, an extended Kalman filter and cascaded Kalman filter stages has been proposed in [25], [26] and [27], respectively. Apart from various options for the navigation filter, various methods are available for aiding the GPS receiver tracking loop (the electronic/software loop used to lock onto satellite signals), including a) velocity information directly from the INS output, and b) an estimation of the line-of-sight vectors from the

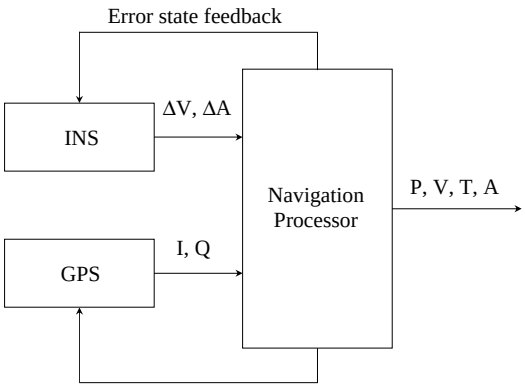

Figure 6: Ultra-tight coupled architecture.

host vehicle to the satellites using INS position and satellite ephemeris data.

Disadvantages - Generally speaking, deep integration is more dependent on the characteristics of INS errors than the other architectures. If the calibration of the INS parameters by GPS measurements is not accurate, the GPS tracking loop will not be able to get useful information from the INS. This increases the time it takes to lock on to the satellites and, in severe cases, can lead to instability. In noisy environments integrity monitoring becomes complicated because GPS observables are contaminated by inertial errors.

Advantages - Tightly coupled systems have been shown to perform better than loosely coupled systems as far as the availability of integrity information is concerned [28]. In fact, on the one hand, the latter systems require at least four GPS satellites to be available to provide a 3-dimensional position solution; on the other hand, tightly coupled systems can produce an integrated position determination with less than four satellites. Moreover, generally speaking, ultra-tight coupling outperforms tightly coupled systems in noisy environments and in terms of anti-jamming capability [25].

6 Integrating Map Knowledge in a Navigation System

6.1 Introduction

The task of map-matching algorithms is, in practice, the integration of positioning data with spatial road network data (roadway centrelines) in order to identify the link on which a vehicle is travelling and to determine its location on the selected link. A number of map-matching algorithms are available in the technical literature [39]. The performance of map matching has been improving over the years thanks to the application of advanced techniques for processing sensor data and to the improvements in the quality of both positioning and spatial road network data. However, these algorithms are not always able to support *intelligent transportation system* (ITS) applications with high required navigation performance, especially in difficult and complex environments such as dense urban areas.

Map-matching algorithms use inputs generated from positioning technologies (such as GPS or GPS integrated with *dead reckoning*, DR) and combine these with data from a high resolution map of a spatial road network to provide an enhanced positioning output. The general purpose of a map-matching algorithm is to identify the correct road segment on which the vehicle is travelling and to determine the vehicle location on that segment. Map-matching not only enables the physical location of the vehicle to be identified, but also improves the positioning accuracy if good spatial road network data are available. This means that the determination of a vehicle location on a particular road identified by a map-matching algorithm depends to a large extent on the quality of the spatial road map used with the algorithm; in fact, a poor quality road map could lead to a large error in map-matched solutions.

It is essential that the map-matching algorithm used in any navigation module meets the specified requirements set for that particular service. Although the performance of a map-matching algorithm depends on the characteristics of input data [40], the technique used in the algorithm can enhance overall performance; for instance, a map-matching algorithm based on fuzzy logic theory may outperfrom an algorithm based on the topological analysis of spatial road network data in the same scenario.

A number of algorithms are available in the techical literature and each has strengths and weaknesses. For instance, some algorithms may perform very well within suburban areas, but may not be appropriate for urban areas and viceversa. The technical literature suggests that the existing map-matching algorithms are not capable of satisfying the requirements of all ITS applications and services, since none of them can satisfy strict positioning requirements, especially within dense urban areas. Therefore, further improvements to map-matching algorithms are essential.

6.2 A Taxonomy of Map-Matching Techniques

Most of the algorithms available in the technical literature employ navigation data from GPS (or GPS integrated with DR sensors) and digital spatial road network data. One of the common assumptions in the literature on map-matching is that the vehicle is essentially constrained to a finite network of roads. While this assumption is valid for most vehicles under usual operating conditions, problems may be encountered for off-roadway situations (such as car parks) or on private land. Most of the studies also report that the digital spatial road network data used for map matching should be of a large scale in order to generate position outputs with fewer errors [37]. Procedures for map-matching vary from those using simple search techniques [44] to those using more advanced techniques, such as extended Kalman filtering, fuzzy logic and belief theory. Map-matching algorithms available in the technical literature can be divided into four groups: *geometric*, *topological*, *probabilistic*, and those based on other *advanced techniques*.

The methods used in the map-matching algorithms vary greatly from using simple search techniques to highly mathematical approaches. The performance and speed of an algorithms largely depends on the technique used in the algorithm itself.

Currently, map-matching algorithms generate outputs exactly on the centreline of a road segment. This may be desirable for many ITS applications. However, some ITS applications require more accurate positioning information. Therefore, the current methods introduce large errors in the location estimation, especially in the case of low resolution spatial road network data. A method should be developed so that the final positioning outputs from the map-matching algorithm can optimally be determined anywhere within the edges of a carriageway.

In the following Paragraphs the main features of different classes of map-matching algorithms are briefly described.

6.2.1 Map-matching based on a geometric analysis

A geometric map-matching algorithm makes use of the geometric information of the spatial road network data by considering only the shape of the links [42], so that the way links are connected to each other is ignored. The most commonly used geometric map-matching algorithm is a simple search algorithm, known as *point-to-point matching*. In this approach each of the position fixes are matched to the closest 'node' or 'shape point' of a road segment. A number of data structures and algorithms exist in the literature to select the closest node or shape point of a road segment from a given point. This approach is both easy to implement and very fast. However, it is very sensitive to the way in which the spatial road network data have been generated and, consequently, can suffer from various problems in practice. For instance, arcs including a larger number of shape points are more likely to be properly matched; for instance, in a straight arc with two end nodes only, all positioning points above the arc match only to

the end nodes of the arc itself.

6.2.2 Map-matching based on a topological analysis

Topology refers to the relationship between entities (points, lines, and polygons). The relationship can be defined as *adjacency* (in the case of polygons), *connectivity* (in the case of lines), or *containment* (in the case of points in polygons). Therefore, any map-matching algorithm making use of the geometry of the links as well as of the connectivity and contiguity of the links is a *topological map-matching algorithm* (e.g., see [34], [42] and [45]).

6.2.3 Probabilistic map-matching algorithms

A probabilistic algorithm requires the definition of an elliptical or rectangular *confidence region* around a position fix obtained from a navigation sensor. In [46] this approach is analysed in the case of GPS navigation and it is suggested that an error region can be identified by means of the error variances associated with the GPS position solution. The error region is then superimposed on the road network to identify a road segment on which the vehicle is travelling. If the error region contains a number of segments, then the evaluation of candidate segments is carried out using heading, connectivity, and closeness criteria. While such criteria are relevant from a theoretical viewpoint, ref. [46] does not provide details about their implementation. Note also that other parameters, like vehicle speed and its distance to downstream junctions, can be exploited to further improve the map-matching process.

6.2.4 Advanced map-matching algorithms

Advanced map-matching algorithms are based on more refined concepts, like Kalman filtering or extended Kalman filtering (e.g., see [49] and [47]), Dempster–Shafer's mathematical theory of evidence [50], flexible state-space modelling and particle filtering [24], interacting multiple models [41], fuzzy logic modelling (e.g., see [47] and [38]) or Bayesian inference [33].

One of the most relevant techniques in this class is represented by *particle filtering*, whose application to vehicle positioning with map matching has been first proposed by Gustafson et al. [24]. When particle filtering is employed, information provided by digital maps are exploited to constrain the possible vehicle positions. In the specific solution devised in [24] the only other inputs to the algorithm are wheel speed and the initial position of the vehicle provided by the driver or acquired from a different source (e.g., a terrestrial wireless communications system or GPS). In that manuscript it is stated that a wrong initial position of the vehicle can be improved to one metre accuracy by the use of particle filters and that this could be used to supplement or replace GPS. More recently, idea of combing particle filtering localization with a digital map has been also investigated in [53], where some experimental results are also shown. Similar principles have been exploited in [54], where, however, particle

filtering is applied to human positioning in an indoor scenario. Further results about this research area can be found in [57] and [58].

6.3 Constraints and limitations

Map-matching algorithms suffer from different problems; the most significant of them are briefly described below.

6.3.1 Initial matching

Most of the map-matching algorithms start with an initial matching procedure which aims at selecting the road segments falling within an error ellipse; this ellipse depends on the errors associated with the navigation device. The initial matching procedure first selects all nodes (i.e., road junctions) or shape points (i.e., road topology) that are within the error ellipse. The segments that originate from (or end in) these nodes or shape points are considered to be candidate segments. Although this process normally identifies the correct segment near a junction or a shape point, there may be some circumstances in which the initial matching process needs to start on a road segment which is further from the junctions or shape points.

6.3.2 Selection of threshold values

Different thresholds are used in various decision-making procedures contained in map-matching algorithms (e.g., the threshold for the minimum speed at which the heading of the vehicle computed from a stand-alone GPS module can be deemed incorrect). Threshold values are commonly derived from a series of field observations on the basis of empirical considerations. A more refined approach would be needed to improve the quality of the above mentioned decision-making processes.

6.3.3 Problems at Y-junctions

The techniques used in existing map-matching algorithms may fail to identify the correct road segment at or near a Y-junction.

6.3.4 Impact of road design parameters in map-matching

Road design parameters, such as turn restrictions at junctions, roadway classification (e.g. one-way, two-way), carriageway width, number of lanes and overpass/underpass information, are normally not included as inputs to existing map-matching algorithms. The availability of such data could potentially improve the performance of map-matching algorithms especially at junctions.

6.3.5 Height data from the navigation sensors

Map-matching algorithms normally do not make use of height data generated by navigation sensors. Height data together with data from a 3-D digital road network map can effectively identify the correct road segment at a section of roadway with fly-overs. However, this result largely depends on the accuracy of height data and the availability of high-quality 3-D road maps.

6.3.6 Spatial road network data quality

Unluckily, spatial road network data may suffer from both geometric and topological errors. It is envisaged that position fixes from a stand-alone GPS, specifically in an open-space environment, could be more accurate than the map-matched positions if a poor quality map is available to the map-matching algorithm. Therefore, the quality of the spatial road map data may significantly affect the performance of map-matching methods.

6.4 Possible Scenarios

Although GPS provides users with their locations in real-time, limitations on system performance and political considerations have suggested that stand-alone GPS cannot always meet all the requirements of a range of ITS services and other *safety-of-life* (SOL) applications. Moreover, the US *Department of Defence* (DoD), which operates GPS, does not guarantee the *Standard Positioning Service* (SPS). One solution to this problem is the development of an augmentation to GPS to improve accuracy, integrity, continuity, and availability. For this reason, Europe has developed a satellite-based regional augmentation system, known as the *European Geostationary Overlay Service* (EGNOS).

The following four scenarios should be considered when analysing the potential impact of EGNOS on the performance of map-matching algorithms [39]:

- *Scenario #1* (combining GPS, DR and map data) - This is the basic scenario on which most of map-matching research is based. In this scenario, a map matching algorithm takes inputs from an integrated GPS/DR and a road map. The quality of the position solution from the GPS/DR is affected by the duration of GPS outages. In such cases, the performance of a map-matching algorithm depends on the performance of DR sensors, especially in dense urban areas where the visibility of GPS satellites is often poor.

- *Scenario #2* (combining GPS, EGNOS, DR and map data) - In this scenario, a GPS receiver will be capable of receiving data transmitted by the different services provided by EGNOS. This will make easier to obtain good quality GPS data due to the availability of differential corrections and marginally better geometry due to the additional EGNOS signal (i.e, the GEO L1 signal) for some instances where the EGNOS GEO satellites

will be visible. This will lead to a marginally better positioning accuracy; consequently, the improvement in the performance of map-matching algorithms is expected to be marginal, especially in urban areas.

- *Scenario #3* (combining GPS, EGNOS(SISNet), DR and map data) - In this scenario, the problem of the unavailability of GEO satellites in urban areas (scenario #2) is addressed to some extent by an internet-based solution called *Signal-In-Space Network* (SISNeT), which provides public access to EGNOS data about wide-area differential correction and integrity data via internet. This makes EGNOS differential correction data continuously available wherever an internet connection is available. If SISNet is available, the visibility of a GEO satellite is not required; note, however, that, if the GEO L1 data are lost, there will be no improvement in satellite geometry; in this case, the improvement in the performance of the map-matching algorithm will be significant and only constrained by the data quality of the spatial road network.

- *Scenario #4* (combining GPS, EGNOS (conventional + SISNet), DR and map data) - This is the combination of scenarios #2 and #3. In this scenario, a GPS receiver will be able to receive both differential correction data via SISNet and the additional data (GEO L1) directly from EGNOS. This will lead to better positioning data at all times and a marginal improvement in geometry for some instances. In this case the performance improvement of map-matching algorithms will be limited by the quality of the spatial road network data provided to them.

It is important to assess the impact of each of the scenarios above not only on the geometric positioning capability, but also on the overall performance. As far as integrity is concerned, the EGNOS integrity service monitors GPS satellite signals to generate integrity information. Such information are broadcasted to users in terms of use/don't use and other parameters employed by users' receivers to accomplish failure detection. The main drawback of this approach is represented by the fact that it does not account for errors local to the user. The other relevant issue is that of the combined use of data from GPS and other sensors (like DR and digital spatial databases). A good approach to monitoring the integrity of map-matching algorithms should account for these issues.

7 A New Solution for Integrated INS/GPS Navigation

7.1 Constraints and requirements

In this Section a new solution to the problem of vehicle navigation is proposed. In developing it, the following constraints have been carefully taken into account:

- The need of making it implementable on commercial hardware platforms (the COMBO-T2: Enhanced TERRA board kit [67] combined with a

DAISY 7 GPS/MEMS module [66] is currently being tested in our labs). This need puts a relevant constraint on the overall computational complexity of the navigation algorithm.

- The fact that commericial GPS modules, such as the DAISY 7 GPS/MEMS module, do not make GPS raw data (i.e., pseudoranges) available. In practice, they generate estimates of heading, speed and position. For this reason, tightly coupled architectures (see Section 5) cannot be adopted in this case.
- Unluckily, the sensor data originating from in-car odometers are not available.
- The processed data are generated by a 3D accelerometer, a 3D gyroscope and a GPS receiver.

The devised solution is expected to achieve a reasonable tradeoff between the need of achieving good performance (in terms of positioning accuracy, integrity, availability, and continuity of service) on low cost hardware by means of advanced signal processing algorithms and that of keeping the overall computational complexity at an acceptable level.

7.2 Derivation of the navigation algorithm

7.2.1 Main features and related work

The proposed solution to vehicular navigation has been mainly inspired by: a) the cascaded estimation architecture proposed in [71] for indoor navigation, based on inertial sensors and combining extended Kalman filtering with particle filtering; b) the approach to vehicle modelling proposed in [7]; c) the experience acquired by the author of this document on the use of extended Kalman filtering for processing the signals generated by inertial sensors for position estimation [43].

Following [71], in the proposed solution an EKF (representing the first stage of the estimation architecture) process IMU data to generate an estimate of the joint probability density functions of: a) the position displacement occurring between two consecutive clock epochs; b) the attitude change, i.e. the variation in the yaw ψ, occuring in the same time interval. Then, these statistical information are combined with the heading and position information coming from a GPS receiver by means of particle filtering methods (implemented in the second stage of the estimation architecture) that allow to incorporate higly nonlinear constraints coming from a digital map. A block diagram describing the architecture of the navigation solution is shown in Fig. 7.

The navigation technique illustrated in this Section has the following relevant features:

1. It is based on rigorous kinematic equations relating the IMU-sensed quantities with the vehicle orientation, speed and acceleration in the 3-D space.

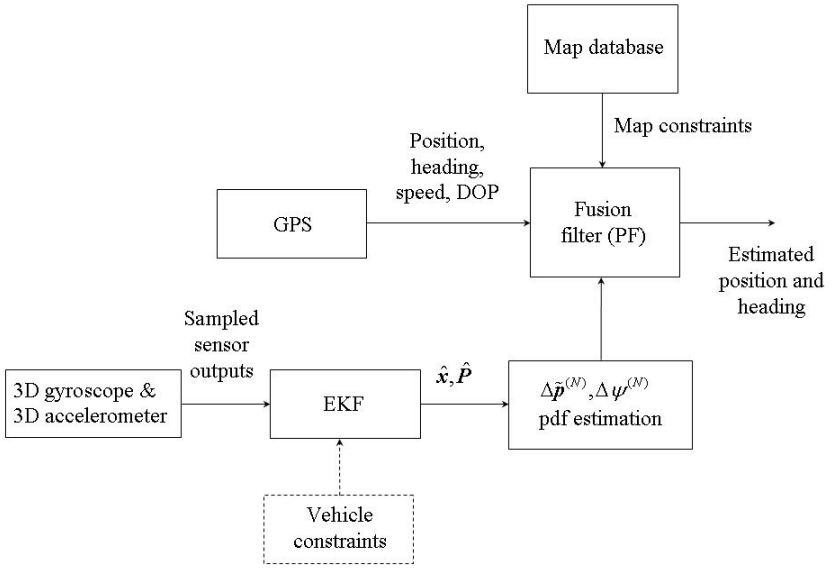

Figure 7: Proposed architecture for vehicular navigation.

2. It tracks vehicle orientation. Note that, in principle, the knowledge of 3D orientation is required because the distance travelled by the vehicle is obtained by double integration of the estimated acceleration[4] and the effect of earth gravity needs always to be removed before integration.

3. Extended Kalman filtering and particle filtering are combined in order to a) reduce the overall computational complexity (with respect to that required by a single fusion filter based on extended Kalman filtering or particle filtering); b) embed map information in the final position estimation in a natural fashion; c) substantially improve the quality of position estimates that, if based on GPS only, are less reliable at low speeds (e.g., at a speed lower than 3.0 m/s; see [75] and [76]) and are certainly unavailable in the absence of GPS coverage.

The remaining part of this Paragraph is organized as follows. The structure of the state vector proposed for the EKF is described in Subsection 7.2.2, whereas the dynamic and measurement models on which it is based are illustrated in Subsection 7.2.3. The EKF algorithm is summarised in Subsection 7.2.3, where the use of pseudo measurements is also described. Finally, the use of particle filtering for position and heading estimation is analysed in Subsection 7.2.5.

[4]If odometer data were available, the accelerometer would be no more needed to estimate the travelled distance [47].

7.2.2 Proposed structure for the state vector

Following [7], we focus on a wheeled vehicle moving on the earth surface. In our model the *body frame* is attached to the vehicle and is aligned with the axes of the IMU; in particular, the IMU is placed at the center of the rear axle of the vehicle and, as far as the body frame is concerned, the y axis is in the direction of the rear axle, the x axis is in the direction of the forward motion of the vehicle and the z axis points downward. Moreover, in our study the discrete-time vector

$$\mathbf{x}_k \triangleq \left[(\mathbf{v}_k)^T, (\mathbf{a}_k)^T, (\mathbf{\Psi}_k)^T, \left(\mathbf{a}_k^b\right)^T, \left(\boldsymbol{\omega}_k^{b,n\triangleright b}\right)^T, (\mathbf{b}_k^a)^T, (\mathbf{b}_k^\omega)^T \right]^T \in \mathbb{R}^{D_x} \quad (52)$$

is adopted to represent the *dynamic state* of the vehicle at time $t = kT_s$ for any integer k, where T_s denotes the *sampling period*. Here,

- The quantity $\mathbf{v}_k \triangleq [v_{x,k}, v_{y,k}, v_{z,k}]^T \in \mathbb{R}^3$ represents the vehicle speed at time $t = kT_s$, with respect to the navigation frame (its components are measured in m/s).
- The quantity $\mathbf{a}_k \triangleq [a_{x,k}, a_{y,k}, a_{z,k}]^T \in \mathbb{R}^3$ represents the vehicle acceleration at time $t = kT_s$, with respect to the navigation frame (its components are measured in m/s^2).
- The vector $\mathbf{\Psi}_k \triangleq [\phi_k, \theta_k, \psi_k]^T \in \mathbb{R}^3$ collects the three Euler angles and describes the orientation of the body frame with respect to the navigation frame.
- The quantity $\mathbf{a}_k^b \triangleq \left[a_{x,k}^b, a_{y,k}^b, a_{z,k}^b\right]^T \in \mathbb{R}^3$ represents the acceleration in body frame (expressed in m/s^2); a noisy and biased measurements of these vector is provided by the employed 3D accelerometer.
- The quantity $\boldsymbol{\omega}_k^{b,n\triangleright b} \triangleq \left[\omega_{x,k}^{b,n\triangleright b}, \omega_{y,k}^{b,n\triangleright b}, \omega_{z,k}^{b,n\triangleright b}\right]^T \in \mathbb{R}^3$ represents the angular velocity, from body to navigation frame, resolved in body coordinate frame (expressed in rad/s), at the time instant $t = kT_s$; note that a noisy and biased measurement of this vector is provided by the employed 3D gyroscope.
- The quantities $\mathbf{b}_k^a \in \mathbb{R}^3$ and $\mathbf{b}_k^\omega \in \mathbb{R}^3$ represent the *bias instability* of the accelerometer and the gyroscope sensors, respectively, expressed in body coordinate frame (they are expressed in m/s^2 and rad/s respectively).
- $D_x = 21$ is the dimension of the state vector.

It is important to point out that:

- The vectors $\mathbf{b}_k^a$ and $\mathbf{b}_k^\omega$ model *stochastic bias instability* and play a complementary role with respect to $\hat{\mathbf{b}}_a$ and $\hat{\mathbf{b}}_\omega$ (see Sec. 4.1), which account for *deterministic biases* and are compensated for at the beginning (after that the employed IMU achieves steady state conditions).

- The bias and the scale factor of inertial sensors are influenced by environmental conditions and, in particular, by temperature; however, the temperature coefficients of accelerometers are of relatively lower quantitative relevance. Moreover, it is well known that scale factor drifts of inertial sensors affect the accuracy of the measurement process to a much lesser extent than their bias drifts.

- Following [65], gyroscope bias instability $\mathbf{b}_k^{\omega}$ of the gyro might not be included in the state vector of an inertial system. This choice is motivated by the fact that temperature variations represent the most important factor determining the bias drift of gyroscopes. For this reason, the bias drift is significant especially after that power is applied to gyroscopes, as a result of device self-heating. If gyroscopes are allowed warm-up and achieve thermal stabilization for few minutes, then their biases are expected to change quite slowly with time. This issue would deserve further investigation in the considered scenario.

- A quaternion $q_k^{n \triangleright b} = (q_{0,k}, q_{1,k}, q_{2,k}, q_{3,k}) \in \mathbb{H}_1$ could be included in the state vector in place of the angle vector $\mathbf{\Psi}_k \triangleq [\phi_k, \theta_k, \psi_k]^T$ to represent the vehicle orientation, i.e. the transformation which produces, given a vector in navigation coordinates, a vector in body coordinates (or the opposite transformation); this would increase the dimensionality of the state vector by one. We will comment further on this point in order to clearly evidence the mathematical problems originating from the use of quaternions in this case.

- The state vector defined in (52) is different from that given in [71], which has been inspired by Foxlin [72] and that consists of 15 variables (namely, position errors, velocity errors, attitude errors, accelerometer biases and gyroscopic biases); it differs also from that adopted in [7], where sensor biases are not included in the dynamic state vector.

- As far as the *observability* of the elements of $\mathbf{x}_k$ (52) is concerned, only $\mathbf{a}_k^b$ and $\boldsymbol{\omega}_k^{b,n \triangleright b}$ are effectively observed through the IMU sensors, since all the other variables are non-observable; however, as discussed later in Subsection 7.2.4, some of the components of the state vector can be *pseudo-observed*, if some constraints originating from modelling vehicle motion are kept into account.

- The choice of including the IMU-sensed quantities $\mathbf{a}_k^b$ and $\boldsymbol{\omega}_k^{b,n \triangleright b}$ in $\mathbf{x}_k$ (52) may seem to be counter-intuitive; however, in the considered scenario this represents a fundamental choice because impulsive noise, due to hardware instability of low-cost sensors or vehicle vibrations, may substantially affect the IMU output.

- In principle, the EKF and the particle filter contained in the proposed architecture can operate at different rates. For instance, in [71] the EKF operates at a lower rate than particle filtering. This is due to the fact the

outputs of inertial sensors can be sampled and processed at a rate higher than that at which data fusion with GPS data is accomplished. In the following it is assumed that the rate of the EKF is N times larger than that of the particle filter (for instance, the EKF could operate at 500 Hz, whereas the PF at 100 Hz, so that $N = 5$).

Finally, it is important to note that at the instant $t = kT_s$ EKF-based processing should aim at producing *joint statistical information* about the following quantities: 1) the change in the vehicle position in the motion plane occurring in the interval $[(k-N)T_s, kT_s]$, that is the vector

$$\boldsymbol{\Delta}\tilde{\mathbf{p}}_k^{(N)} = \left[\Delta p_{x,k}^{(N)}, \Delta p_{y,k}^{(N)}\right]^T \triangleq \tilde{\mathbf{p}}_k - \tilde{\mathbf{p}}_{k-N}, \tag{53}$$

where $\tilde{\mathbf{p}}_k \triangleq [p_{x,k}, p_{y,k}]^T$; 2) the change in vehicle heading occurring in the same interval $[(k-N)T_s, kT_s]$, i.e. the phase variation

$$\Delta\psi_k^{(N)} \triangleq \psi_k - \psi_{k-N}. \tag{54}$$

In practice, the vector $\boldsymbol{\Delta}\tilde{\mathbf{p}}_k^{(N)}$ (53) and the phase change $\Delta\psi_k^{(N)}$ (54) are collected in the vector

$$\Delta\mathbf{r}_k \triangleq \left[\Delta p_{x,k}^{(N)}, \Delta p_{y,k}^{(N)}, \Delta\psi_k^{(N)}\right]^T, \tag{55}$$

which is modelled as a Gaussian vector $\mathcal{N}\left(\Delta\mathbf{r}; \overline{\Delta\mathbf{r}_k}, \mathbf{C}_{\Delta r,k}\right)$; the evaluation of the elements of the vector mean $\overline{\Delta\mathbf{r}_k}$ and its covariance matrix $\mathbf{C}_{\Delta r,k}$ can be accomplished as follows. The displacement $\boldsymbol{\Delta}\tilde{\mathbf{p}}_k^{(N)}$(53) can be expressed as

$$\boldsymbol{\Delta}\tilde{\mathbf{p}}_k^{(N)} = \sum_{l=k-N+1}^{k} \boldsymbol{\Delta}\tilde{\mathbf{p}}_l \tag{56}$$

where

$$\boldsymbol{\Delta}\tilde{\mathbf{p}}_l = [\Delta p_{x,l}, \Delta p_{y,l}]^T \triangleq \tilde{\mathbf{p}}_l - \tilde{\mathbf{p}}_{l-1} \tag{57}$$

denotes the change in the vehicle position in its motion plane occurring in the interval $[(l-1)T_s, lT_s]$. Consequently, the mean value $\overline{\boldsymbol{\Delta}\tilde{\mathbf{p}}_k^{(N)}}$ of $\boldsymbol{\Delta}\tilde{\mathbf{p}}_k^{(N)}$ (53) can be evaluated as

$$\overline{\boldsymbol{\Delta}\tilde{\mathbf{p}}_k^{(N)}} \triangleq E\left\{\boldsymbol{\Delta}\tilde{\mathbf{p}}_k^{(N)}\right\} = \sum_{l=k-N+1}^{k} \overline{\boldsymbol{\Delta}\tilde{\mathbf{p}}_l}, \tag{58}$$

where

$$\overline{\boldsymbol{\Delta}\mathbf{p}_l} \triangleq E\left\{\boldsymbol{\Delta}\tilde{\mathbf{p}}_l\right\}. \tag{59}$$

Similarly, the covariance matrix $\mathbf{C}_{\Delta\tilde{p}^{(N)},k}$ of $\boldsymbol{\Delta}\tilde{\mathbf{p}}_k^{(N)}$(53) can be computed as

$$\begin{aligned}\mathbf{C}_{\Delta\tilde{p}^{(N)},k} &\triangleq E\left\{\left[\boldsymbol{\Delta}\tilde{\mathbf{p}}_k^{(N)} - E\left\{\boldsymbol{\Delta}\tilde{\mathbf{p}}_k^{(N)}\right\}\right]\left[\boldsymbol{\Delta}\tilde{\mathbf{p}}_k^{(N)} - E\left\{\boldsymbol{\Delta}\tilde{\mathbf{p}}_k^{(N)}\right\}\right]^T\right\} \\ &= \textstyle\sum_{l=k-N+1}^{k} \mathbf{C}_{\Delta\tilde{p},l}\end{aligned} \tag{60}$$

if the quantities $\{\boldsymbol{\Delta}\tilde{\mathbf{p}}_l\}$ are assumed independent; here, we have that

$$\mathbf{C}_{\Delta\tilde{p},l} \triangleq E\left\{\left[\boldsymbol{\Delta}\tilde{\mathbf{p}}_l - E\left\{\boldsymbol{\Delta}\tilde{\mathbf{p}}_l\right\}\right]\left[\boldsymbol{\Delta}\tilde{\mathbf{p}}_l - E\left\{\boldsymbol{\Delta}\tilde{\mathbf{p}}_l\right\}\right]^T\right\}. \tag{61}$$

As far as the evaluation of $\boldsymbol{\Delta}\tilde{\mathbf{p}}_l$ (57) is concerned, the standard *linear* model (based on a first order Taylor expansion of a standard equation for the motion of a rigid body)

$$\boldsymbol{\Delta}\tilde{\mathbf{p}}_l = \tilde{\mathbf{v}}_l \cdot T_s + \frac{1}{2}\tilde{\mathbf{a}}_l \cdot T_s^2 + \mathbf{n}_{p,l} \tag{62}$$

can be adopted, where $\mathbf{n}_{\tilde{p},k}$ is an AGN vector describing model inaccuracies and characterized by the covariance matrix $\mathbf{C}_{\tilde{p}} = \sigma_p^2\mathbf{I}_2$, whereas $\tilde{\mathbf{v}}_l \triangleq [v_{x,l}, v_{y,kl}]^T$ and $\tilde{\mathbf{a}}_l \triangleq [a_{x,l}, a_{y,l}]^T$ denote the velocity and acceleration vectors, respectively, in the motion plane. Consequently, the expectation $\overline{\boldsymbol{\Delta}\mathbf{p}_l}$ (59) can be evaluated as

$$\overline{\boldsymbol{\Delta}\mathbf{p}_l} = \overline{\tilde{\mathbf{v}}_l} \cdot T_s + \frac{1}{2}\overline{\tilde{\mathbf{a}}_l} \cdot T_s^2 \tag{63}$$

where the quantities

$$\overline{\tilde{\mathbf{v}}_l} \triangleq E\left\{\tilde{\mathbf{v}}_l\right\} \tag{64}$$

and

$$\overline{\tilde{\mathbf{a}}_l} \triangleq E\left\{\tilde{\mathbf{a}}_l\right\} \tag{65}$$

are estimated by the EKF. Similarly, the covariance matrix $\mathbf{C}_{\Delta\tilde{p},l}$ (61) can be evaluated as

$$\mathbf{C}_{\Delta\tilde{p},l} = T_s^2 \cdot \mathbf{C}_{\tilde{v},l} + \frac{1}{4}T_s^4 \cdot \mathbf{C}_{\tilde{a},l} + T_s^3 \cdot \mathbf{C}_{\tilde{v}\tilde{a},l} + \mathbf{C}_{\tilde{p}}, \tag{66}$$

where

$$\mathbf{C}_{\tilde{v},l} \triangleq E\left\{\left[\tilde{\mathbf{v}}_l - E\left\{\tilde{\mathbf{v}}_l\right\}\right]\left[\tilde{\mathbf{v}}_l - E\left\{\tilde{\mathbf{v}}_l\right\}\right]^T\right\}, \tag{67}$$

$$\mathbf{C}_{\tilde{a},l} \triangleq E\left\{\left[\tilde{\mathbf{a}}_l - E\left\{\tilde{\mathbf{a}}_l\right\}\right]\left[\tilde{\mathbf{a}}_l - E\left\{\tilde{\mathbf{a}}_l\right\}\right]^T\right\} \tag{68}$$

and

$$\mathbf{C}_{\tilde{v}\tilde{a},l} \triangleq E\left\{\left[\tilde{\mathbf{v}}_l - E\left\{\tilde{\mathbf{v}}_l\right\}\right]\left[\tilde{\mathbf{a}}_l - E\left\{\tilde{\mathbf{a}}_l\right\}\right]^T\right\} \tag{69}$$

are estimated by the EKF (since, as shown above, vehicle velocity and acceleration are included in its state vector).

A conceptually related approach can be adopted for the evaluation of the mean and covariance of the phase variation $\Delta\psi_k^{(N)}$(54), since this quantity can be expressed as

$$\Delta\psi_k^{(N)} = \sum_{l=k-N+1}^{k} \Delta\psi_l, \tag{70}$$

where

$$\Delta\psi_l \triangleq \psi_l - \psi_{l-1} \tag{71}$$

and the phase increments $\{\Delta\psi_l\}$ can be modelled as *independent* random variables. Consequently, the expectation $\overline{\Delta\psi_k^{(N)}}$ of $\Delta\psi_k^{(N)}$(53) can be evaluated as

$$\overline{\Delta\psi_k^{(N)}} \triangleq E\left\{\Delta\psi_k^{(N)}\right\} = \sum_{l=k-N+1}^{k} \overline{\Delta\psi_l}, \tag{72}$$

where

$$\overline{\Delta\psi_l} \triangleq E\left\{\psi_l\right\} - E\left\{\psi_{l-1}\right\} \tag{73}$$

and $E\left\{\psi_l\right\}$ and $E\left\{\psi_{l-1}\right\}$ are estimated by the EKF (since the Euler angles are included in its state). Similarly, the variance $\sigma^2_{\Delta\psi^{(N)},k}$ of $\Delta\psi_k^{(N)}$(53) can be computed as

$$\begin{aligned}\sigma^2_{\Delta\psi^{(N)},k} &\triangleq E\left\{\left[\Delta\psi_k^{(N)} - \overline{\Delta\psi_k^{(N)}}\right]^2\right\} \\ &= \textstyle\sum_{l=k-N+1}^{k} \sigma^2_{\Delta\psi,l},\end{aligned} \tag{74}$$

where

$$\sigma^2_{\Delta\psi,l} \triangleq E\left\{\left[\Delta\psi_l - \overline{\Delta\psi_l}\right]^2\right\}. \tag{75}$$

Unluckily, the quantity $\sigma^2_{\Delta\psi,l}$ (75) is not estimated by the EKF, since the phase variation $\Delta\psi_l$ is not included in the state vector $\mathbf{x}_l$ (52). This quantity can be evaluated as follows. The phase variation $\Delta\psi_l$ can be approximated as (see (14))

$$\Delta\psi_l = \left[X_l + Y_l\right] T_s, \tag{76}$$

where

$$X_l = \omega_{y,l}^{b,n\triangleright b} \frac{\sin\phi_l}{\cos\theta_l} \tag{77}$$

and

$$Y_l = \omega_{z,l}^{b,n\triangleright b} \frac{\cos\phi_l}{\cos\theta_l}. \tag{78}$$

Consequently, if the random vectors $\boldsymbol{\omega}_k^{b,n\triangleright b}$ and $\boldsymbol{\Psi}_k$ are assumed *independent* and Gaussian (in particular, $\omega_{y,l}^{b,n\triangleright b} \epsilon \mathcal{N}\left(\omega_y^b; \bar{\omega}_{y,l}^b, \sigma^2_{\omega_y^b,l}\right)$, $\omega_{z,l}^{b,n\triangleright b} \epsilon \mathcal{N}\left(\omega_z^b; \bar{\omega}_{z,l}^b, \sigma^2_{\omega_z^b,l}\right)$, $\phi_l \epsilon \mathcal{N}\left(\phi; \bar{\phi}_l, \sigma^2_{\phi,l}\right)$, $\theta_l \epsilon \mathcal{N}\left(\theta; \bar{\theta}_l, \sigma^2_{\theta,l}\right)$ and $\psi_l \epsilon \mathcal{N}\left(\theta; \bar{\psi}_l, \sigma^2_{\psi,l}\right)$), the variance $\sigma^2_{\Delta\psi,l}$ can be expressed as

$$\sigma^2_{\Delta\psi,l} = \left[\sigma^2_{X,l} + \sigma^2_{Y,l} + 2\mathrm{cov}\left\{X_l, Y_l\right\}\right] T_s^2, \tag{79}$$

where $\sigma^2_{X,l}$, $\sigma^2_{Y,l}$ and $\mathrm{cov}\left\{X_l, Y_l\right\}$ denote the variance of X_l, the variance of Y_l, and the covariance of X_l and Y_l, respectively. It is not difficult to show that, if $\sigma^2_{\phi,l}$ is small, the following approximations hold:

$$\bar{\phi}_{s,l} \triangleq E\left\{\sin\phi_l\right\} \cong \sin\bar{\phi}_l \left[1 - \frac{1}{2}\sigma^2_{\phi,l}\right], \tag{80}$$

$$\bar{\phi}_{c,l} \triangleq E\left\{\cos\phi_l\right\} \cong \cos\bar{\phi}_l \left[1 - \frac{1}{2}\sigma^2_{\phi,l}\right], \tag{81}$$

$$\bar{\phi}_{t,l} \triangleq E\left\{\tan\phi_l\right\} \cong \tan\bar{\phi}_l\left[1+\frac{1}{\cos^2\bar{\theta}_l}\sigma^2_{\phi,l}\right], \tag{82}$$

$$\bar{\phi}_{s^2,l} \triangleq E\left\{\sin^2\phi_l\right\} \cong \sin^2\bar{\phi}_l + \left(\cos^2\bar{\phi}_l - \sin^2\bar{\phi}_l\right)\sigma^2_{\phi,l}, \tag{83}$$

$$\bar{\phi}_{c^2,l} \triangleq E\left\{\cos^2\phi_l\right\} \cong \cos^2\bar{\phi}_l + \left(\sin^2\bar{\phi}_l - \cos^2\bar{\phi}_l\right)\sigma^2_{\phi,l}, \tag{84}$$

$$\bar{\phi}_{sc,l} \triangleq E\left\{\sin\phi_l\cos\phi_l\right\} = \frac{1}{2}E\left\{\sin 2\phi_l\right\} \cong \frac{1}{2}\sin 2\bar{\phi}_l\left[1-2\sigma^2_{\phi,l}\right], \tag{85}$$

$$\bar{\phi}_{c^{-1},l} \triangleq E\left\{\frac{1}{\cos\phi_l}\right\} \cong \frac{1}{\cos\bar{\phi}_l}\left[1+\left(\frac{1}{2}+\tan^2\bar{\phi}_l\right)\sigma^2_{\phi,l}\right] \tag{86}$$

and

$$\bar{\phi}_{c^{-2},l} \triangleq E\left\{\frac{1}{\cos^2\phi_l}\right\} \cong \frac{1}{\cos^2\bar{\phi}_l}\left[1+\left(1+3\tan^2\bar{\phi}_l\right)\sigma^2_{\phi,l}\right]. \tag{87}$$

Similar approximations hold for the trigonometric functions of θ_l and ψ_l if $\sigma^2_{\theta,l}$ and $\sigma^2_{\psi,l}$ are small, respectively. These approximations can be employed to simplify the evaluation of $\sigma^2_{X,l}$, $\sigma^2_{Y,l}$ and $\mathrm{cov}\left\{X_l, Y_l\right\}$, since

$$\sigma^2_{X,l} = E\left\{X_l^2\right\} - \left(E\left\{X_l\right\}\right)^2 = \left[\left(\bar{\omega}^b_{y,l}{}^2 + \sigma^2_{\omega^b_y,l}\right)\bar{\phi}_{s^2,l}\bar{\theta}_{c^{-2},l} - \left(\bar{\omega}^b_{y,l}\bar{\phi}_{s,l}\bar{\theta}_{c^{-1},l}\right)^2\right], \tag{88}$$

$$\sigma^2_{Y,l} = E\left\{Y_l^2\right\} - \left(E\left\{Y_l\right\}\right)^2 = \left[\left(\bar{\omega}^b_{z,l}{}^2 + \sigma^2_{\omega^b_z,l}\right)\bar{\phi}_{c^2,l}\bar{\theta}_{c^{-2},l} - \left(\bar{\omega}^b_{z,l}\bar{\phi}_{c,l}\bar{\theta}_{c^{-1},l}\right)^2\right] \tag{89}$$

and

$$\begin{aligned}\mathrm{cov}\left\{X_l, Y_l\right\} &= E\left\{X_l Y_l\right\} - E\left\{X_l\right\}E\left\{Y_l\right\} \\ &= \bar{\omega}^b_{y,l}\bar{\omega}^b_{z,l}\left[\bar{\phi}_{sc,l}\bar{\theta}_{c^{-2},l} - \bar{\phi}_{s,l}\bar{\phi}_{c,l}\left(\bar{\theta}_{c^{-1},l}\right)^2\right].\end{aligned} \tag{90}$$

Finally, the covariance between $\Delta p^{(N)}_{x,k}$ (or $\Delta p^{(N)}_{y,k}$)) and $\Delta\psi^{(N)}_k$ can be evaluated as follows. Since

$$\begin{aligned}\mathrm{cov}\left\{\Delta p^{(N)}_{x,k}, \Delta\psi^{(N)}_k\right\} &= E\left\{\Delta p^{(N)}_{x,k}\Delta\psi^{(N)}_k\right\} - E\left\{\Delta p^{(N)}_{x,k}\right\}E\left\{\Delta\psi^{(N)}_k\right\} \\ &= E\left\{\Delta p^{(N)}_{x,k}\Delta\psi^{(N)}_k\right\} - \overline{\Delta p^{(N)}_{x,k}}\;\overline{\Delta\psi^{(N)}_k},\end{aligned} \tag{91}$$

the correlation $E\left\{\Delta p^{(N)}_{x,k}\Delta\psi^{(N)}_k\right\}$ only has to be evaluated. This quantity can be expressed as

$$E\left\{\Delta p^{(N)}_{x,k}\Delta\psi^{(N)}_k\right\} = \sum_{l=k-N+1}^{k} E\left\{\Delta p_{x,l}\Delta\psi_l\right\}, \tag{92}$$

where (see (62) and (76))

$$\begin{aligned}E\left\{\Delta p_{x,l}\Delta\psi_l\right\} &= T_s^2 E\left\{\left[v_{x,l} + \tfrac{1}{2}a_{x,l}\cdot T_s + n_{px,l}\right]\left[X_l + Y_l\right]\right\} \\ &= T_s^2 E\left\{\left[v_{x,l} + \tfrac{1}{2}a_{x,l}\cdot T_s\right]\left[\omega^{b,n\triangleright b}_{y,l}\frac{\sin\phi_l}{\cos\theta_l} + \omega^{b,n\triangleright b}_{z,l}\frac{\cos\phi_l}{\cos\theta_l}\right]\right\}.\end{aligned} \tag{93}$$

As (see (105) and (106) below)

$$\begin{aligned} a_{x,l} = &\left(\cos\theta_l \cos\psi_l\right) a^b_{x,l} + \left(\sin\phi_l \sin\theta_l \cos\psi_l - \cos\phi_l \sin\psi_l\right) a^b_{y,l} \\ &+ \left(\cos\phi_l \sin\theta_l \cos\psi_l + \sin\phi_l \sin\psi_l\right) a^b_{z,l} \end{aligned} \tag{94}$$

and the vectors $\mathbf{v}_l$, $\mathbf{a}^b_l$, $\boldsymbol{\omega}^{b,n\triangleright b}_k$ and $\boldsymbol{\Psi}_k$ can be deemed *independent*, the expectation (93) can be evaluated as

$$\begin{aligned} &E\left\{\Delta p_{x,l} \Delta\psi_l\right\} \\ &= T_s^2 \left[E\left\{v_{x,l}\omega^{b,n\triangleright b}_{y,l} \tfrac{\sin\phi_l}{\cos\theta_l}\right\} + E\left\{v_{x,l}\omega^{b,n\triangleright b}_{z,l} \tfrac{\cos\phi_l}{\cos\theta_l}\right\}\right. \\ &\left. + \tfrac{1}{2}T_s E\left\{a_{x,l}\omega^{b,n\triangleright b}_{y,l} \tfrac{\sin\phi_l}{\cos\theta_l}\right\} + \tfrac{1}{2}T_s E\left\{a_{x,l}\omega^{b,n\triangleright b}_{z,l} \tfrac{\cos\phi_l}{\cos\theta_l}\right\}\right] \\ &= T_s^2 \bar{v}_{x,l}\bar{\theta}_{c^{-1},l}\left[\bar{\omega}^b_{y,l}\bar{\phi}_{s,l} + \bar{\omega}^b_{z,l}\bar{\phi}_{c,l}\right] \\ &+ \tfrac{1}{2}T_s^3 \bar{\omega}^b_{y,l}\left[\bar{\phi}_{s,l}\bar{\psi}_{c,l}\bar{a}^b_{x,l} + \left(\bar{\phi}_{s^2,l}\bar{\theta}_{t,l}\bar{\psi}_{c,l} - \bar{\phi}_{sc,l}\bar{\theta}_{c^{-1},l}\bar{\psi}_{s,l}\right)\bar{a}^b_{y,l}\right. \\ &\left. + \left(\bar{\phi}_{sc,l}\bar{\theta}_{t,l}\bar{\psi}_{c,l} + \bar{\phi}_{s^2,l}\bar{\theta}_{c^{-1},l}\bar{\psi}_{s,l}\right)\bar{a}^b_{z,l}\right] \\ &+ \tfrac{1}{2}T_s^3 \bar{\omega}^b_{z,l}\left[\bar{\phi}_{c,l}\bar{\psi}_{c,l}\bar{a}^b_{x,l} + \left(\bar{\phi}_{sc,l}\bar{\theta}_{t,l}\bar{\psi}_{c,l} - \bar{\phi}_{c^2,l}\bar{\theta}_{c^{-1},l}\bar{\psi}_{s,l}\right)\bar{a}^b_{y,l}\right. \\ &\left. + \left(\bar{\phi}_{c^2,l}\bar{\theta}_{t,l}\psi_{c,l} + \bar{\phi}_{sc,l}\bar{\theta}_{c^{-1},l}\bar{\psi}_{s,l}\right)\bar{a}^b_{z,l}\right]. \end{aligned} \tag{95}$$

Similarly, since (see (105) and (106) below)

$$\begin{aligned} a_{y,l} = &\left(\cos\theta_l \sin\psi_l\right) a^b_0 + \left(\sin\phi_l \sin\theta_l \sin\psi_l + \cos\phi_l \cos\psi_l\right) a^b_1 \\ &+ \left(\cos\phi_l \sin\theta_l \sin\psi_l - \sin\phi_l \cos\psi_l\right) a^b_2, \end{aligned} \tag{96}$$

we have that

$$\begin{aligned} &E\left\{\Delta p_{y,l} \Delta\psi_l\right\} \\ &= T_s^2 \left[E\left\{v_{y,l}\omega^{b,n\triangleright b}_{y,l} \tfrac{\sin\phi_l}{\cos\theta_l}\right\} + E\left\{v_{xy,l}\omega^{b,n\triangleright b}_{z,l} \tfrac{\cos\phi_l}{\cos\theta_l}\right\}\right. \\ &\left. + \tfrac{1}{2}T_s E\left\{a_{y,l}\omega^{b,n\triangleright b}_{y,l} \tfrac{\sin\phi_l}{\cos\theta_l}\right\} + \tfrac{1}{2}T_s E\left\{a_{y,l}\omega^{b,n\triangleright b}_{z,l} \tfrac{\cos\phi_l}{\cos\theta_l}\right\}\right] \\ &= T_s^2 \bar{v}_{y,l}\bar{\theta}_{c^{-1},l}\left[\bar{\omega}^b_{y,l}\bar{\phi}_{s,l} + \bar{\omega}^b_{z,l}\bar{\phi}_{c,l}\right] \\ &+ \tfrac{1}{2}T_s^3 \bar{\omega}^b_{y,l}\left[\bar{\phi}_{s,l}\bar{\psi}_{s,l}\bar{a}^b_{x,l} + \left(\bar{\phi}_{s^2,l}\bar{\theta}_{t,l}\bar{\psi}_{s,l} + \bar{\phi}_{sc,l}\bar{\theta}_{c^{-1},l}\bar{\psi}_{c,l}\right)\bar{a}^b_{y,l}\right. \\ &\left. + \left(\bar{\phi}_{sc,l}\bar{\theta}_{t,l}\bar{\psi}_{s,l} - \bar{\phi}_{s^2,l}\bar{\theta}_{c^{-1},l}\bar{\psi}_{c,l}\right)\bar{a}^b_{z,l}\right] \\ &+ \tfrac{1}{2}T_s^3 \bar{\omega}^b_{z,l}\left[\bar{\phi}_{c,l}\bar{\psi}_{s,l}\bar{a}^b_{x,l} + \left(\bar{\phi}_{sc,l}\bar{\theta}_{t,l}\bar{\psi}_{s,l} + \bar{\phi}_{c^2,l}\bar{\theta}_{c^{-1},l}\bar{\psi}_{c,l}\right)\bar{a}^b_{y,l}\right. \\ &\left. + \left(\bar{\phi}_{c^2,l}\bar{\theta}_{t,l}\psi_{s,l} - \bar{\phi}_{sc,l}\bar{\theta}_{c^{-1},l}\bar{\psi}_{c,l}\right)\bar{a}^b_{z,l}\right]. \end{aligned} \tag{97}$$

7.2.3 Dynamic and measurement models

To develop an algorithm for the sequential estimation of the state $\mathbf{x}_k$ (52), the dynamic models for every element of $\mathbf{x}_k$ (52) and the models of the measurements available for state estimation need to be clearly defined. The *dynamic models* adopted in our work can be summarised as follows:

1. The standard *linear* model

$$\mathbf{v}_{k+1} = \mathbf{v}_k + \mathbf{a}_k \cdot T_s + \mathbf{n}_{v,k} \tag{98}$$

based on a first order Taylor expansion of a standard equation for the motion of a rigid body is used for velocity; here $\mathbf{n}_{v,k}$ represents an *additive Gaussian noise* (AGN) vector characterized by the covariance matrices $\mathbf{C}_v = \sigma_v^2 \mathbf{I}_3$ and representing modelling errors (note that $\sigma_v^2 = \sigma_p^2 / T_s^2$, where σ_p^2 has been introduced right after eq. (62)). We will show how $\mathbf{a}_k$ can be related to the other state variables later.

2. A standard discrete-time model for rigid body angular motion is adopted for the vector $\mathbf{\Psi}_k \triangleq [\phi_k, \theta_k, \psi_k]^T$ (e.g., see [7, Sec. II, eqs. (5)-(7)]). This means that the *nonlinear* model

$$\mathbf{\Psi}_{k+1} = \mathbf{\Psi}_k + T_s \mathbf{A}_{s\omega}(\mathbf{\Psi}_k) \boldsymbol{\omega}_k^{b,n \triangleright b} + \mathbf{n}_{\Psi,k} \tag{99}$$

is used, where

$$\mathbf{A}_{\mathbf{s}\omega}(\mathbf{\Psi}) \triangleq \begin{bmatrix} 1 & \sin\phi \tan\theta & \cos\phi \tan\theta \\ 0 & \cos\phi & -\sin\phi \\ 0 & \frac{\sin\phi}{\cos\theta} & \frac{\cos\phi}{\cos\theta} \end{bmatrix} \tag{100}$$

and $\mathbf{n}_{\Psi,k}$ is an AGN term, characterized by the covariance matrix $\mathbf{C}_\Psi = \sigma_\Psi^2 \mathbf{I}_4$, accounting for model inaccuracies.

3. The random walk models

$$\mathbf{a}_{k+1}^b = \mathbf{a}_k^b + \mathbf{n}_{a^b,k} \tag{101}$$

and

$$\boldsymbol{\omega}_{k+1}^{b,n \triangleright b} = \boldsymbol{\omega}_k^{b,n \triangleright b} + \mathbf{n}_{\omega^b,k} \tag{102}$$

are adopted for $\mathbf{a}_{k+1}^b$ and $\boldsymbol{\omega}_k^{b,n \triangleright b}$, respectively. Here $\mathbf{n}_{a^b,k}$ and $\mathbf{n}_{\omega^b,k}$ represent AGN vectors (assumed to be mutually independent), characterized by the covariance matrices $\mathbf{C}_{a^b} = \sigma_{a^b}^2 \mathbf{I}_3$ and $\mathbf{C}_{\omega^b} = \sigma_{\omega^b}^2 \mathbf{I}_3$, respectively.

4. The autoregressive models of order 1 [70]

$$\mathbf{b}_{k+1}^a = \mathrm{diag}\{\boldsymbol{\beta}^a\} \mathbf{b}_k^a + \mathbf{n}_{b^a,k} \tag{103}$$

and

$$\mathbf{b}_{k+1}^\omega = \mathrm{diag}\{\boldsymbol{\beta}^\omega\} \mathbf{b}_k^\omega + \mathbf{n}_{b^\omega,k} \tag{104}$$

can be used for the bias instability of accelerometer and gyroscope sensors, respectively (autoregressive modelling of order 1 is considered a good approximation for $1/f$ noise, from which bias instability originates). Here $\boldsymbol{\beta}^a$ and $\boldsymbol{\beta}^\omega$ are the three-dimansional vectors of AR(1) coefficients. Since the bias instability has a very long correlation time (roughly, greater than 1000 sec [69]), such coefficients have to be chosen very close to 1, to avoid that the tracked values of bias instability decrease very quickly with k (in practice, following [43], $\boldsymbol{\beta}^a \triangleq \boldsymbol{\beta}^\omega \triangleq [0.9999, 0.9999, 0.9999]^T$ could be selected).

5. Given the model (101) for $\mathbf{a}_{k+1}^b$, the vehicle acceleration $\mathbf{a}_{k+1}$ (measured in m/s^2) can be evaluated as

$$\mathbf{a}_{k+1} = \mathbf{C}_b^n\left(\boldsymbol{\Psi}_{k+1}\right)\mathbf{a}_{k+1}^b + \mathbf{g}, \tag{105}$$

where (see (4))

$$\mathbf{C}_b^n \triangleq \begin{bmatrix} \cos\theta\cos\psi & \sin\phi\sin\theta\cos\psi - \cos\phi\sin\psi & \cos\phi\sin\theta\cos\psi + \sin\phi\sin\psi \\ \cos\theta\sin\psi & \sin\phi\sin\theta\sin\psi + \cos\phi\cos\psi & \cos\phi\sin\theta\sin\psi - \sin\phi\cos\psi \\ -\sin\theta & \sin\phi\cos\theta & \cos\phi\cos\theta \end{bmatrix}. \tag{106}$$

Then, substituting (101) in (105) yields

$$\mathbf{a}_{k+1} = \mathbf{C}_b^n\left(\boldsymbol{\Psi}_{k+1}\right)\mathbf{a}_k^b + \mathbf{g} + \mathbf{C}_b^n\left(\boldsymbol{\Psi}_{k+1}\right)\mathbf{n}_{a^b,k}. \tag{107}$$

If we define

$$\boldsymbol{\Delta}\mathbf{C}_b^n\left(\boldsymbol{\Psi}_k, \boldsymbol{\Delta}\boldsymbol{\Psi}_{k+1}\right) \triangleq \mathbf{C}_b^n\left(\boldsymbol{\Psi}_{k+1}\right) - \mathbf{C}_b^n\left(\boldsymbol{\Psi}_k\right), \tag{108}$$

where

$$\Delta\boldsymbol{\Psi}_{k+1} \triangleq \left[\Delta\phi_{k+1}, \Delta\theta_{k+1}, \Delta\psi_{k+1}\right]^T = \boldsymbol{\Psi}_{k+1} - \boldsymbol{\Psi}_k \tag{109}$$

(107) can be rewritten as

$$\mathbf{a}_{k+1} = \mathbf{C}_b^n\left(\boldsymbol{\Psi}_k\right)\mathbf{a}_k^b + \mathbf{g} + \boldsymbol{\Delta}\mathbf{C}_b^n\left(\boldsymbol{\Psi}_k, \boldsymbol{\Delta}\boldsymbol{\Psi}_{k+1}\right)\mathbf{a}_k^b + \mathbf{C}_b^n\left(\boldsymbol{\Psi}_{k+1}\right)\mathbf{n}_{a^b,k} \tag{110}$$

or, in more compact form, as

$$\mathbf{a}_{k+1} = \mathbf{C}_b^n\left(\boldsymbol{\Psi}_k\right)\mathbf{a}_k^b + \mathbf{g} + \mathbf{n}_{a,k}, \tag{111}$$

where

$$\mathbf{n}_{a,k} \triangleq \boldsymbol{\Delta}\mathbf{C}_b^n\left(\boldsymbol{\Psi}_k, \boldsymbol{\Delta}\boldsymbol{\Psi}_{k+1}\right)\mathbf{a}_k^b + \mathbf{C}_b^n\left(\boldsymbol{\Psi}_{k+1}\right)\mathbf{n}_{a^b,k} \tag{112}$$

can be interpreted as an additive noise term; note that is term is correlated with the noise affecting the accelerometer output, the measured acceleration $\mathbf{a}_k^b$ and the phase variation vector $\boldsymbol{\Delta}\boldsymbol{\Psi}_{k+1}$. In this manuscript, following [43], we model it as AGN characterized by the covariance matrix $\mathbf{C}_a = \sigma_a^2\mathbf{I}_3$, with $\sigma_a^2 > \sigma_{a^b}^2$ and neglect its correlation with the noise vector affecting the accelerometer output (see (103)).

It is important to note that:

- If the vehicle rotation was described by the quaternion $q_k^{n\triangleright b}$ (in place of the vector $\boldsymbol{\Psi}_k$), the dynamic model

$$q_{k+1}^{n\triangleright b} = \exp\left(-\frac{T_s}{2}\boldsymbol{\omega}_k^{b,n\triangleright b}\right) \odot q_k^{n\triangleright b} \tag{113}$$

would be adopted for $q_k^{n\triangleright b}$, where $\exp(\cdot)$ and $\odot$ denote the quaternion exponential operator and the quaternion multiplication operator, respectively (the corresponding operations are defined in the Appendix). The

validity of the last equation, like that of (99), is subject to the assumption that the angular velocity $\boldsymbol{\omega}_k^{b,n\triangleright b}$ measured at the instant kT_s is constant in the interval $[kT_s, (k+1)T_s]$; consequently, to account for model inaccuracy, an AGN term $\mathbf{n}_{q,k}$ (characterized by the covariance matrix $\mathbf{C}_q = \sigma_q^2\mathbf{I}_4$) should be inserted in the right hand side of (113) (e.g, see [43]), so turning it into

$$q_{k+1}^{n\triangleright b} = \exp\left(-\frac{T_s}{2}\boldsymbol{\omega}_k^{b,n\triangleright b}\right) \odot q_k^{n\triangleright b} + \mathbf{n}_{q,k}. \tag{114}$$

It is also important to mention that, if the gyroscope, after bias removal, produced an accurate estimate $\hat{\boldsymbol{\omega}}_k^{b,n\triangleright b}$ of $\boldsymbol{\omega}_k^{b,n\triangleright b}$, $\boldsymbol{\omega}_k^{b,n\triangleright b}$ and $\mathbf{b}_k^{\omega}$ could be removed from the state vector $\mathbf{x}_k$ (52) in order to reduces its dimensionality, as suggested in [65]. In this case, following [65], the *nonlinear* model

$$q_{k+1}^{n\triangleright b} = \exp\left(-\frac{T_s}{2}\hat{\boldsymbol{\omega}}_k^{b,n\triangleright b}\right) \odot q_k^{n\triangleright b} + \mathbf{n}_{q,k} \tag{115}$$

could be used for the vehicle orientation in place of (113), where

$$\mathbf{n}_{q,k} = -\frac{T_s}{2}\boldsymbol{\Xi}_k\left(q_k^{n\triangleright b}\right)\mathbf{n}_{\omega,k} \tag{116}$$

and (see [65, eq. (9)])

$$\boldsymbol{\Xi}_k\left(q_k^{n\triangleright b}\right) \triangleq \begin{bmatrix} q_{0,k} & -q_{3,k} & q_{2,k} \\ q_{3,k} & q_{0,k} & -q_{1,k} \\ -q_{2,k} & q_{1,k} & q_{0,k} \\ -q_{1,k} & -q_{2,k} & -q_{3,k} \end{bmatrix}. \tag{117}$$

It is worth stressing that the model (115) is based on the assumptions that: a) the estimate $\hat{\boldsymbol{\omega}}_k^{b,n\triangleright b}$ is affected by discrete time AGN noise vector process $\{\mathbf{n}_{\omega,k}\}$ (the covariance matrix of $\mathbf{n}_{\omega,k}$ is $\mathbf{C}_\omega = \sigma_\omega^2\mathbf{I}_3$ for any k); b) the elements of $\mathbf{n}_{\omega,k}$ are small enough that a first order approximation can be used in evaluating the quaternion multiplication in (113). Moreover, when using (114) or (115) it should not be forgotten that: a) a quaternion representing a valid rotation must have a unit norm so that its four components are interdependent; b) the unit-norm property must be always preserved by including a normalization step (accomplished by dividing any quaternion by its norm).

- Four of seven the dynamic models illustrated above are *linear,* but two (namely, (99) and (105)) are *nonlinear* because of the presence of trigonometric functions. For this reason, a standard Kalman filter cannot be adopted for state estimation in this case. This relevant feature of our state model is better evidenced by condensing it in the state transition vector equation

$$\mathbf{x}_{k+1} = \mathbf{f}_{\mathbf{x}}\left(\mathbf{x}_k\right) + \mathbf{M}\mathbf{g} + \mathbf{n}_k, \tag{118}$$

where

$$\mathbf{f}_{\mathbf{x}}\left(\mathbf{x}_k\right) \triangleq \left[\begin{array}{ccccccc} \mathbf{I}_3 & T_s\mathbf{I}_3 & \mathbf{0}_{3,3} & \mathbf{0}_{3,3} & \mathbf{0}_{3,3} & \mathbf{0}_{3,3} & \mathbf{0}_{3,3} \\ \mathbf{0}_{3,3} & \mathbf{0}_{3,3} & \mathbf{0}_{3,3} & \mathbf{C}_b^n\left(\boldsymbol{\Psi}_k\right) & \mathbf{0}_{3,3} & \mathbf{0}_{3,3} & \mathbf{0}_{3,3} \\ \mathbf{0}_{3,3} & \mathbf{0}_{3,3} & \mathbf{I}_3 & \mathbf{0}_{3,3} & T\mathbf{A}_{s\omega}\left(\boldsymbol{\Psi}_k\right) & \mathbf{0}_{3,3} & \mathbf{0}_{3,3} \\ \mathbf{0}_{3,3} & \mathbf{0}_{3,3} & \mathbf{0}_{3,3} & \mathbf{I}_3 & \mathbf{0}_{3,3} & \mathbf{0}_{3,3} & \mathbf{0}_{3,3} \\ \mathbf{0}_{3,3} & \mathbf{0}_{3,3} & \mathbf{0}_{3,3} & \mathbf{0}_{3,3} & \mathbf{I}_3 & \mathbf{0}_{3,3} & \mathbf{0}_{3,3} \\ \mathbf{0}_{3,3} & \mathbf{0}_{3,3} & \mathbf{0}_{3,3} & \mathbf{0}_{3,3} & \mathbf{0}_{3,3} & \mathrm{diag}\left\{\boldsymbol{\beta}^a\right\} & \mathbf{0}_{3,3} \\ \mathbf{0}_{3,3} & \mathbf{0}_{3,3} & \mathbf{0}_{3,3} & \mathbf{0}_{3,3} & \mathbf{0}_{3,3} & \mathbf{0}_{3,3} & \mathrm{diag}\left\{\boldsymbol{\beta}^\omega\right\} \end{array}\right] \mathbf{x}_k, \tag{119}$$

$$\mathbf{M} \triangleq \left[\mathbf{0}, \mathbf{I}_3, \mathbf{0}_{3,3}, \mathbf{0}_{3,3}, \mathbf{0}_{3,3}, \mathbf{0}_{3,3}, \mathbf{0}_{3,3}\right]^T \tag{120}$$

and

$$\mathbf{n}_k \triangleq \left[\mathbf{n}_{v,k}, \mathbf{n}_{a,k}, \mathbf{n}_{\Psi,k}, \mathbf{n}_{a^b,k}, \mathbf{n}_{\omega^b,k}, \mathbf{n}_{b^a,k}, \mathbf{n}_{b^\omega,k}\right]^T. \tag{121}$$

The *measurement* models relate the IMU sensed quantities with the state vector (52) and are given by

$$\mathbf{z}_k^a = \mathbf{a}_k^b + \mathbf{b}_k^a + \mathrm{diag}\{\mathbf{w}^a\}\mathbf{m}_{a,k} \tag{122}$$

and

$$\mathbf{z}_k^\omega = \boldsymbol{\omega}_k^{b,n\triangleright b} + \mathbf{b}_k^\omega + \mathrm{diag}\{\mathbf{w}^\omega\}\mathbf{m}_{\omega,k}, \tag{123}$$

where $\mathbf{z}_k^f$ and $\mathbf{z}_k^\omega$ denote the *calibrated* angular velocity and acceleration measurements from the IMU, respectively, both expressed in the body frame, the vectors $\mathbf{w}^\omega$ and $\mathbf{w}^\omega$ account for asymmetries in the random walk of the sensors on different axes, and $\mathbf{m}_{a,k}$ and $\mathbf{m}_{\omega,k}$ represent the AGN affecting acceleration and angular velocity measurements, respectively (these characterized by the covariance matrices $\mathbf{C}_{z,a} = \sigma_{z,a}^2\mathbf{I}_3$ and $\mathbf{C}_{z,\omega} = \sigma_{z,\omega}^2\mathbf{I}_3$, respectively). Note that: a) both (122) and (123) are *linear*; b) the vectors $\mathbf{z}_k^a$ and $\mathbf{z}_k^\omega$ can be collected in the D_z-dimensional measurement vector (with $D_z = 6$)

$$\mathbf{z}_k \triangleq \left[\left(\mathbf{z}_k^a\right)^T, \left(\mathbf{z}_k^\omega\right)^T\right]^T = \mathbf{f}_{\mathbf{z}}\left(\mathbf{x}_k\right) + \mathbf{m}_k \tag{124}$$

where

$$\mathbf{f}_{\mathbf{z}}\left(\mathbf{x}_k\right) \triangleq \left[\begin{array}{c} \mathbf{a}_k^b + \mathbf{b}_k^a \\ \boldsymbol{\omega}_k^{b,n\triangleright b} + \mathbf{b}_k^\omega \end{array}\right] \tag{125}$$

and

$$\mathbf{m}_k \triangleq \left[\left(\mathrm{diag}\{\mathbf{w}^a\}\mathbf{m}_{a,k}\right)^T, \left(\mathrm{diag}\{\mathbf{w}^\omega\}\mathbf{m}_{\omega,k}\right)^T\right]^T \tag{126}$$

is the AGN vector affecting $\mathbf{z}_k$ (124). From a statistical viewpoint (118) leads to the conclusion that the pdf of $\mathbf{x}_{k+1}$conditioned on $\mathbf{x}_k$ is given by

$$f\left(\mathbf{x}_{k+1}\left|\mathbf{x}_k\right.\right) = \mathcal{N}\left(\mathbf{x}_{k+1}; \mathbf{f}_{\mathbf{x}}\left(\mathbf{x}_k\right) + \mathbf{M}\mathbf{g}, \mathbf{C}_n\right), \tag{127}$$

where $\mathbf{C}_n$ is the (diagonal) covariance matrix of the vector $\mathbf{n}_k$ (121). Similarly, the pdf of $\mathbf{z}_k$ conditioned on $\mathbf{x}_k$ is given by (see (124))

$$f(\mathbf{z}_k|\mathbf{y}_k) = \mathcal{N}\left(\mathbf{z}_k; \mathbf{f}_{\mathbf{z}}\left(\mathbf{x}_k\right), \mathbf{C}_m\right), \tag{128}$$

where $\mathbf{C}_m$ is the (diagonal) covariance matrix of the vector $\mathbf{m}_k$.

Finally, it is important to mention that:

- In the technical literature some *theoretical* indications are available about the variance of some noise terms; for instance, the variance of the noise terms in (98) can be assessed considering that they originate from the truncation of a Taylor series (i.e., they account for the error due to higher-order terms; see [73, Sec. 4.3]).

- In practice, because of model approximations/simplifications, such theoretical indications are not useful and *careful tuning* is needed for the noise variances appearing in the state model.

- If a quaternion $q_k^{n\triangleright b}$ was used in place of the angle vector $\boldsymbol{\Psi}_k$, the state vector would become

$$\mathbf{x}_k \triangleq \left[\left(\mathbf{v}_k\right)^T, \left(\mathbf{a}_k\right)^T, q_k^{n\triangleright b}, \left(\mathbf{a}_k^b\right)^T, \left(\boldsymbol{\omega}_k^{b,n\triangleright b}\right)^T, \left(\mathbf{b}_k^a\right)^T, \left(\mathbf{b}_k^\omega\right)^T \right]^T, \quad (129)$$

the function $\mathbf{f}_{\mathbf{x}}\left(\mathbf{x}_k\right)$ appearing in the state transition vector equation (118) would turn into[5]

$$\mathbf{f}_{\mathbf{x}}\left(\mathbf{x}_k\right) \triangleq \begin{bmatrix} \mathbf{I}_3 & T_s\mathbf{I}_3 & \mathbf{0}_{3,3} & \mathbf{0}_{3,4} & \mathbf{0}_{3,3} & \mathbf{0}_{3,3} & \mathbf{0}_{3,3} \\ \mathbf{0}_{3,3} & \mathbf{I}_3 & \mathbf{0}_{3,3} & \mathbf{R}^T\left(q_k^{n\triangleright b}\right) & \mathbf{0}_{3,3} & \mathbf{0}_{3,3} & \mathbf{0}_{3,3} \\ \mathbf{0}_{4,3} & \mathbf{0}_{4,3} & \exp\left(-\frac{T_s}{2}\boldsymbol{\omega}_k^{b,n\triangleright b}\right) & \mathbf{0}_{4,3} & \mathbf{0}_{3,3} & \mathbf{0}_{4,3} & \mathbf{0}_{4,3} \\ \mathbf{0}_{3,3} & \mathbf{0}_{3,3} & \mathbf{0}_{3,3} & \mathbf{I}_3 & \mathbf{0}_{3,3} & \mathbf{0}_{3,3} & \mathbf{0}_{3,3} \\ \mathbf{0}_{3,3} & \mathbf{0}_{3,3} & \mathbf{0}_{3,3} & \mathbf{0}_{3,4} & \mathbf{I}_3 & \mathbf{0}_{3,3} & \mathbf{0}_{3,3} \\ \mathbf{0}_{3,3} & \mathbf{0}_{3,3} & \mathbf{0}_{3,3} & \mathbf{0}_{3,4} & \mathbf{0}_{3,3} & \mathrm{diag}\left\{\boldsymbol{\beta}^a\right\} & \mathbf{0}_{3,3} \\ \mathbf{0}_{3,3} & \mathbf{0}_{3,3} & \mathbf{0}_{3,3} & \mathbf{0}_{3,4} & \mathbf{0}_{3,3} & \mathbf{0}_{3,3} & \mathrm{diag}\left\{\boldsymbol{\beta}^\omega\right\} \end{bmatrix} \mathbf{x}_k \quad (130)$$

and the noise vector $\mathbf{n}_k$ (121) would become

$$\mathbf{n}_k \triangleq \left[\left(\mathbf{n}_{v,k}\right)^T, \left(\mathbf{n}_{a,k}\right)^T, \left(\mathbf{n}_{q,k}\right)^T, \left(\mathbf{n}_{a^b,k}\right)^T, \left(\mathbf{n}_{\omega^b,k}\right)^T, \left(\mathbf{n}_{b^a,k}\right)^T, \left(\mathbf{n}_{b^\omega,k}\right)^T \right]^T. \quad (131)$$

7.2.4 State estimation via extended Kalman filtering

The EKF is an extension of the Kalman filter and represents a sub-optimal estimator for non-linear, Gaussian models; its has has been widely adopted in many signal processing areas, thanks to its relatively low computational complexity and its ease of use. For these reasons, it represents a good choice for the implementation of a filter whose state vector has a significant dimensionality ($D_x = 21$ in (52)). In this Paragraph we briefly describe its implementation in our scenario.

Extended Kalman filtering is based on the propagation of the first two (estimated) moments of the posterior pdf $f(\mathbf{x}_k|\mathbf{z}_{0:k})$ (where $\mathbf{z}_{0:k}$ is the vector resulting from the ordered concatenation of the vectors $\{\mathbf{z}_l, l = 0, 1, ..., k\}$), namely the

[5] Note that in evaluating the product between $\exp\left(-\frac{T_s}{2}\boldsymbol{\omega}_k^{b,n\triangleright b}\right)$ and the quaternion $q_k^{n\triangleright b}$ contained in $\mathbf{x}_k$, quaternion multiplication must be used.

estimated mean state vector $\hat{\mathbf{x}}_k$ and the *estimated state vector covariance matrix* $\hat{\mathbf{P}}_k$. It consists of two distinct steps, called *prediction step* and *update step*, which are described in detail below for the considered scenario.

Prediction step - Given the quantities $\hat{\mathbf{x}}_k$ and $\hat{\mathbf{P}}_k$ referred to the k-th iteration, the standard EKF *prediction* step is expressed by (see (118))

$$\hat{\mathbf{x}}_{k+1|k} = \mathbf{f}_{\mathbf{x}}\left(\hat{\mathbf{x}}_k\right) + \mathbf{M}\mathbf{g} \tag{132}$$

and

$$\hat{\mathbf{P}}_{k+1|k} = \mathbf{J}_x\left(\hat{\mathbf{x}}_k\right)\hat{\mathbf{P}}_k\left(\mathbf{J}_x\left(\hat{\mathbf{x}}_k\right)\right)^T + \mathbf{C}_n, \tag{133}$$

where $\hat{\mathbf{x}}_{k+1|k}$ and $\hat{\mathbf{P}}_{k+1|k}$ represent the $(k+1)$-th state mean and covariance matrix, respectively, *predicted* on the basis of the information originating from the k-th step and

$$\mathbf{J}_x\left(\mathbf{x}\right) \triangleq \frac{\partial \mathbf{f}_{\mathbf{x}}\left(\mathbf{x}\right)}{\partial \mathbf{x}} \tag{134}$$

is the $D_x \times D_x$ Jacobian matrix for the (non-linear) state model (118). Since (see (119))

$$\mathbf{f}_{\mathbf{x}}\left(\mathbf{x}\right) = \begin{bmatrix} \mathbf{v} + T_s\mathbf{a} \\ \mathbf{C}_b^n\left(\boldsymbol{\Psi}\right)\mathbf{a}^b \\ \Psi + T_s\mathbf{A}_{s\omega}\left(\boldsymbol{\Psi}\right)\boldsymbol{\omega}^{b,n\triangleright b} \\ \mathbf{a}^b \\ \boldsymbol{\omega}^{b,n\triangleright b} \\ \mathrm{diag}\left\{\boldsymbol{\beta}^a\right\}\mathbf{b}_k^a, \\ \mathrm{diag}\left\{\boldsymbol{\beta}^\omega\right\}\mathbf{b}^\omega \end{bmatrix}, \tag{135}$$

$\mathbf{J}_x\left(\mathbf{x}\right)$ (134) is given by

$$\mathbf{J}_x\left(\mathbf{x}\right) = \begin{bmatrix} \mathbf{I}_3 & T_s\mathbf{I}_3 & \mathbf{0}_{3,3} & \mathbf{0}_{3,3} & \mathbf{0}_{3,3} & \mathbf{0}_{3,3} & \mathbf{0}_{3,3} \\ \mathbf{0}_{3,3} & \mathbf{0}_{3,3} & \mathbf{A}\left(\boldsymbol{\Psi},\mathbf{a}^b\right) & \mathbf{C}_b^n\left(\boldsymbol{\Psi}\right) & \mathbf{0}_{3,3} & \mathbf{0}_{3,3} & \mathbf{0}_{3,3} \\ \mathbf{0}_{3,3} & \mathbf{0}_{3,3} & \mathbf{B}\left(\boldsymbol{\Psi},\boldsymbol{\omega}^{b,n\triangleright b}\right) & \mathbf{0}_{3,3} & T_s\mathbf{A}_{s\omega}\left(\boldsymbol{\Psi}\right) & \mathbf{0}_{3,3} & \mathbf{0}_{3,3} \\ \mathbf{0}_{3,3} & \mathbf{0}_{3,3} & \mathbf{0}_{3,3} & \mathbf{I}_3 & \mathbf{0}_{3,3} & \mathbf{0}_{3,3} & \mathbf{0}_{3,3} \\ \mathbf{0}_{3,3} & \mathbf{0}_{3,3} & \mathbf{0}_{3,3} & \mathbf{0}_{3,3} & \mathbf{I}_3 & \mathbf{0}_{3,3} & \mathbf{0}_{3,3} \\ \mathbf{0}_{3,3} & \mathbf{0}_{3,3} & \mathbf{0}_{3,3} & \mathbf{0}_{3,3} & \mathbf{0}_{3,3} & \mathrm{diag}\left\{\boldsymbol{\beta}^a\right\} & \mathbf{0}_{3,3} \\ \mathbf{0}_{3,3} & \mathbf{0}_{3,3} & \mathbf{0}_{3,3} & \mathbf{0}_{3,3} & \mathbf{0}_{3,3} & \mathbf{0}_{3,3} & \mathrm{diag}\left\{\boldsymbol{\beta}^\omega\right\} \end{bmatrix}, \tag{136}$$

where

$$\begin{aligned} &\mathbf{A}\left(\boldsymbol{\Psi},\mathbf{a}^b\right) \triangleq \tfrac{\partial}{\partial \boldsymbol{\Psi}}\left[\mathbf{C}_b^n\left(\boldsymbol{\Psi}\right)\mathbf{a}^b\right] = \\ &\tfrac{\partial}{\partial \boldsymbol{\Psi}}\begin{bmatrix} \left(\cos\theta\cos\psi\right)a_0^b + \left(\sin\phi\sin\theta\cos\psi - \cos\phi\sin\psi\right)a_1^b \\ + \left(\cos\phi\sin\theta\cos\psi + \sin\phi\sin\psi\right)a_2^b \\ \left(\cos\theta\sin\psi\right)a_0^b + \left(\sin\phi\sin\theta\sin\psi + \cos\phi\cos\psi\right)a_1^b \\ + \left(\cos\phi\sin\theta\sin\psi - \sin\phi\cos\psi\right)a_2^b \\ \left(-\sin\theta\right)a_0^b + \left(\sin\phi\cos\theta\right)a_1^b + \left(\cos\phi\cos\theta\right)a_2^b \end{bmatrix} \\ &= \begin{bmatrix} d_{1,1} & d_{1,2} & d_{1,3} \\ d_{2,1} & d_{2,2} & d_{2,3} \\ d_{3,1} & d_{3,2} & d_{3,3} \end{bmatrix} \end{aligned} \tag{137}$$

with

$$d_{1,1} = \left(\cos\phi\sin\theta\cos\psi + \sin\phi\sin\psi\right) a_1^b + \left(-\sin\phi\sin\theta\cos\psi + \cos\phi\sin\psi\right) a_2^b, \tag{138}$$

$$d_{1,2} = \left(-\sin\theta\cos\psi\right) a_0^b + \left(\sin\phi\cos\theta\cos\psi\right) a_1^b + \left(\cos\phi\cos\theta\cos\psi+\right) a_2^b, \tag{139}$$

$$\begin{array}{c} d_{1,3} = \left(-\cos\theta\sin\psi\right) a_0^b + \left(-\sin\phi\sin\theta\sin\psi - \cos\phi\cos\psi\right) a_1^b \\ + \left(-\cos\phi\sin\theta\sin\psi + \sin\phi\cos\psi\right) a_2^b, \end{array} \tag{140}$$

$$d_{2,1} = \left(\cos\phi\sin\theta\sin\psi - \sin\phi\cos\psi\right) a_1^b + \left(-\sin\phi\sin\theta\sin\psi - \cos\phi\cos\psi\right) a_2^b, \tag{141}$$

$$d_{2,2} = \left(-\sin\theta\sin\psi\right) a_0^b + \left(\sin\phi\cos\theta\sin\psi\right) a_1^b + \left(\cos\phi\cos\theta\sin\psi\right) a_2^b, \tag{142}$$

$$\begin{array}{c} d_{2,3} = \left(\cos\theta\cos\psi\right) a_0^b + \left(\sin\phi\sin\theta\cos\psi - \cos\phi\sin\psi\right) a_1^b \\ + \left(\cos\phi\sin\theta\cos\psi + \sin\phi\sin\psi\right) a_2^b, \end{array} \tag{143}$$

$$d_{3,1} = \left(\cos\phi\cos\theta\right) a_1^b + \left(-\sin\phi\cos\theta\right) a_2^b, \tag{144}$$

$$d_{3,2} = \left(-\cos\theta\right) a_0^b + \left(-\sin\phi\sin\theta\right) a_1^b + \left(-\cos\phi\sin\theta\right) a_2^b \tag{145}$$

and

$$d_{3,3} = 0. \tag{146}$$

Moreover, we have that

$$\mathbf{B}\left(\mathbf{\Psi}, \boldsymbol{\omega}^{b,n\triangleright b}\right) \triangleq \mathbf{I}_3 + T_s \frac{\partial}{\partial \mathbf{\Psi}} \left[\mathbf{A}_{s\omega}\left(\mathbf{\Psi}\right) \boldsymbol{\omega}^{b,n\triangleright b}\right] \tag{147}$$

with

$$\begin{array}{c} \frac{\partial}{\partial \mathbf{\Psi}} \left[\mathbf{A}_{s\omega}\left(\mathbf{\Psi}\right) \boldsymbol{\omega}^{b,n\triangleright b}\right] \\ = \frac{\partial}{\partial \mathbf{\Psi}} \left\{ \begin{array}{c} \omega_x^{b,n\triangleright b} + \omega_y^{b,n\triangleright b} \sin\phi\tan\theta + \omega_z^{b,n\triangleright b} \cos\phi\tan\theta \\ \omega_y^{b,n\triangleright b} \cos\phi - \omega_z^{b,n\triangleright b} \sin\phi \\ \omega_y^{b,n\triangleright b} \frac{\sin\phi}{\cos\theta} - \omega_z^{b,n\triangleright b} \frac{\cos\phi}{\cos\theta} \end{array} \right\} \\ \left[\begin{array}{ccc} \tan\theta \left[\omega_y^{b,n\triangleright b} \cos\phi - \omega_z^{b,n\triangleright b} \sin\phi\right] & \frac{1}{\cos^2\theta} \left[\omega_y^{b,n\triangleright b} \sin\phi + \omega_z^{b,n\triangleright b} \cos\phi\right] & 0 \\ -\omega_y^{b,n\triangleright b} \sin\phi - \omega_z^{b,n\triangleright b} \cos\phi & 0 & 0 \\ \frac{1}{\cos\theta} \left[\omega_y^{b,n\triangleright b} \cos\phi + \omega_z^{b,n\triangleright b} \sin\phi\right] & \frac{\sin\theta}{\cos^2\theta} \left[\omega_y^{b,n\triangleright b} \sin\phi - \omega_z^{b,n\triangleright b} \cos\phi\right] & 0 \end{array} \right]. \end{array} \tag{148}$$

Note that, if (130) were used in place of (119), (135) would be replaced by

$$\mathbf{f}_{\mathbf{x}}\left(\mathbf{x}\right) = \left[\begin{array}{c} \mathbf{v} + T_s \mathbf{a} \\ \mathbf{R}^T\left(q^{n\triangleright b}\right) \mathbf{a}^b \\ \exp\left(-\frac{T_s}{2} \boldsymbol{\omega}^{b,n\triangleright b}\right) \odot q^{n\triangleright b} \\ \mathbf{a}^b \\ \boldsymbol{\omega}^{b,n\triangleright b} \\ \operatorname{diag}\left\{\boldsymbol{\beta}^a\right\} \mathbf{b}_k^a, \\ \operatorname{diag}\left\{\boldsymbol{\beta}^\omega\right\} \mathbf{b}^\omega \end{array} \right] \tag{149}$$

and, consequently, the associated Jacobian $\mathbf{J}_x(\mathbf{x})$ would become

$$\mathbf{J}_x(\mathbf{x}) = \begin{bmatrix} \mathbf{I}_3 & T_s\mathbf{I}_3 & \mathbf{0}_{3,4} & \mathbf{0}_{3,3} & \mathbf{0}_{3,3} & \mathbf{0}_{3,3} & \mathbf{0}_{3,3} \\ \mathbf{0}_{3,3} & \mathbf{0}_{3,3} & T_s\mathbf{D}\left(q^{n\triangleright b}, \mathbf{a}^b\right) & \mathbf{R}^T\left(q^{n\triangleright b}\right) & \mathbf{0}_{3,3} & \mathbf{0}_{3,3} & \mathbf{0}_{3,3} \\ \mathbf{0}_{4,3} & \mathbf{0}_{4,3} & \mathbf{E}\left(q^{n\triangleright b}, \boldsymbol{\omega}^{b,n\triangleright b}\right) & \mathbf{0}_{4,3} & \mathbf{F}\left(q^{n\triangleright b}, \boldsymbol{\omega}^{b,n\triangleright b}\right) & \mathbf{0}_{4,3} & \mathbf{0}_{4,3} \\ \mathbf{0}_{3,3} & \mathbf{0}_{3,3} & \mathbf{0}_{3,4} & \mathbf{I}_3 & \mathbf{0}_{3,3} & \mathbf{0}_{3,3} & \mathbf{0}_{3,3} \\ \mathbf{0}_{3,3} & \mathbf{0}_{3,3} & \mathbf{0}_{3,4} & \mathbf{0}_{3,3} & \mathbf{I}_3 & \mathbf{0}_{3,3} & \mathbf{0}_{3,3} \\ \mathbf{0}_{3,3} & \mathbf{0}_{3,3} & \mathbf{0}_{3,4} & \mathbf{0}_{3,3} & \mathbf{0}_{3,3} & \mathrm{diag}\left\{\boldsymbol{\beta}^a\right\} & \mathbf{0}_{3,3} \\ \mathbf{0}_{3,3} & \mathbf{0}_{3,3} & \mathbf{0}_{3,4} & \mathbf{0}_{3,3} & \mathbf{0}_{3,3} & \mathbf{0}_{3,3} & \mathrm{diag}\left\{\boldsymbol{\beta}^\omega\right\} \end{bmatrix}, \tag{150}$$

where (e.g., see (3) and [10, Sec. 4])

$$\begin{aligned} \mathbf{D}\left(q^{n\triangleright b}, \mathbf{a}^b\right) &\triangleq \tfrac{\partial}{\partial q^{n\triangleright b}}\left[\mathbf{R}^T\left(q^{n\triangleright b}\right)\mathbf{a}^b\right] = \\ \tfrac{\partial}{\partial q^{n\triangleright b}}&\begin{bmatrix} \left(2q_0^2+2q_1^2-1\right)a_0^b + \left(2q_1q_2+2q_0q_3\right)a_1^b + \left(2q_1q_3-2q_0q_2\right)a_2^b \\ \left(2q_1q_2-2q_0q_3\right)a_0^b + \left(2q_0^2+2q_2^2-1\right)a_1^b + \left(2q_2q_3+2q_0q_1\right)a_2^b \\ \left(2q_1q_3+2q_0q_2\right)a_0^b + \left(2q_2q_3-2q_0q_1\right)a_1^b + \left(2q_0^2+2q_3^2-1\right)a_2^b \end{bmatrix} \\ = \begin{bmatrix} 4q_0a_0^b+2q_3a_1^b-2q_2a_2^b & 4q_1a_0^b+2q_2a_1^b+2q_3a_2^b & 2q_1a_1^b-2q_0a_2^b & 2q_0a_1^b+2q_1a_2^b \\ -2q_3a_0^b+4q_0a_1^b+2q_1a_2^b & 2q_2a_0^b+2q_0a_2^b & 2q_1a_0^b+4q_2a_1^b+2q_3a_2^b & -2q_0a_0^b+2q_2a_2^b \\ 2q_2a_0^b-2q_1a_1^b+4q_0a_2^b & 2q_3a_0^b-2q_0a_1^b & 2q_0a_0^b+2q_3a_1^b & 2q_1a_0^b+2q_2a_1^b+4q_3a_2^b \end{bmatrix}, \end{aligned} \tag{151}$$

$$\begin{aligned} \mathbf{E}\left(q^{n\triangleright b}, \boldsymbol{\omega}^{b,n\triangleright b}\right) &\triangleq \tfrac{\partial}{\partial q^{n\triangleright b}}\left[\exp\left(-\tfrac{T_s}{2}\boldsymbol{\omega}^{b,n\triangleright b}\right)\odot q^{n\triangleright b}\right] = \tfrac{\partial}{\partial q^{n\triangleright b}}\left[\left[\exp\left(-\tfrac{T_s}{2}\boldsymbol{\omega}^{b,n\triangleright b}\right)\right]_L q^{n\triangleright b}\right] \\ &= \left[\exp\left(-\tfrac{T_s}{2}\boldsymbol{\omega}^{b,n\triangleright b}\right)\right]_L \end{aligned} \tag{152}$$

and

$$\begin{aligned} \mathbf{F}\left(q^{n\triangleright b}, \boldsymbol{\omega}^{b,n\triangleright b}\right) &\triangleq \tfrac{\partial}{\partial \boldsymbol{\omega}^{b,n\triangleright b}}\left[\exp\left(-\tfrac{T_s}{2}\boldsymbol{\omega}^{b,n\triangleright b}\right)\odot q^{n\triangleright b}\right] \\ = -\tfrac{T_s}{2}\left(q^{n\triangleright b}\right)_R &\begin{bmatrix} -\frac{\mathbf{v}^T}{\|\mathbf{v}\|}\sin\|\mathbf{v}\| \\ \frac{1}{\|\mathbf{v}\|}\left[\mathbf{I}_3 - \frac{\mathbf{v}\mathbf{v}^T}{\|\mathbf{v}\|^2}\right]\sin\|\mathbf{v}\| + \frac{\mathbf{v}\mathbf{v}^T}{\|\mathbf{v}\|^2}\cos\|\mathbf{v}\| \end{bmatrix}_{\mathbf{v}=-\frac{T_s}{2}\boldsymbol{\omega}^{b,n\triangleright b}}. \end{aligned} \tag{153}$$

Here (see (3), and (212) and (213) in the Appendix)

$$\mathbf{R}^T\left(q^{n\triangleright b}\right) = \begin{bmatrix} 2q_0^2+2q_1^2-1 & 2q_1q_2+2q_0q_3 & 2q_1q_3-2q_0q_2 \\ 2q_1q_2-2q_0q_3 & 2q_0^2+2q_2^2-1 & 2q_2q_3+2q_0q_1 \\ 2q_1q_3+2q_0q_2 & 2q_2q_3-2q_0q_1 & 2q_0^2+2q_3^2-1 \end{bmatrix}, \tag{154}$$

$$\begin{aligned} \left[\exp\left(-\tfrac{T_s}{2}\boldsymbol{\omega}^{b,n\triangleright b}\right)\right]_L &= \left[\left(\cos\|\mathbf{v}\|, \tfrac{\mathbf{v}}{\|\mathbf{v}\|}\sin\|\mathbf{v}\|\right)_{\mathbf{v}=[v_1,v_2,v_3]^T=-\frac{T_s}{2}\boldsymbol{\omega}^{b,n\triangleright b}}\right]_L \\ = \begin{bmatrix} \cos\|\mathbf{v}\| & -\frac{v_1}{\|\mathbf{v}\|}\sin\|\mathbf{v}\| & -\frac{v_2}{\|\mathbf{v}\|}\sin\|\mathbf{v}\| & -\frac{v_3}{\|\mathbf{v}\|}\sin\|\mathbf{v}\| \\ \frac{v_1}{\|\mathbf{v}\|}\sin\|\mathbf{v}\| & \cos\|\mathbf{v}\| & -\frac{v_3}{\|\mathbf{v}\|}\sin\|\mathbf{v}\| & \frac{v_2}{\|\mathbf{v}\|}\sin\|\mathbf{v}\| \\ \frac{v_2}{\|\mathbf{v}\|}\sin\|\mathbf{v}\| & \frac{v_3}{\|\mathbf{v}\|}\sin\|\mathbf{v}\| & \cos\|\mathbf{v}\| & -\frac{v_1}{\|\mathbf{v}\|}\sin\|\mathbf{v}\| \\ \frac{v_3}{\|\mathbf{v}\|}\sin\|\mathbf{v}\| & -\frac{v_2}{\|\mathbf{v}\|}\sin\|\mathbf{v}\| & \frac{v_1}{\|\mathbf{v}\|}\sin\|\mathbf{v}\| & \cos\|\mathbf{v}\| \end{bmatrix}_{\mathbf{v}=[v_1,v_2,v_3]^T=-\frac{T_s}{2}\boldsymbol{\omega}^{b,n\triangleright b}} \end{aligned} \tag{155}$$

and

$$\left(q^{n\triangleright b}\right)_R = \begin{bmatrix} q_0 & -q_1 & -q_2 & -q_3 \\ q_1 & q_0 & q_3 & -q_2 \\ q_2 & -q_3 & q_0 & q_1 \\ q_3 & q_2 & -q_1 & q_0 \end{bmatrix}. \tag{156}$$

Note also that, if the angular acceleration signal is sampled fast enough, the norm of the vector $-\frac{T_s}{2}\boldsymbol{\omega}^{b,n\triangleright b}$ can be deemed small, and a small angle approximation can be used in (153); this leads to the approximate expression

$$\begin{aligned} &\tfrac{\partial}{\partial \boldsymbol{\omega}^{b,n\triangleright b}}\left[\exp\left(-\tfrac{T_s}{2}\boldsymbol{\omega}^{b,n\triangleright b}\right)\odot q^{n\triangleright b}\right] \\ &\cong -\tfrac{T_s}{2}\left(q^{n\triangleright b}\right)_R \begin{bmatrix} \frac{T_s}{2}\left(\boldsymbol{\omega}^{b,n\triangleright b}\right)^T \\ \mathbf{I}_3 \end{bmatrix}. \end{aligned} \tag{157}$$

Prediction step - In the EKF *update* step the observation vector $\mathbf{z}_k$ (124) is processed. This step evolves as follows. First, the *innovation residual*

$$\mathbf{s}_{k+1|k} \triangleq \mathbf{z}_k - \mathbf{f}_{\mathbf{z}}\left(\hat{\mathbf{x}}_{k+1|k}\right) \tag{158}$$

and its estimated covariance matrix

$$\mathbf{S}_{k+1|k} = \mathbf{J}_z\left(\hat{\mathbf{x}}_{k+1|k}\right)\hat{\mathbf{P}}_{k+1|k}\left(\mathbf{J}_z\left(\hat{\mathbf{x}}_{k+1|k}\right)\right)^T + \mathbf{C}_m \tag{159}$$

are evaluated; here

$$\mathbf{J}_z\left(\mathbf{x}\right) \triangleq \frac{\partial \mathbf{f}_{\mathbf{z}}\left(\mathbf{x}\right)}{\partial \mathbf{x}} \tag{160}$$

is the $D_z \times D_x$ Jacobian matrix for the (linear) measurement model (124); it is not difficult to show that

$$\mathbf{J}_z\left(\mathbf{x}\right) = \begin{bmatrix} \mathbf{0}_{3,3} & \mathbf{0}_{3,3} & \mathbf{0}_{4,3} & \mathbf{I}_3 & \mathbf{0}_{3,3} & \mathbf{I}_3 & \mathbf{0}_{3,3} \\ \mathbf{0}_{3,3} & \mathbf{0}_{3,3} & \mathbf{0}_{4,3} & \mathbf{0}_{3,3} & \mathbf{I}_3 & \mathbf{0}_{3,3} & \mathbf{I}_3 \end{bmatrix}. \tag{161}$$

Then, $\mathbf{s}_{k+1|k}$ (158) and $\mathbf{S}_{k+1|k}$ (159) are processed to compute the so called *Kalman gain*

$$\mathbf{K}_{k+1|k} = \hat{\mathbf{P}}_{k+1|k}\left(\mathbf{J}_z\left(\hat{\mathbf{x}}_{k+1|k}\right)\right)^T \mathbf{S}_{k+1|k}^{-1}$$

and the new estimates

$$\hat{\mathbf{x}}_{k+1} = \hat{\mathbf{x}}_{k+1|k} + \mathbf{K}_{k+1|k}\mathbf{s}_{k+1|k} \tag{162}$$

and

$$\hat{\mathbf{P}}_{k+1} = \left[\mathbf{I} - \mathbf{K}_{k+1|k}\mathbf{J}_z\left(\hat{\mathbf{x}}_{k+1|k}\right)\right]\hat{\mathbf{P}}_{k+1|k} \tag{163}$$

of the state vector mean and of its covariance matrix, respectively. A well-known feature of the EKF is represented by the fact that at the end of the k-th step only $\hat{\mathbf{x}}_k$ and $\hat{\mathbf{P}}_k$ need to be saved, since the posterior distribution of the state vector $f(\mathbf{x}_k|\mathbf{z}_{0:k})$ is estimated as $\mathcal{N}\left(\mathbf{x}_k; \hat{\mathbf{x}}_k, \hat{\mathbf{P}}_k\right)$. Actually, as already stated above, in the considered scenario at the end of the k-th step the EKF output is

processed to generate the joint pdf of the vector $\Delta\mathbf{r}_k \triangleq \left[\Delta p_{x,k}^{(N)}, \Delta p_{y,k}^{(N)}, \Delta\psi_k^{(N)}\right]^T$ modelled as a Gaussian vector $\mathcal{N}\left(\Delta\mathbf{r}_k; \overline{\Delta\mathbf{r}_k}, \mathbf{C}_{\Delta r,k}\right)$. It is important to note that, from a mathematical viewpoint, the evaluation of this pdf would become much more complicated if a quaternion was used in place of the Euler angles to represent the vehicle orientation. In fact, it is known that, given a quaternion $q_k^{n\triangleright b} = (q_{0,k}, q_{1,k}, q_{2,k}, q_{3,k})^T$, the associated heading can be evaluated as (see (7))

$$\psi_k = \arctan\left(R_k\right), \tag{164}$$

where

$$R_k \triangleq \frac{2q_{1,k}q_{2,k} - 2q_{0,k}q_{3,k}}{2q_{0,k}^2 + 2q_{1,k}^2 - 1}. \tag{165}$$

This equation shows that ψ_k is characterized by a *strongly nonlinear dependence* on the quaternion $q_k^{n\triangleright b}$ and that, even if we assume a Gaussian pdf for $q_k^{n\triangleright b}$, the pdf of ψ_k cannot be easily evaluated. From (164) it is also inferred that the heading variation $\Delta\psi_k$ (54) can be expressed as

$$\Delta\psi_k = \arctan\left(R_k\right) - \arctan\left(R_{k-1}\right), \tag{166}$$

where the quantity R_k can be represented as

$$R_k = R_{k-1} + \Delta R_k \tag{167}$$

and the variation ΔR_k can be deemed small if the sampling rate is high. Then, the approximate expression

$$\Delta\psi_k \cong \frac{\Delta R_k}{1 + R_{k-1}^2} \tag{168}$$

based on the Taylor series of $\arctan(x)$ can be adopted to relate $\Delta\psi_k$ to $q_k^{n\triangleright b}$ and $q_{k-1}^{n\triangleright b}$. However, even if this approximation is adopted, the pdf of $\Delta\psi_k$ cannot be easily evaluated.

The use of the EKF requires a proper inizialization and the exploitation of some form of a priori knowledge to mitigate the effects of sensor biases (which, unluckily, are not directly observed). These issues are briefly discussed below.

Inizialization - If we assume that the tracking operation starts with the vehicle being still (this can be enforced stopping any vehicle movement at its startup), reasonable initial values for speed and velocity are $\mathbf{v}_0 = \mathbf{0}$ and $\mathbf{a}_0 = \mathbf{0}$. Regarding the initial orientation (i.e., $\mathbf{\Psi}_0$) a simple orientation filter and a magnetometer could be employed to obtain the initial values of the Euler angles; note that an orientation filter exploits only accelerometer measurements to detect the orientation of the sensor with respect to the gravity field and assumes that the sensor is still (so that the sensed acceleration is just the gravity vector in the body frame). Regarding the initial state vector elements $\mathbf{a}_0^b$ and $\boldsymbol{\omega}_0^{b,n\triangleright b}$, the natural initial value for the first is $\mathbf{a}_0^b = \mathbf{C}_b^n\left(\mathbf{\Psi}_0\right)\mathbf{g}$, while the latter may be just initialized as $\boldsymbol{\omega}_0^{b,n\triangleright b} = \mathbf{0}$ (assuming the vehicle to be still). Finally,

the initial BI values $\mathbf{b}_0^a$ and $\mathbf{b}_0^\omega$ may be set to zero if we assume, as already stated above, that they represent the fine components of the sensor biases.

A priori knowledge for sensor bias mitigation - Any bias in the sensed accelerations and angular velocities quickly disrupts the INS accuracy, since such measurements are continuously integrated. To counteract these error sources (which are very relevant in MEMS) some form of a priori knowledge about the vehicle motion can be exploited. In practice, the constraints (17) and (18), which refer to two components of the vector $\mathbf{v}_k^b \triangleq \left[v_{x,k}^b, v_{y,k}^b, v_{z,k}^b\right]^T$ (denoting the vehicle speed resolved in body coordinate frame at the time instant $t = kT_s$) are exploited. Consequently, it is required that

$$v_{y,k}^b = n_{y,k}^b \tag{169}$$

and

$$v_{z,k}^b = n_{z,k}^b \tag{170}$$

respectively, where $\left\{n_{y,k}^b\right\}$ and $\left\{n_{z,k}^b\right\}$ are Gaussian white noise processes with zero mean and variance $\left(\sigma_{v,y}^b\right)^2$ and $\left(\sigma_{v,z}^b\right)^2$, respectively (the values of these variances can be chosen to reflect the extent of the violation of the ideal constaints $v_{y,k}^b = 0$ and $v_{z,k}^b = 0$). The constraints (169) and (170) can be easily turned into a vector constraint on the system state. In fact, since

$$\mathbf{v}_k^b = \mathbf{C}_b^n \left(\mathbf{\Psi}_k\right)^T \mathbf{v}_k, \tag{171}$$

they can be rewritten as

$$\left[\begin{array}{c} 0 \\ 0 \end{array}\right] = \left[\begin{array}{c} v_{y,k}^b \\ v_{z,k}^b \end{array}\right] = \mathbf{g}\left(\mathbf{\Psi}_k, \mathbf{v}_k\right) + \left[\begin{array}{c} m_{vy,k} \\ m_{vz,k} \end{array}\right], \tag{172}$$

where $m_{vy,k}$ and $m_{vz,k}$ are noise terms (having variance $\left(\sigma_{v,y}^b\right)^2$ and $\left(\sigma_{v,z}^b\right)^2$, respectively) and

$$\mathbf{g}\left(\mathbf{\Psi}_k, \mathbf{v}_k\right) = \left[\begin{array}{c} v_{x,k}\left(\sin\phi\sin\theta\cos\psi - \cos\phi\sin\psi\right) \\ +v_{y,k}^b\left(\sin\phi\sin\theta\sin\psi + \cos\phi\cos\psi\right) + v_{z,k}^b\sin\phi\cos\theta \\ v_{x,k}\left(\cos\phi\sin\theta\cos\psi + \sin\phi\sin\psi\right) \\ +v_{y,k}^b\left(\cos\phi\sin\theta\sin\psi - \sin\phi\cos\psi\right) + v_{z,k}^b\cos\phi\cos\theta \end{array}\right]. \tag{173}$$

Eq. (172) can be reformulated as

$$\mathbf{0}_2 = \mathbf{z}_{pm,k} = \mathbf{h}\left(\mathbf{x}_k, \mathbf{m}_{v,k}\right), \tag{174}$$

where $\mathbf{m}_{v,k} = [m_{vy,k}, m_{vz,k}]^T$ is a noise vector and $\mathbf{z}_{pm,k} = [v_{y,k}^b, v_{z,k}^b]^T$ is interpreted as a sort of measurement (dubbed *pseudo measurement*) which is forced to be equal to zero. The vector $\mathbf{z}_{pm,k}$ can be included in the measurement vector (124), which becomes

$$\mathbf{z}_k \triangleq \left[\left(\mathbf{z}_k^a\right)^T, \left(\mathbf{z}_k^\omega\right)^T, \left(\mathbf{z}_{pm,k}\right)^T\right]^T = \tilde{\mathbf{f}}_{\mathbf{z}}\left(\mathbf{x}_k\right) + \tilde{\mathbf{m}}_k, \tag{175}$$

where

$$\tilde{\mathbf{f}}_{\mathbf{z}}\left(\mathbf{x}_k\right) \triangleq \left[\begin{array}{c} \mathbf{a}_k^b + \mathbf{b}_k^a \\ \boldsymbol{\omega}_k^{b,n\triangleright b} + \mathbf{b}_k^{\omega} \\ \mathbf{g}\left(\boldsymbol{\Psi}_k, \mathbf{v}_k\right) \end{array}\right] \tag{176}$$

and

$$\mathbf{m}_k \triangleq \left[\left(\mathbf{m}_{a,k}\right)^T, \left(\mathbf{m}_{\omega,k}\right)^T, \left(\mathbf{m}_{v,k}\right)^T\right]^T. \tag{177}$$

The Jacobian matrix for the nonlinear measurement model (175) is

$$\mathbf{J}_z\left(\mathbf{x}\right) = \left[\begin{array}{ccccccc} \mathbf{0}_{3,3} & \mathbf{0}_{3,3} & \mathbf{0}_{3,3} & \mathbf{I}_3 & \mathbf{0}_{3,3} & \mathbf{I}_3 & \mathbf{0}_{3,3} \\ \mathbf{0}_{3,3} & \mathbf{0}_{3,3} & \mathbf{0}_{3,3} & \mathbf{0}_{3,3} & \mathbf{I}_3 & \mathbf{0}_{3,3} & \mathbf{I}_3 \\ \mathbf{M}_{\mathbf{v}} & \mathbf{0}_{2,3} & \mathbf{M}_{\Psi} & \mathbf{0}_{2,3} & \mathbf{0}_{2,3} & \mathbf{0}_{2,3} & \mathbf{0}_{2,3} \end{array}\right], \tag{178}$$

where

$$\mathbf{M}_{\mathbf{v}} = \left[\begin{array}{ccc} \sin\phi\sin\theta\cos\psi - \cos\phi\sin\psi & \sin\phi\sin\theta\sin\psi + \cos\phi\cos\psi & \sin\phi\cos\theta \\ \cos\phi\sin\theta\cos\psi + \sin\phi\sin\psi & \cos\phi\sin\theta\sin\psi - \sin\phi\cos\psi & \cos\phi\cos\theta \end{array}\right] \tag{179}$$

and

$$\mathbf{M}_{\boldsymbol{\Psi}} = \left[\begin{array}{ccc} m_{\Psi,1,1} & m_{\Psi,1,2} & m_{\Psi,1,3} \\ m_{\Psi,2,1} & m_{\Psi,2,2} & m_{\Psi,2,3} \end{array}\right], \tag{180}$$

with

$$\begin{array}{c} m_{\Psi,1,1} = v_{x,k}\left(\cos\phi\sin\theta\cos\psi + \sin\phi\sin\psi\right) \\ +v_{y,k}^b\left(\cos\phi\sin\theta\sin\psi - \sin\phi\cos\psi\right) + v_{z,k}^b\cos\phi\cos\theta, \end{array} \tag{181}$$

$$\begin{array}{c} m_{\Psi,1,2} = v_{x,k}\left(\sin\phi\cos\theta\cos\psi\right) \\ +v_{y,k}^b\left(\sin\phi\cos\theta\sin\psi\right) - v_{z,k}^b\sin\phi\sin\theta, \end{array} \tag{182}$$

$$\begin{array}{c} m_{\Psi,1,3} = v_{x,k}\left(-\sin\phi\sin\theta\sin\psi - \cos\phi\cos\psi\right) \\ +v_{y,k}^b\left(\sin\phi\sin\theta\cos\psi - \cos\phi\sin\psi\right), \end{array} \tag{183}$$

$$\begin{array}{c} m_{\Psi,2,1} = v_{x,k}\left(-\sin\phi\sin\theta\cos\psi + \cos\phi\sin\psi\right) \\ +v_{y,k}^b\left(-\sin\phi\sin\theta\sin\psi - \cos\phi\cos\psi\right) - v_{z,k}^b\sin\phi\cos\theta, \end{array} \tag{184}$$

$$\begin{array}{c} m_{\Psi,2,2} = v_{x,k}\left(\cos\phi\cos\theta\cos\psi\right) \\ +v_{y,k}^b\left(\cos\phi\cos\theta\sin\psi\right) - v_{z,k}^b\cos\phi\sin\theta \end{array} \tag{185}$$

and

$$\begin{array}{c} m_{\Psi,2,3} = v_{x,k}\left(-\cos\phi\sin\theta\sin\psi + \sin\phi\cos\psi\right) \\ +v_{y,k}^b\left(\cos\phi\sin\theta\cos\psi + \sin\phi\sin\psi\right). \end{array} \tag{186}$$

If the pseudo-measurements are employed, when evaluating the *innovation residual* $\mathbf{s}_{k+1|k}$ according to (158), the vector

$$\mathbf{z}_k \triangleq \left[\left(\mathbf{z}_k^a\right)^T, \left(\mathbf{z}_k^{\omega}\right)^T, \left(\mathbf{0}_2\right)^T\right]^T \tag{187}$$

is used, where $\mathbf{0}_2 = [0, 0]^T$.

7.2.5 Position estimation via particle filtering

As explained in the previous Subsection, the mean state vector $\hat{\mathbf{x}}_k$ and the state covariance matrix $\hat{\mathbf{P}}_k$ generated by the EKF are processed to estimate the joint pdf of $\Delta\tilde{\mathbf{p}}_k^{(N)}$ (53) and $\Delta\psi_k^{(N)}$ (54), i.e. the pdf of the vector $\Delta\mathbf{r}_k \triangleq \left[\Delta p_{x,k}^{(N)}, \Delta p_{y,k}^{(N)}, \Delta\psi_k^{(N)}\right]^T$. However, since the particle filter runs N times more slowly than the EKF, the parameters of these joint pdf are updated every NT_ss; in the following we assume that this occurs when the time index k of the EKF is a multiple of N. These statistical information are then fused with the information about position and heading coming from the GPS module and from those coming from the available map to generate the final estimates $\hat{\mathbf{p}}_l = [\hat{p}_{x,l}, \hat{p}_{y,l}]^T$ and $\hat{\psi}_l$ of the 2D position vector $\tilde{\mathbf{p}}_l = [p_{x,l}, p_{y,l}]^T$ and heading ψ_l, respectively, with $l = k/N$ (note that the clock interval for the particle filter is $T_s^{'} = NT_s$). In[71] the adoption of the 6D state vector

$$\mathbf{x}_l^{PF} \triangleq \left[\tilde{\mathbf{p}}_l^T, \psi_l, \boldsymbol{\Delta}\tilde{\mathbf{p}}_l^T, \Delta\psi_l\right]^T \tag{188}$$

is proposed for the particle filter employed in an architecture similar to that shown in Fig. 7. As a matter of fact, this represents the optimal choice because of the nature of the data processed by the particle filter; in fact, the input data originating from the EKF refer to$\boldsymbol{\Delta}\tilde{\mathbf{p}}_l^{(N)}$ and $\Delta\psi_l^{(N)}$, whereas those coming from the GPS refer to $\tilde{\mathbf{p}}_l$ and ψ_l. It is well known, however, that particle filtering performs quite well in a 3D space and that in higher dimensions the particle representation becomes soon too sparse to be a meaningful representation of a pdf [58]. For this reason, a smaller state vector has been adopted and, in particular, following [53], the 4D state vector

$$\mathbf{x}_l^{PF} \triangleq \left[\mathbf{r}_l^T, L_l\right]^T \tag{189}$$

has been selected, where

$$\mathbf{r}_l \triangleq [p_{x,l}, p_{y,l}, \psi_l]^T \tag{190}$$

is a vector collecting the 2D position and the yaw, and L_l represents a link to the map database [53]. In the following we concentrate on how the pdf of $\mathbf{r}_l$ (190) can be estimated via particle filtering; in fact, L_l can be easily related to $\mathbf{r}_l$ (see below). Estimating such a pdf raises the problem of how the *differential* information extracted from the EKF can be combined with the *absolute* information coming from the GPS module. To show how this can be accomplished, we need to define a *measurement model* and a *state model* for the particel filter. In principle, in the considered problem the l-th *measurement* vector $\mathbf{z}_l$consists of two contributions, i.e. the 3D vector

$$\mathbf{z}_l^{INS} = \overline{\Delta\mathbf{r}_k} = \mathbf{r}_l - \mathbf{r}_{l-1} + \mathbf{n}_l^{INS} \tag{191}$$

coming from the INS (always available) and the 3D vector

$$\mathbf{z}_l^{GPS} = \mathbf{r}_l + \mathbf{n}_l^{GPS} \tag{192}$$

from the GPS module (sometimes unavailable); here $\mathbf{n}_l^{INS}$ and $\mathbf{n}_l^{GPS}$ denote the zero mean (Gaussian) noise contributions affecting INS and GPS data and characterized by the covariance matrices $\mathbf{C}_{\Delta r,k}$ (evaluated in the first stage) and $\mathbf{C}_{GPS,l}$, respectively[6] (statistical independence can be assumed between these noise vectors). In this case defining a *state model* requires developing a probabilistic model for the vehicle movements. Following [71], a simple movement model is adopted here. If a state transition $\mathbf{r}_{l-1} \rightarrow \mathbf{r}_l$ violates some constraint originating from the map (e.g., it is associated with a path intersecting the walls of a building), $p(\mathbf{r}_l|\mathbf{r}_{l-1}) = 0$ is selected. On the contrary, if no constraint is violated, a simple Markovian model is assumed; in practice, it is assumed that: a) the sequence $\{\mathbf{r}_l - \mathbf{r}_{l-1}\}$ is a Gaussian process, consisting of independent vectors; b) for any l $(\mathbf{r}_l - \mathbf{r}_{l-1})$ is characterized by a zero mean and a covariance matrix $\mathbf{C}_{nr,l}$, and its elements are independent (their variances can be adapted to the vehicle speed, estimated by $|\overline{\Delta \mathbf{r}_k}|/T_s^{'}$).

It is worth mentioning that particle filtering is employed to approximate the posterior pdf $p(\mathbf{r}_l/\mathbf{z}_{0:l})$ of $\mathbf{r}_l$ at step l, given the vector $\mathbf{z}_{0:l} \triangleq [\mathbf{z}_0^T, \mathbf{z}_1^T, ..., \mathbf{z}_l^T]^T$ (which contains the available noisy observations available up to that step), as a sum of weighted delta functions associated with a set of N_p distinct particles, i.e. as

$$p(\mathbf{r}_l/\mathbf{Z}_l) \approx \sum_{j=0}^{N_p-1} w_l^{(j)} \cdot \delta\left(\mathbf{r}_l - \mathbf{r}_l^{(j)}\right). \tag{193}$$

For any j the j-th particle is drawn according to a so-called *proposal* (or *importance*) *density* $q\left(\mathbf{r}_l \left| \mathbf{r}_{l-1}^{(j)}, \mathbf{z}_l \right.\right)$, which, in principle, should be also used for the evaluation of the particle weigths; in fact, the weight $w_l^{(j)}$ for the j-th particle $\mathbf{r}_l^{(j)}$ should be evaluated as [77]

$$w_l^{(j)} \propto w_{l-1}^{(j)} \frac{p\left(\mathbf{z}_l/\mathbf{r}_l^{(j)}\right) p\left(\mathbf{r}_l^{(j)}/\mathbf{r}_{l-1}^{(j)}\right)}{q\left(\mathbf{r}_l^{(j)} \left| \mathbf{r}_{l-1}^{(j)}, \mathbf{z}_l \right.\right)}, \tag{194}$$

where $p(\mathbf{z}_l/\mathbf{r}_l)$ $(p(\mathbf{r}_l/\mathbf{r}_{l-1}))$ denotes the pdf of $\mathbf{z}_l$ $(\mathbf{r}_l)$ conditioned on $\mathbf{r}_l$ $(\mathbf{r}_{l-1})$. Note also that:

- The *optimal* choice of the proposal density is given by

$$q\left(\mathbf{r}_l \left| \mathbf{r}_{l-1}^{(j)}, \mathbf{z}_l \right.\right) = p\left(\mathbf{r}_l \left| \mathbf{r}_{l-1}^{(j)}, \mathbf{z}_l \right.\right) = \frac{p\left(\mathbf{z}_l \left| \mathbf{r}_l, \mathbf{r}_{l-1}^{(j)} \right.\right) p\left(\mathbf{r}_l \left| \mathbf{r}_{l-1}^{(j)} \right.\right)}{p\left(\mathbf{z}_l \left| \mathbf{r}_{l-1}^{(j)} \right.\right)}. \tag{195}$$

[6]Note that, when the quality of GPS data improves in terms of position and heading accuracy, the diagonal elements of $\mathbf{C}_{GPS,l}$ become smaller. The accuracy depends on two factors, the measurement quality and the user-to-satellite geometry. The measurement quality is described by the variance of the measurement error, which for a typical pseudorange is in the range of 0.3 to 30 m, depending on the error conditions. The geometry is described by the so called "G" matrix [60].

If this choice is made, (194) turns into

$$w_l^{(j)} \propto w_{l-1}^{(j)} p\left(\mathbf{z}_l/\mathbf{r}_{l-1}^{(j)}\right) = w_{l-1}^{(j)} \int p\left(\mathbf{z}_l/\tilde{\mathbf{r}}_l, \mathbf{r}_{l-1}^{(j)}\right) p\left(\tilde{\mathbf{r}}_l/\mathbf{r}_{l-1}^{(j)}\right) d\tilde{\mathbf{r}}_l. \quad (196)$$

- A proper choice (even if not the optimal one) for the proposal density is often the *prior*

$$q\left(\mathbf{r}_l \left| \mathbf{r}_{l-1}^{(j)}, \mathbf{z}_l \right.\right) = p\left(\mathbf{r}_l \left| \mathbf{r}_{l-1}^{(j)} \right.\right), \quad (197)$$

so that (194) yields

$$w_l^{(j)} \propto w_{l-1}^{(j)} p\left(\mathbf{z}_l/\mathbf{r}_l^{(j)}\right). \quad (198)$$

In the considered problem, in formulating the proposal density we assume that $\mathbf{z}_l$ consists of the INS differential information only; this choice is motivated by the fact that INS data are always available and, consequently, are able to drive the navigation system continuosly. In practice, this means that INS data only are exploited in the generation of new particles according to a given proposal density; GPS data, however, can still play an important role, since when available, can be used, for instance, to define a *confidence region*, such that particles falling outside it are discarded, as discussed in more detail below. Under this assumption the optimal proposal density (197) becomes[7]

$$\begin{aligned} q\left(\mathbf{r}_l \left| \mathbf{r}_{l-1}^{(j)}, \mathbf{z}_l^{INS} \right.\right) &= p\left(\mathbf{r}_l \left| \mathbf{r}_{l-1}^{(j)}, \mathbf{z}_l^{INS} \right.\right) \\ = \mathcal{N}\left(\mathbf{r}_l; \mathbf{r}_{l-1}^{(j)} + \mathbf{z}_l^{INS}, \mathbf{C}_{\Delta r,k}\right) &= \mathcal{N}\left(\mathbf{r}_l; \mathbf{r}_{l-1}^{(j)} + \overline{\Delta \mathbf{r}_k}, \mathbf{C}_{\Delta r,k}\right). \end{aligned} \quad (199)$$

Moreover, the weight update equation (196) becomes

$$\begin{aligned} w_l^{(j)} \propto w_{l-1}^{(j)} p\left(\mathbf{z}_l^{INS}/\mathbf{r}_{l-1}^{(j)}\right) &= w_{l-1}^{(j)} \int p\left(\mathbf{z}_l^{INS}/\tilde{\mathbf{r}}_l, \mathbf{r}_{l-1}^{(j)}\right) p\left(\tilde{\mathbf{r}}_l/\mathbf{r}_{l-1}^{(j)}\right) d\tilde{\mathbf{r}}_l \\ &= w_{l-1}^{(j)} \int \mathcal{N}\left(\overline{\Delta \mathbf{r}_k}; \tilde{\mathbf{r}}_l - \mathbf{r}_{l-1}^{(j)}, \mathbf{C}_{\Delta r,k}\right) p\left(\tilde{\mathbf{r}}_l/\mathbf{r}_{l-1}^{(j)}\right) d\tilde{\mathbf{r}}_l \\ &= w_{l-1}^{(j)} \int \mathcal{N}\left(\tilde{\mathbf{r}}_l; \overline{\Delta \mathbf{r}_k} + \mathbf{r}_{l-1}^{(j)}, \mathbf{C}_{\Delta r,k}\right) p\left(\tilde{\mathbf{r}}_l/\mathbf{r}_{l-1}^{(j)}\right) d\tilde{\mathbf{r}}_l. \end{aligned} \quad (200)$$

The integral

$$\begin{aligned} &\int \mathcal{N}\left(\tilde{\mathbf{r}}_l; \mathbf{z}_l^{INS} + \mathbf{r}_{l-1}^{(j)}, \mathbf{C}_{\Delta r,k}\right) p\left(\tilde{\mathbf{r}}_l/\mathbf{r}_{l-1}^{(j)}\right) d\tilde{\mathbf{r}}_l \\ &= \int \mathcal{N}\left(\tilde{\mathbf{r}}_l; \overline{\Delta \mathbf{r}_k} + \mathbf{r}_{l-1}^{(j)}, \mathbf{C}_{\Delta r,k}\right) p\left(\tilde{\mathbf{r}}_l/\mathbf{r}_{l-1}^{(j)}\right) d\tilde{\mathbf{r}}_l \end{aligned} \quad (201)$$

appearing in the right hand side of (200) does not admit a closed form solution, but can be approximated with an arbitray accuracy by means of particle-filtering methods [78]. This requires generating $\tilde{N}_p$ particles $\left\{\mathbf{y}_l^{(q)}, q = 0, 1, ..., \tilde{N}_p - 1\right\}$ (independent of the index j of $\mathbf{r}_{l-1}^{(j)}$and consequently to be computed only once

[7] Note that the Gaussian density $\mathcal{N}\left(\Delta \mathbf{r}; \overline{\Delta \mathbf{r}_k}, \mathbf{C}_{\Delta r,k}\right)$ is the pdf of the vector $\Delta \mathbf{r}_k \triangleq \left[\Delta p_{x,k}^{(N)}, \Delta p_{y,k}^{(N)}, \Delta \psi_k^{(N)}\right]^T$ generated by processing INS data only.

for any l), which are drawn from the pdf $\mathcal{N}(\mathbf{y}_l; \mathbf{0}, \mathbf{C}_{\Delta r,k})$; in fact, given these particles, the integral (201) is approximated as

$$\begin{array}{l} \int \mathcal{N}\left(\tilde{\mathbf{r}}_l; \overline{\Delta \mathbf{r}_k} + \mathbf{r}_{l-1}^{(j)}, \mathbf{C}_{\Delta r,k}\right) p\left(\tilde{\mathbf{r}}_l / \mathbf{r}_{l-1}^{(j)}\right) d\tilde{\mathbf{r}}_l \\ \cong \frac{1}{\tilde{N}_p} \sum_{q=0}^{\tilde{N}_p - 1} p\left(\mathbf{y}_l^{(q)} + \overline{\Delta \mathbf{r}_k} + \mathbf{r}_{l-1}^{(j)} / \mathbf{r}_{l-1}^{(j)}\right) d\tilde{\mathbf{r}}_l, \end{array} \tag{202}$$

where

$$p\left(\mathbf{y}_l^{(q)} + \overline{\Delta \mathbf{r}_k} + \mathbf{r}_{l-1}^{(j)} / \mathbf{r}_{l-1}^{(j)}\right) = 0 \tag{203}$$

if the state transition $\mathbf{r}_{l-1} \rightarrow \mathbf{r}_l$ does not satisfy map constraints and

$$p\left(\mathbf{y}_l^{(q)} + \overline{\Delta \mathbf{r}_k} + \mathbf{r}_{l-1}^{(j)} / \mathbf{r}_{l-1}^{(j)}\right) = \mathcal{N}\left(\mathbf{y}_l^{(q)} + \overline{\Delta \mathbf{r}_k}; \mathbf{0}, \mathbf{C}_{nr,l}\right) \tag{204}$$

if satisfies them.

Given a proposal density and weight update equation, particle filtering operates in a recursive fashion; the l-th recursion (with $l = 1, 2, ...$) evolves through the following steps for the j-th particle (with $j = 0, 1, ..., N_p - 1$) [77, Sec. V]:

1. Draw $\mathbf{r}_l^{(j)} \sim q\left(\mathbf{r}_l \left| \mathbf{r}_{l-1}^{(j)}, \mathbf{z}_l \right.\right)$;

2. Assign the weight $w_l^{(j)}$ to the the particle $\mathbf{r}_l^{(j)}$ according to (200).

Once the set $\left\{\tilde{w}_l^{(j)}, w_l^{(j)}\right\}$ collecting all the N_p new particles and their weights is available, the *total weight*

$$W = \sum_{j=0}^{N_p - 1} w_l^{(j)} \tag{205}$$

is computed, and *weight normalization* is accomplished evaluating

$$\tilde{w}_l^{(j)} = w_l^{(j)} W^{-1} \tag{206}$$

and assigning the new weight $\tilde{w}_l^{(j)}$ to $\mathbf{r}_l^{(j)}$ (with $j = 0, 1, ..., N_p - 1$). A common problem with the particle filter described above is the so called *degeneracy* phenomenon; this means that, after a few iterations, all but one particle are characterized by negligible weights. Degeneracy can be measured by evaluating the estimate

$$\widehat{N_{eff}} = \frac{1}{\sum_{j=0}^{N_p - 1} \left(\tilde{w}_l^{(j)}\right)^2} \tag{207}$$

of the so called *effective sample size* N_{eff}, whose value cannot exceed N_p; in fact, a small N_{eff} indicates severe degeneracy. This problem can be mitigated by properly choosing the proposal density and/or by using *resampling* when $\widehat{N_{eff}}$ (207) drops below a given threshold N_T. Resampling eliminates particles with small weights and concentrates on particles on large weights. In practice,

if a resampling step is added to the particle filter described above (after weight normalization, evaluating $\widehat{N_{eff}}$ (207) and checking if the inequality $\widehat{N_{eff}} < N_T$ holds), a new set of particles $\left\{\check{\mathbf{r}}_l^{(j)},\ j = 0, 1, ..., N_p - 1\right\}$ is generated by resampling (with replacement) N_p times from the density

$$\sum_{j=0}^{N_p-1} \tilde{w}_l^{(j)} \cdot \delta\left(\mathbf{r}_l - \mathbf{r}_l^{(j)}\right), \tag{208}$$

so that $\Pr\left\{\check{\mathbf{r}}_l^{(j)} = \mathbf{r}_l^{(j)}\right\} = \tilde{w}_l^{(j)}$; then, all the particle weights are reset to $1/N_p$. An efficient resapling procedure (known as *systematic resampling*) can be found in [77, Alg.2, p. 180].

In the particle filter described above INS information only has been exploited to derive the proposal density (199) and the weight update equation (200). GPS data have not been exploited; in addition map information has played a limited role, being employed only in the evaluation of the integral (201). Let us now discuss how these additional information can be employed. First of all, GPS data are needed for particle inizialization, since information about absolute position are available through GPS only. In other words, it is assumed that for $l = 0$ the j-th sample $\mathbf{r}_0^{(j)}$ is drawn from $\mathcal{N}\left(\mathbf{r}_0; \mathbf{z}_0^{GPS}, \mathbf{C}_{GPS,0}\right)$ and that the weight $\tilde{w}_0^{(j)} = 1/N_p$ is assigned to it (with $j = 0, 1, ..., N_p - 1$). For $l > 0$, when reliable GPS information are available, they can be exploited to evaluate the weight

$$w_{l,G}^{(j)} = \mathcal{N}\left(\mathbf{r}_l^{(j)}; \mathbf{z}_l^{GPS}, \mathbf{C}_{GPS,l}\right) \tag{209}$$

to be multiplied by $w_l^{(j)}$; in this way particle weighting is influenced by GPS data and particles falling out of a specific confidence region loose relevance.

Map information can be also processed to modify particle weights; in doing so, however, two different issues should be considered, as discussed in detail below.

1. If the speed of a given particle is different from zero (i.e., $\mathbf{r}_l^{(j)}$ and $\mathbf{r}_{l-1}^{(j)}$ differ), such a particle should be on a road segment. If it is not on road segment, a low probability should be assigned to it [53, 79]. In addition, if the particle is on a road segment, different weights should be assigned on the basis of its speed and of the type of road (i.e., of the *functional road class*, FRC). For instance, its is very unlikely that a particle can travel at high speed on a residential road. A table listing the weights to be associated to a particle on the basis of its speed and of the FRC parameter can be found in [53]; the weight to be associated to $\mathbf{r}_l^{(j)}$ on the basis of its speed and road type is denoted $w_{l,SR}^{(j)}$ in the following. Note also that, when a particle is associated with a road segment, its link to the map database (denoted L_l above) is uniquely identified.

2. Maps provide *topological information*, which, in principle, can be also exploited in particle filtering. In practice, a road network consists of nodes

and edges. Edges are made of several vertices, and can be unidirectional or bidirectional (i.e., they allow traffic flow in one or both directions). If a particle is established to be on a road segment (uniquely identified by a link to the map), only some locations (i.e., road segments) can be reached in the network when the particle is updated. If the new road segment is reachable from the previous location, then the probability of being on the new segment is higher than that associated with an impossible location. Topological information can accounted for by adding another weight in the weight update equation (such a weight is denoted $w_{l,T}^{(j)}$ in the following). For instance, if the previous road of the $j-$th particle is not known, $w_{l,T}^{(j)}$ =0.5 could be selected; on the contrary, if its known, $w_{l,T}^{(j)}$ =1 ($w_{l,T}^{(j)}$ =0) could be set if the new location is reachable (unreachable). Note that this idea is closely related to concept of *hospitability map* developed in [80] for target state estimation an aims at guiding the particle filter to more probable areas.

Consequently, GPS and map information can be incorporated in the particle filter by replacing the weight update equation (200) with

$$w_l^{(j)} \propto w_{l-1}^{(j)} p\left(\mathbf{z}_l^{INS}/\mathbf{r}_{l-1}^{(j)}\right) \cdot w_{l,G}^{(j)} \cdot w_{l,Z}^{(j)} \cdot w_{l,T}^{(j)}. \tag{210}$$

Unluckily, the impact of this change in the weight update equation on the performance of particle filtering cannot be assessed theoretically; for this reason, extensive computer simulations are needed.

8 Conclusions

After discussing some fundamental issues in vehicular navigation, a two stage architecture has been developed. It relies on a vehicle model available in the technical literature and combines extended Kalman filtering with particle filtering. Particle filtering allows to include strongly nonlinear constraints originating from map knowledge in the position estimation process and to reduce the dimensionality of the extended Kalman filter.

The theoretical framework provided by CNIT fully achieves the objectives of WP2 of the Proof-of-Concept. This report completely describes the theoretical framework in all its parts.

The next steps in the Proof of Concept will be the implementation in MATLAB of the theoretical framework presented in this report and the subsequent integration and validation on the platforms and sensors acquired as part of the procurement plan of the Proof of Concept.

Appendix - Quaternion Algebra

In this Appendix some basic notions about *quaternion algebra* are briefly illustrated, since quaternions can be used for the representation of the orientation in the 3-D space of sensors used for navigation. A good introductory text about such entities and a suggested reading is ref. [61].

Quaternions are *hyper-complex numbers* of rank 4. Hyper-complex numbers are extensions of real numbers in which some of ordinary field properties (closure, associativity, commutativity, existence of zero and identity elements, distributivity) do not necessary hold. Real numbers may be considered as hyper-complex numbers of rank 1 (that satisfy the field properties under ordinary addition and multiplication). The "ordinary" complex numbers may be considered as hyper-complex numbers of rank 2 (they also satisfy the field properties). Quaternions are hyper-complex numbers of rank 4 and satisfy all field properties except for the commutative law for multiplication. Their algebra is commonly denoted $\mathbb{H}$ [8, 61]. A quaternion $q \in \mathbb{H}$ is a 4-tuple of real numbers and is usually denoted $q = (q_0, q_1, q_2, q_3)$. Alternatively it is represented as $q = (q_0, \mathbf{q})$, where q_0 is its *scalar* part and $\mathbf{q}$ is its *vector* part. Special quaternion groups are:

1. *Unit* quaternions, i.e., quaternions q such that their norm is $\|q\| = 1$; their algebra is denoted $\mathbb{H}_1$ in this document.

2. *Pure* quaternions, i.e., quaternions q such that their scalar part is $q_0 = 0$; their algebra is denoted $\mathbb{H}_0$ in this document.

3. *Scalar* quaternions, i.e., quaternions q such that their vector part is $\mathbf{q} = \mathbf{0}$; their algebra is denoted $\mathbb{H}_s$ in this document.

Quaternion operations in $\mathbb{H}$ can be briefly described as follows (see also [10, Appendix A]).

- Addition: $p + q \triangleq (p_0 + q_0, \mathbf{p} + \mathbf{q})$, where $+$ denotes ordinary vector addition in $\mathbb{R}$ and $p = (p_0, p_1, p_2, p_3) = (p_0, \mathbf{p})$;

- Multiplication: $p \odot q \triangleq (p_0 q_0 - \mathbf{p} \cdot \mathbf{q}, p_0\mathbf{q} + q_0\mathbf{p} + \mathbf{p} \times \mathbf{q})$, where $\cdot$ and $\times$ denote ordinary dot and vector products in $\mathbb{R}^3$, respectively;

- Conjugation: $(q)^* \triangleq (q_0, -\mathbf{q})$;

- Norm: $\|q\| \triangleq \sqrt{q_0^2 + \mathbf{q} \cdot \mathbf{q}} = \sqrt{(q)^* \cdot q}$, where $\sqrt{\cdot}$ denotes the ordinary square root in $\mathbb{R}$;

- Inverse: $q^{-1} \triangleq (q)^* / \|q\|^2$;

- Exponential: this is defined as a power series similar to the matrix exponential; in the specific case of a quaternion exponential of a vector $q = (0, \mathbf{q})$, we have that $\exp(q) \triangleq \left(\cos\|\mathbf{q}\|, \frac{\mathbf{q}}{\|\mathbf{q}\|}\sin\|\mathbf{q}\|\right)$, where $\sin(\cdot)$ and $\cos(\cdot)$ denote ordinary sine and cosine functions, respectively, in $\mathbb{R}$.

Note that: a) the operations defined above also hold in $\mathbb{H}_0$, $\mathbb{H}_1$ and $\mathbb{H}_s$; b) the multiplication of quaternions can be also expressed, using a matrix/vector notation, as

$$p \odot q = p_L q = q_R p, \tag{211}$$

where

$$p_L = \begin{bmatrix} p_0 & -p_1 & -p_2 & -p_3 \\ p_1 & p_0 & -p_3 & p_2 \\ p_2 & p_3 & p_0 & -p_1 \\ p_3 & -p_2 & p_1 & p_0 \end{bmatrix} \tag{212}$$

and

$$q_R = \begin{bmatrix} q_0 & -q_1 & -q_2 & -q_3 \\ q_1 & q_0 & q_3 & -q_2 \\ q_2 & -q_3 & q_0 & q_1 \\ q_3 & q_2 & -q_1 & q_0 \end{bmatrix}, \tag{213}$$

and $\cdot_L$ and $\cdot_R$ denote the left and right multiplication operators, respectively. Finally, the mapping between real numbers and quaternions can be represented as

$$a \in \mathbb{R} \leftrightarrow (a, \mathbf{0}) \in \mathbb{H}_s \tag{214}$$

so that each real number in $\mathbb{R}$ is a *scalar* quaternion and viceversa (so that $\mathbb{R} \subset \mathbb{H}_s \subset \mathbb{H}$). Moreover, quaternions can be easily related to real vectors of $\mathbb{R}^3$, since

$$\mathbf{a} \in \mathbb{R}^3 \leftrightarrow (0, \mathbf{a}) \in \mathbb{H}_0, \tag{215}$$

so that each real vector in $\mathbb{R}^3$ is a *pure* quaternion and viceversa (however, $\mathbb{R}^3$ is not a subset of $\mathbb{H}_0$; the mapping (215) represents an isomorphism).

References

[1] Y. K. Tham, H. Wang, and E. K. Teoh, "Adaptative state estimation for 4-wheel steerable industrial vehicles", *Proc. of the 37th IEEE Conf. Decision Control*, Tampa, FL, 1998, pp. 4509–4514.

[2] R. Toledo-Moreo, M. Zamora-Izquierdo, B. Ubeda-Minarro and A. Gomez-Skarmeta, "High-integrity IMM-EKF-based road vehicle navigation with low-cost GPS/SBAS/INS", *IEEE Trans. Intell. Transp. Syst.*, vol. 8, no. 4, pp.491-511, Sep. 2007.

[3] N. K. Weiss, M. Schaefer and K. C. J. Dietmayer, "IMM object tracking for high dynamic driving maneuvers", *Proc. IEEE Intell. Veh. Symp.*, Parma, Italy, pp. 825–830, June 2004.

[4] L. Zhao and C. Thorpe, "Qualitative and quantitative car tracking from a range image sequence", *Proc. IEEE Conf. Comput. Vis. and Pattern Recog.*, pp. 496–501, 1998.

[5] K. Weiss, N. Kaempchen, and A. Kirchner, "Multiple-model tracking for the detection of lane change maneuvers", *Proc. IEEE Intell. Veh. Symp.*, Parma, Italy, pp. 937–942, June 2004.

[6] S. Godha and E. Cannon, "GPS/MEMS INS integrated system for navigation in urban areas", *GPS Solut.*, vol. 11, no. 3, pp. 193–203, July 2007.

[7] G. Dissanayake, S. Sukkarieh, E. Nebot and H. Durrant-Whyte, "The aiding of a low-cost strapdown inertial measurement unit using vehicle model constraints for land vehicle applications", *IEEE Trans. Robot. Autom.*, vol. 17, no. 5, pp. 731–747, Oct. 2001.

[8] J. Diebel, *Representing Attitude: Euler Angles, Unit Quaternions, and Rotation Vectors*, Stanford University, Tech. Rep., 2006.

[9] I. Skog and P. Handel, "In-Car Positioning and Navigation Technologies - A Survey", *IEEE Trans. Intell. Transp. Syst.*, vol.10, no.1, pp.4-21, March 2009.

[10] J. Hol, *Pose Estimation and Calibration Algorithms for Vision and Inertial Sensors*, Ph.D. dissertation, Linköping University, 2008.

[11] J. B. Kuipers, *Quaternions and Rotation Sequences: A Primer with Applications to Orbits, Aerospace, and Virtual Reality.* Princeton University Press, 1999.

[12] S. Julier and H. Durrant-Whyte, "On the role of process models in autonomous land vehicle navigation systems", *IEEE Trans. Robot. Autom.*, vol. 19, no. 1, pp. 1–14, Feb. 2003.

[13] J. Huang and H.-S. Tan, "A low-order DGPS-based vehicle positioning system under urban environment", *IEEE/ASME Trans. Mechatron.*, vol. 5, no. 1/2, pp. 567–575, Oct. 2006.

[14] N. El-Sheimy and X. Niu, "The promise of MEMS to the navigation community", *Inside GPS*, vol. 2, no. 2, pp. 46–56, Mar./Apr. 2007.

[15] D. Bevly, J. Ryu, and J. Gerdes, "Integrating INS sensors with GPS measurements for continuous estimation of vehicle sideslip, roll, and tire cornering stiffness", *IEEE Trans. Intell. Transp. Syst.*, vol. 7, no. 4, pp. 483–493, Dec. 2006.

[16] S. Julier and H. Durrant-Whyte, "Process models for the high-speed navigation of road vehicles", *Proc. IEEE Int. Conf. Robot. Autom.*, Nagoya, Japan, pp. 101–105, May 1995.

[17] S. Rezaei and R. Sengupta, "Kalman filter-based integration of DGPS and vehicle sensors for localization", *IEEE Trans. Control Syst. Technol.*, vol. 15, no. 6, pp. 1080–1088, Nov. 2007.

[18] C. Tan and S. Park, "Design of accelerometer-based inertial navigation systems," *IEEE Trans. Instrum. Meas.*, vol. 54, no. 6, pp. 2520–2530, Dec. 2005.

[19] J. Chen, S. Lee and D. DeBra, "Gyroscope free strapdown inertial measurement unit by six linear accelerometers", *J. Guid. Control Dyn.* , vol. 17, no. 2, pp. 286–290, 1994.

[20] E. Abbott and D. Powell, "Land-vehicle navigation using GPS", *Proc. IEEE*, vol. 87, no. 1, pp. 145–162, Jan. 1999.

[21] P. Batista, C. Silvestre, P. Oliveira and B. Cardeira, "Accelerometer Calibration and Dynamic Bias and Gravity Estimation: Analysis, Design, and Experimental Evaluation", *IEEE Trans. Control Syst. Technol.*, vol. 19, no. 5, pp. 1128-1137, Sep. 2011.

[22] M. Sipos, P. Paces, J. Rohac and P. Novacek, "Analyses of Triaxial Accelerometer Calibration Algorithms", *IEEE Sensors J.*, vol. 12, no. 5, pp. 1157-1165, May 2012.

[23] J. Gautier, GPS/INS generalized evaluation tool for the design and testing of integrated navigation systems. PhD Thesis, Stanford University, USA, 2003.

[24] F. Gustafsson, F. Gunnarsson, N. Bergman, U. Forssell, J. Jansson, R. Karlsson and P. Nordlund, "Particle filters for positioning, navigation, and tracking", *IEEE Trans. Sig. Proc.*, vol. 50, pp. 425–435, 2002.

[25] D. Gustafson and J. Dowdle, "Deeply integrated code tracking: comparative performance analysis", *Proc. of ION GPS/GNSS 2003*, Portland, Oregon, pp. 2553–2561, 2003.

[26] H-S. Kim, S-C. Bu, G-I. Jee, C. Gook, C.-G. Park, "An ultra-tightly coupled GPS/INS integration using federated Kalman filter", *Proc. of ION GPS/GNSS 2003*, Portland, Oregon, USA, 2003.

[27] K. L. Gold and A. K. Brown, "A Hybrid Integrity solution for Precision Landing and Guidance", *Proc. of IEEE PLANS*, California, USA, pp. 165–174, 2004.

[28] Y. C. Lee and S. D. Ericson, "Analysis of Coast Times Upon Loss of GPS Signals for Integrated GPS/ Inertial Systems", *Air Traffic Control Quarterly*, vol. 12, no. 1, pp. 27–51, 2004.

[29] U. I. Bhatti and W. Y. Ochieng, "Failure Modes and Models for Integrated GPS/INS Systems", *Journal of Navigation*, vol. 60, pp. 327-348, 2007.

[30] U. I. Bhatti, W. Y. Ochieng and S. Feng, "Integrity of an integrated GPS/INS system in the presence of slowly growing errors. Part I: A critical review", *GPS Solutions*, Springer-Verlag, vol. 11, pp. 173-181, 2007

[31] U. I. Bhatti, W. Y. Ochieng and S. Feng, "Integrity of an integrated GPS/INS system in the presence of slowly growing errors. Part II: analysis", *GPS Solutions*, Springer-Verlag, 2007, vil. 11, pp. 183-192, 2007

[32] S. Kim and J. Kim, "Adaptive fuzzy-network based C-measure map-matching algorithm for car navigation system", *IEEE Trans. Ind. Electr.*, vol. 48, no. 2, pp. 432–440, 2001.

[33] J. Pyo, D. Shin and T. Sung, "Development of a map-matching method using the multiple hypothesis technique", *IEEE Proc. Intell. Transp. Syst.*, pp. 23–27, 2001.

[34] M. A. Quddus, W. Y. Ochieng, L. Zhao and R. B. Noland, "A general map-matching algorithm for transport telematics applications", *GPS Solutions*, vol. 7, no. 3, pp. 157–167, 2003.

[35] S. Syed and M. E. Cannon, "Fuzzy logic-based map-matching algorithm for vehicle navigation system in urban canyons", *Proc. of the Institute of Navigation* (ION) *national technical meeting*, California, USA, Jan. 26–28, 2004.

[36] W. Y. Ochieng, M. A. Quddus and R. B. Noland, "Map-matching in complex urban road networks", *Brazilian Journal of Cartography* (*Revista Brasileira de Cartografia*), vol. 55, no. 2, pp. 1–18, 2004.

[37] M. A. Quddus, R. B. Noland and W. Y. Ochieng, "The effects of navigation sensors and digital map quality on the performance of mapmatching algorithms", presented at the *Transportation Research Board* (TRB) *Annual Meeting of the Transportation Research Board*, Washington D.C., Jan. 2006.

[38] M. A. Quddus, R. B. Noland and W. Y. Ochieng, "A high accuracy fuzzy logic-based map-matching algorithm for road transport", *Journal of Intelligent Transportation Systems: Technology, Planning, and Operations*, vol. 10, no.3, pp. 103–115, 2006.

[39] M. A. Quddus, W. Y. Ochieng and R. B. Noland, "Current map-matching algorithms for transport applications: State-of-the-art and future research directions", *Transportation Research Part C*, vol. 15, no.5, pp. 312–328, 2007.

[40] W. Chen, Z. Li, M. Yu and Y. Chen, "Effects of sensor errors on the performance of map-matching", *Journal of Navigation*, 2005.

[41] Y. Cui and S. S. Ge, "Autonomous vehicle positioning with GPS in urban canyon environments", *IEEE Transactions on Robotics and Automation*, vol. 19, no. 1, pp. 15–25, 2003.

[42] J. S. Greenfeld, "Matching GPS observations to locations on a digital map", *Proc. of the 81st Annual Meeting of the Transportation Research Board*, Washington D.C., January 2002.

[43] F. Montorsi, F. Pancaldi and G. M. Vitetta, "Design and implementation of an inertial navigation system for pedestrians based on a low-cost MEMS IMU", *Proc. of the 2013 IEEE Int. Conf. Commun.* (ICC 2013), pp. 57-61, 9-13 June 2013.

[44] J. S. Kim, J. H. Lee, T. H. Kang, W. Y. Lee and Y. G. Kim, "Node based map-matching algorithm for car navigation system", *Proc. of the 29th ISATA Symposium*, Florence, Italy, vol. 10, pp. 121–126, 1996.

[45] W. Chen, M. Yu, Z.-L. Li and Y.-Q. Chen, "Integrated vehicle navigation system for urban applications", *Proc. of the 7th International Conference on Global Navigation Satellite Systems* (GNSS), European Space Agency, Graz, Austria, pp. 15–22, April 22–24, 2003.

[46] Y. Zhao, Vehicle Location and Navigation System, Artech House, Inc., MA, 1997.

[47] D. Obradovic, H. Lenz and M. Schupfner, "Fusion of map and sensor data in a modern car navigation system", *Journal of VLSI Signal Processing*, vol. 45, pp. 112–122, 2006.

[48] D. Obradovic, H. Lenz and M. Schupfner, "Fusion of Sensor Data in Siemens Car Navigation System", *IEEE Trans. Veh. Tech.*, vol. 56, no.1, pp. 43-50, Jan. 2007.

[49] Q. Li, Z. Fang, H. Li and H. Xiao, "Integrating GPS, GYRO, vehicle speed sensor, and digital map to provide accurate and real-time position in an intelligent navigation system", *Proc. of the International Society for Optical Engineering*, pp. 1–11, 2005.

[50] M. E. El Najjar and P. Bonnifait, "A Road-matching method for precise vehicle localization using Kalman filtering and belief theory", *Autonomous Robots*, vol. 19, no. 2, pp. 173–191, 2005.

[51] IEEE Standard Specification Format Guide and Test Procedure for Linear, Single-Axis, Nongyroscopic Accelerometers, 1999.

[52] IEEE Standard Specication Format Guide and Test Procedure for Single-Axis Interferometric Fiber Optic Gyros, IEEE Std 952-1997, 1998.

[53] A. U. Peker, O. Tosun and T. Acarman, "Particle filter vehicle localization and map-matching using map topology", *Proc. of the 2011 IEEE Intell. Veh. Symp.* (IV), pp.2 48-253, 5-9 June 2011.

[54] Chih-Hao Chao, Chun-Yuan Chu and An-Yeu Wu, "Location-Constrained Particle Filter human positioning and tracking system", *2008 IEEE Workshop on Signal Processing Systems* (SiPS 2008), pp.73-76, 8-10 Oct. 2008.

[55] Yun-Ki Kim, Seung-Hwan Choi and Jang-Myung Lee, "Enhanced outdoor localization of multi-GPS/INS fusion system using Mahalanobis Distance", *Proc. of the 2013 10th International Conference on Ubiquitous Robots and Ambient Intelligence* (URAI), pp. 488-492, Oct. 2013.

[56] X. Niu, S. Nasser, C. Goodall and N. El-Sheimi, "A Universal Approach for Processing any MEMS Inertial Sensor Configuration for Land-Vehicle Navigation", *Journal of Navigation*, vol. 60, pp. 233-245, 2007.

[57] A. Eidehall, T. B. Schon and F. Gustafsson, "The marginalized particle filter for automotive tracking applications", *Proc. of the 2005 IEEE Intell. Veh. Symp.*, pp. 370-375, June 2005.

[58] F. Gustafsson, "Particle filter theory and practice with positioning applications", *IEEE Aerospace and Electronic Systems Magazine*, vol. 25, no. 7, pp. 53-82, July 2010.

[59] D. Huang, H. Leung and N. El-Sheimy, "Expectation Maximization Based GPS/INS Integration for Land-Vehicle Navigation", I*EEE Transactions on Aerospace and Electronic Systems*, vol. 43, no. 3, pp. 1168-1177, July 2007.

[60] B. W. Parkinson and J. J. Spilker (Eds.), Global Positioning System: Theory & Applications, Volume I, Progress in Astronautics and Aeronautics, American Institute of Austronatics and Aeronautics, 1st edition, 1996.

[61] J. B. Kuipers, Quaternions and Rotation Sequences: A Primer with Applications to Orbits, Aerospace, and Virtual Reality. Princeton University Press, 1999.

[62] M. George and S. Sukkarieh, "Tightly Coupled INS/GPS with Bias Estimation for UAV Applications", *Proc. of the Australiasian Conference on Robotics and Automation* (ACRA) 2005, Sydney, Australia, 5-7 Dec. 2005.

[63] J. Wendel and G. F. Trommer, "Tightly coupled GPS/INS integration for missile applications", *Aerospace Science and Technology*, vol. 8, 627– 634, 2004.

[64] J. Zhou, S. Knedlik and O. Loffeld, "INS/GPS for High-Dynamic UAV-Based Applications", *International Journal of Navigation and Observation*, 2012.

[65] A. M. Sabatini, "Quaternion-based extended Kalman filter for determining orientation by inertial and magnetic sensing", *IEEE Transactions on Biomedical Engineering*, vol.53, no.7, pp.1346,-1356, July 2006.

[66] DAISY-7: GPS-MEMS module, technical documentation available at www.acmesystems.it.

[67] COMBO-T2: Enhanced TERRA board kit, technical documentation available at www.acmesystems.it.

[68] A. Wahdan, J. Georgy, W. F. Abdelfatah and A. Noureldin, "Magnetometer Calibration for Portable Navigation Devices in Vehicles Using a Fast and Autonomous Technique", to appear on the *IEEE Trans. Intell. Transp. Syst.*

[69] M. El-Diasty, S. Pagiatakis, "A Rigorous Temperature-Dependent Stochastic Modelling and Testing for MEMS-Based Inertial Sensor Errors", *Sensors*, vol. 9, no. 11, pp. 8473-8489, 2009.

[70] N. El-Sheimy, H. Hou and X. Niu, "Analysis and Modeling of Inertial Sensors Using Allan Variance", *IEEE Transactions on Instrumentation and Measurement*, vol. 57, no. 1, pp. 140-149, Jan. 2008.

[71] B. Krach and P. Robertson, "Integration of foot-mounted inertial sensors into a Bayesian location estimation framework", *Proc. of the 5th Workshop on Positioning, Navigation and Communication* (WPNC 2008), pp. 55-61, 27 March 2008.

[72] E. Foxlin, "Pedestrian tracking with shoe-mounted inertial sensors", *IEEE Computer Graphics and Applications*, vol. 25, no. 6, pp. 38-46, Nov.-Dec. 2005.

[73] X. Rong Li and V. Jilkov, "Survey of maneuvering target tracking. Part I. Dynamic models", *IEEE Trans. Aerosp. and Electron. Syst.*, vol. 39, no. 4, pp. 1333- 1364, Oct. 2003.

[74] J. Hol, Pose Estimation and Calibration Algorithms for Vision and Inertial Sensors, Ph.D. dissertation, Linköping University, 2008.

[75] G. Taylor, G. Blewitt, D. Steup, S. Corbett and A. Car, "Road reduction filtering for GPS-GIS navigation", *Transactions in GIS*, vol. 5, no. 3, pp. 193–207, 2001.

[76] W. Y. Ochieng, M. A. Quddus and R. B. Noland, "Map-matching in complex urban road networks", *Brazilian Journal of Cartography* (*Revista Brasileira de Cartografia*), vol. 55, no. 2, pp. 1–18, 2004.

[77] M. S. Arulampalam, S. Maskell, N. Gordon and T. Clapp, "A Tutorial on Particle Filters for Online Nonlinear/Non-Gaussian Bayesian Tracking", *IEEE Trans. Sig. Proc.*, vol. 50, no. 2, Feb. 2002.

[78] J. Dauwels, S. Korl and H.-A. Loeliger, "Particle Methods as Message Passing", *Proc. of the 2006 IEEE Int. Symp. Inf. Theory*, pp. 2052-2056, 9-14 July 2006.

[79] Sang Min Oh, S. Tariq, B. N. Walker and F. Dellaert, "Map-based priors for localization", *Proc. of the 2004 IEEE/RSJ International Conference on Intelligent Robots and Systems* (IROS 2004), vol. 3, pp. 2179-2184, 28 Sept.-2 Oct. 2004.

[80] Z. M. Kassas, U. Ozguner and J. Layne, "Out-of-surveillance target state estimation: a combined hospitability and synthetic inclination approach", *Proc. of the 43rd IEEE Conference on Decision and Control* (CDC 2004), vol. 1, pp. 710-715, 17 Dec. 2004.

European Commission
EUR 27042 EN – Joint Research Centre – Institute for the Protection and Security of the Citizen

Title: Theoretical framework for In-Car Navigation based on Integrated GPS/IMU Technologies

Authors: Giorgio M. Vitetta, Gianmarco Baldini

Luxembourg: Publications Office of the European Union

2015 – 65 pp. – 21.0 x 29.7 cm

EUR – Scientific and Technical Research series – ISSN 1831-9424

ISBN 978-92-79-44729-7

doi:10.2788/509569

LB-NA-27042 -EN-N

JRC Mission

As the Commission's in-house science service, the Joint Research Centre's mission is to provide EU policies with independent, evidence-based scientific and technical support throughout the whole policy cycle.

Working in close cooperation with policy Directorates-General, the JRC addresses key societal challenges while stimulating innovation through developing new methods, tools and standards, and sharing its know-how with the Member States, the scientific community and international partners.

Serving society
Stimulating innovation
Supporting legislation

doi:10.2788/509569

ISBN 978-92-79-44729-7

Publications Office